Cooperative Localization in Mobile Underwater Acoustic Sensor Networks

Zur Erlangung des akademischen Grades eines
Doktors der Ingenieurwissenschaften
(Dr.-Ing.)

bei der Fakultät für Informatik
des Karlsruher Instituts für Technologie (KIT)

eingereichte
DISSERTATION

von

Sergej Neumann M.Sc.

*"Uncertainty that comes from knowledge (knowing what you don't know)
is different from uncertainty coming from ignorance."*
Isaac Asimov

Abstract (English Version)

The exploration and monitoring of large deep-sea environments become an increasingly interesting endeavour for science and industry. These vast, inaccessible and remote spaces can only be probed efficiently by unmanned submersibles. For a long time, teams of Autonomous Underwater Vehicles (AUV) were economically prohibitive and could only be investigated through simulations. With the emergence of cheaper and more reliant AUV, the simultaneous deployment of several unmanned crafts becomes a viable option. This trend is likely to accelerate with the growing demand on underwater exploration and monitoring.

With the absence of satellite navigation, underwater localization still poses a major technical difficulty for deep diving vehicles. As a consequence thereof, new strategies for underwater localization need to be developed that allow the efficient deployment of multiple submersibles in a scalable manner. The simultaneous deployment of multiple vehicles will not only allow for completely new types of cooperation, but will also enable each individual vehicle to benefit from navigation information obtained by other members of the group.

In order to navigate, every AUV needs the ability of self-localization. In this work a cooperative localization approach is proposed, which enhances the self-localization capabilities of a group of AUVs by sharing navigation data. The proposed method is based on message exchange via acoustic ultra-short base-line (USBL) modems. A USBL modem allows the transmission of data packages as well as the measurement of the relative direction of a transmitting device. When a vehicle transmits a data package with its own location, others can use this information, in conjunction with a relative measurement to the sender, for self-referencing. This work proposes an approach to merge the measurement with the transmitted position, while also accounting for their respective inaccuracies. In order to quantify the measurement uncertainty of the complex USBL modem, a sensor model has been elaborated.

Existing cooperative localization schemes have been analysed to identify desirable properties. Based on this analysis and with a focus on scalability and practical applicability the Deep-Sea Network Localization (DNL) approach was developed. DNL is designed as an intermediate layer between the USBL and the navigation system of a vehicle. It merges communication data and measurements from USBL to provide a position fix and heading estimation to the navigation system, similar to a GPS sensor. The practical functionality of USBL model and DNL has been evaluated with data from sea trials in the Baltic Sea and the Middle Atlantic Ocean. A cooperative localization approach usually depends on many factors. Network topology needs to be considered as well as the navigation capability of each individual member of the

network. Also the communication scheme, that is, which vehicle shares its information in which intervals, plays an important role. Therefore, the performance of DNL was investigated during several multi-vehicle experiments in simulation with varying communication schemes and network topologies. In these experiments an unmanned surface vehicle provided geo-reference for multiple underwater vehicle by forwarding its global position via DNL.

The multi-vehicle experiments can be categorized in two groups, single-hop and multi-hop. In the single-hop case all submersibles have direct access to the transmissions of the surface vehicle, while in the multi-hop case only one underwater vehicle receives the updates from the surface vehicle and relays its own updated position believe to the other members of the group. Results from the single-hop experiments confirm that, with DNL, the localization error can be bound for a group of submersibles. Here the localization accuracy correlates with the combined uncertainty of surface vehicle position and USBL measurement.

In the multi-hop case, a similar observation was made. When the communication is strictly unidirectional from the underwater relay to the other submersibles, the localization error of the group is bound at a margin that approximates the combined uncertainty of relay position and USBL measurement. However, the cooperative localization performance declines if all members of the group share their position with one another. This counter intuitive behaviour can be traced back to the range estimation as one part of the DNL approach. For the given set-up, the range estimation is necessary because the considered USBL class can only measure the direction but not the distance to a sending counterpart. The last experiment demonstrates how this drawback can be overcome by using a relatively new USBL sensor class that is able to measure the range as well as the relative direction.

The two major contributions of this work are an elaborate USBL sensor model and the novel cooperative localization DNL. With the sensor model it is possible to predict measurement deviations and even correct some error sources while DNL provides a scalable cooperative localization approach for mobile underwater networks. Because of its design as intermediate layer it can be easily integrated into existing navigation solutions to provide long-term navigation stability for large fleets of deep diving submersibles. Both, USBL model and DNL are resourceful enough that they can run on the computer of a standard USBL device without disturbing its original driver, which makes their integration effectively free of charge.

Abstract (German Version)

Die großflächige Erkundung und Überwachung von Tiefseegebieten gewinnt mehr und mehr an Bedeutung für Industrie und Wissenschaft. Diese schwer zugänglichen Areale in der Tiefsee können nur mittels Teams unbemannter Tauchbote effizient erkundet werden. Aufgrund der hohen Kosten, war bisher ein Einsatz von mehreren autonomen Unterwasserfahrzeugen (AUV) wirtschaftlich undenkbar, wodurch AUV-Teams nur in Simulationen erforscht werden konnten. In den letzten Jahren konnte jedoch eine Entwicklung hin zu günstigeren und robusteren AUVs beobachtet werden. Somit wird der Einsatz von AUV-Teams in Zukunft zu einer realen Option. Die wachsende Nachfrage nach Technologien zur Unterwasseraufklärung und Überwachung könnte diese Entwicklung noch zusätzlich beschleuningen.

Eine der größten technischen Hürden für tief tauchende AUVs ist die Unterwasserlokalisierug. Satelitengestüzte Navigation ist in der Tiefe nicht möglich, da Radiowellen bereits nach wenigen Metern im Wasser stark an Intensität verlieren. Daher müssen neue Ansätze für die Unterwasserlokalisierung entwickelt werden die sich auch für Fahrzeugenverbände skalieren lassen. Der Einsatz von AUV-Teams ermöglicht nicht nur völlig neue Möglichkeiten der Kooperation, sondern erlaubt auch jedem einzelnen AUV von den Navigationsdaten der anderen Fahrzeuge im Verband zu profitieren, um die eigene Lokalisierung zu verbessern.

In dieser Arbeit wird ein kooperativer Lokalisierungsansatz vorgestellt, welcher auf dem Nachrichtenaustausch durch akustische Ultra-Short Base-Line (USBL) Modems basiert. Ein akustisches Modem ermöglicht die Übertragung von Datenpaketen im Wasser, wärend ein USBL-Sensor die Richtung einer akustischen Quelle bestimmen kann. Durch die Kombination von Modem und Sensor entsteht ein wichtiges Messinstrument für die Unterwasserlokalisierung. Wenn ein Fahrzeug ein Datenpaket mit seiner eignen Position aussendet, können andere Fahrzeuge mit einem USBL-Modem diese Nachricht empfangen. In Verbindung mit der Richtungsmessung zur Quelle, können diese Daten von einem Empfangenden AUV verwendet werden, um seine eigene Positionsschätzung zu verbessern. Diese Arbeit schlägt einen Ansatz zur Fusionierung der empfangenen Nachricht mit der Richtungsmessung vor, welcher auch die jeweiligen Messungenauigkeiten berücksichtigt. Um die Messungenauigkeit des komplexen USBL-Sensors bestimmen zu können, wurde zudem ein detailiertes Sensormodell entwickelt.

Zunächst wurden existierende Ansätze zur kooperativen Lokalisierung (CL) untersucht, um daraus eine Liste von erwünschten Eigenschaften für eine CL abzuleiten. Darauf aufbauend wurde der Deep-Sea Network Lokalisation (DNL) Ansatz entwick-

elt. Bei DNL handelt es sich um eine CL Methode, bei der die Skalierbarkeit sowie die praktische Anwendbarkeit im Fokus stehen. DNL ist als eine Zwischenschicht konzipiert, welche USBL-Modem und Navigationssystem miteinander verbindet. Es werden dabei Messwerte und Kommunikationsdaten des USBL zu einer Standorbestimmung inklusive Richtungsschätzung fusioniert und an das Navigationssystem weiter geleitet, ähnlich einem GPS-Sensor.

Die Funktionalität von USBL-Modell und DNL konnten evaluiert werden anhand von Messdaten aus Seeerprobungen in der Ostsee sowie im Mittelatlantik. Die Qualität einer CL hängt häufig von vielen unterschiedlichen Faktoren ab. Die Netzwerktopologie muss genauso berücksichtig werden wie die Lokalisierungsfähigkeiten jedes einzelnen Teilnehmers. Auch das Kommunikationsverhalten der einzelnen Teilnehmer bestimmt, welche Informationen im Netzwerk vorhanden sind und hat somit einen starken Einfluss auf die CL. Um diese Einflussfaktoren zu untersuchen, wurden eine Reihe von Szenarien simuliert, in denen Kommunikationsverhalten und Netzwerktopologie für eine Gruppe von AUVs variiert wurden. In diesen Experimenten wurden die AUVs durch ein Oberflächenfahrzeug unterstützt, welches seine geo-referenzierte Position über DNL an die getauchten Fahrzeuge weiter leitete.

Anhand der untersuchten Topologie können die Experimente eingeteilt werden in Single-Hop und Multi-Hop. Single-Hop bedeutet, dass jedes AUV sich in der Sende-Reichweite des Oberflächenfahrzeugs befindet und dessen Positionsdaten auf direktem Wege erhält. Wie die Ergebnisse der Single-Hop Experimente zeigen, kann der Lokalisierungsfehler der AUVs eingegrenzt werden, wenn man DNL verwendet. Dabei korreliert der Lokalisierungsfehler mit der kombinierten Ungenauigkeit von USBL-Messung und Oberflächenfahrzeugposition.

Bei den Multi-Hop Experimenten wurde die Topoligie so geändert, dass sich nur eines der AUVs in direkter Sendereichweite des Oberflächenfahrzeugs befindet. Dieses AUV verbessert seine Position mit den empfangen Daten des Oberflächenfahrzeugs und sendet wiederum seine verbesserte Postion an die anderen AUVs. Auch hier konnte gezeigt werden, dass sich der Lokalisierungfehler der Gruppe mit DNL einschränken lässt. Ändert man nun das Schema der Kommunikation so, dass alle AUVs zyklisch ihre Position senden, zeigte sich eine Verschlechterung der Lokalisierungsqualität der Gruppe. Dieses unerwartet Ergebnis konnte auf einen Teil des DNL-Algorithmus zurück geführt werden. Da die verwendete USBL-Klasse nur die Richtung eines Signals misst, nicht jedoch die Entfernung zum Sender, wird in der DNL-Schicht eine Entfernungsschätzung vorgenommen. Wenn die Kommunikation nicht streng unidirektional ist, entsteht eine Rückkopplungsschleife, was zu fehlerhaften Entfernungsschätzungen führt. Im letzten Experiment wird gezeigt wie sich dieses Problem vermeiden lässt, mithilfe einer relativ neue USBL-Klasse, die sowohl Richtung als auch Entfernung zum Sender misst.

Die zwei wesentlichen Beiträge dieser Arbeit sind das USBL-Model zum einen und zum anderen, der neue kooperative Lokalisierungsansatz DNL. Mithilfe des Sensormodells lassen sich nicht nur Messabweichungen einer USBL-Messung bestimmen, es kann auch dazu genutzt werden, einige Fehlereinflüsse zu korrigieren. Mit DNL wurde eine skalierbare CL-Methode entwickelt, die sich gut für den den Einsatz bei

mobilen Unterwassersensornetzwerken eignet. Durch das Konzept als Zwischenschicht, lässt sich DNL einfach in bestehende Navigationslösungen integrieren, um die Langzeitstabilität der Navigation für große Verbände von tiefgetauchten Fahrzeugen zu gewährleisten. Sowohl USBL-Model als auch DNL sind dabei so ressourcenschonend, dass sie auf dem Computer eines Standard USBL laufen können, ohne die ursprüngliche Funktionalität einzuschränken, was den praktischen Einsatz zusätzlich vereinfacht.

I declare that I have developed and written the enclosed thesis completely by myself, and have not used sources or means without declaration in the text. **Karlsruhe, 25.06.2021**

. . . .

        (Sergej Neumann)

Contents

1. Introduction

1.1. Motivation

Deep-sea environments remain one of the least understood ecosystems in the world. Despite a growing interest in the treasures of the abyssal areas, scientist only begin to understand this vast space that takes up 95% of the habitable environment of our planet. These remote places can only be observed by specialized machinery that withstands the high pressure of the water column above and only few of those machines exist. Current observation methods are very limited in space and time as they often require human experts to deploy and operate the devices. Due to its vastness and inaccessibility, the deep-sea remains a mostly unknown territory that is only scarcely probed.

However, recent advancements in underwater sensor and communication technology now make it feasible to apply a system of automated robots for this task. Automated systems yield the promise to examine extensive deep-sea areas quicker and cheaper as they can be deployed in large numbers without requiring a human operator in the loop, however some technical hurdles need yet to be overcome. In order to build a reliable automated system of this kind, the robots need to form a network in which they cooperate and navigate autonomously, in depths where satellite navigation is not available. Measurements recorded by the robots can only be interpreted when the context, like the position, of the recording is known. The motivation of this work is to contribute to the solution of the localization problem with an cooperative localization scheme.

Before diving into the technical details of the problem, this section will give some insights into the possible application areas for such a automated monitoring system. Putting the technical problem into perspective of the application will help to guide the design decisions of the subsequent solution approach.

1.1.1. Deep-Sea Mining and Impact Monitoring

Polymetallic nodules, also called manganese nodules, have attracted a growing economic interest in the recent past. These are metal rich rock accretions that form at high pressures on the sea bottom at around 4000m to 6000m depth. Their composition varies from deposit to deposit and includes manganese, cobalt, nickel as well as

1

other metals and trace elements, many of which are required in hightech devices like cars, smart phones and wind turbines.

An increasing demand of those elements, has made the exploitation of those resources economically interesting. In 2010, The International Seabed Authority, which is responsible for the regulation of mining operations in international waters, has issued an report for the Clarion Clipperton Zone, one of the most attractive deposits in the pacific ocean. The report estimates that the deposit may exceed 21 billion tonnes of nodules. Later in 2016, the German Federal Institute for Geosciences and Natural Resources investigated an area of 75.000 square km in the Clarion Clipperton Zone, covered by the German license [1]. In their report, the estimated dry weight of the manganese nodules in this area amounts to 600 million tonnes.

While there is currently no complete system available to exploit those resources, a rising demand increase the incentive to develop the necessary infrastructure. In this application, the role of mobile underwater sensor networks can be twofold.

- Deposit Assessment: The the known nodule fields extend over a widespread area with varying nodule size and density. An assessment of the site can help distinguish high-yield areas from those with minor resource capacity. Current techniques can only give a rough estimate. For their estimate, the German Federal Institute for Geosciences and Natural Resources utilized box corer that where released on a cable from a ship. This approach only allows for a very sporadic probing as depicted in figure 1.1. A team of autonomous underwater vehicles, which operates close to the sea bed, could create a detailed assessment of the deposit by producing an accurate map of the nodule density in this area.

- Impact Monitoring: An important regulatory precondition for every mining operation is the monitoring of its impact on the local environment, during and after the operation. It is known that deep-sea life cycles are often much slower than those on the surface. As a result, the exploitation will have a long time effect on the deep-sea fauna [2]. It is impossible to evaluate the consequences from the surface. For this purpose, a team of autonomous underwater vehicles could monitor the impact on large scales, helping to protect that environment from overexploitation.

In both application scenarios, the potential advantages of an automated submersible fleet arise from the close proximity to the sea bed and the ability to cover a vast area through higher numbers of vehicles. The demand for a multi vehicle system that is able to monitor large deep-sea areas gave rise to the project Subsea Monitoring via Intelligent Swarms which will be discussed in the following section.
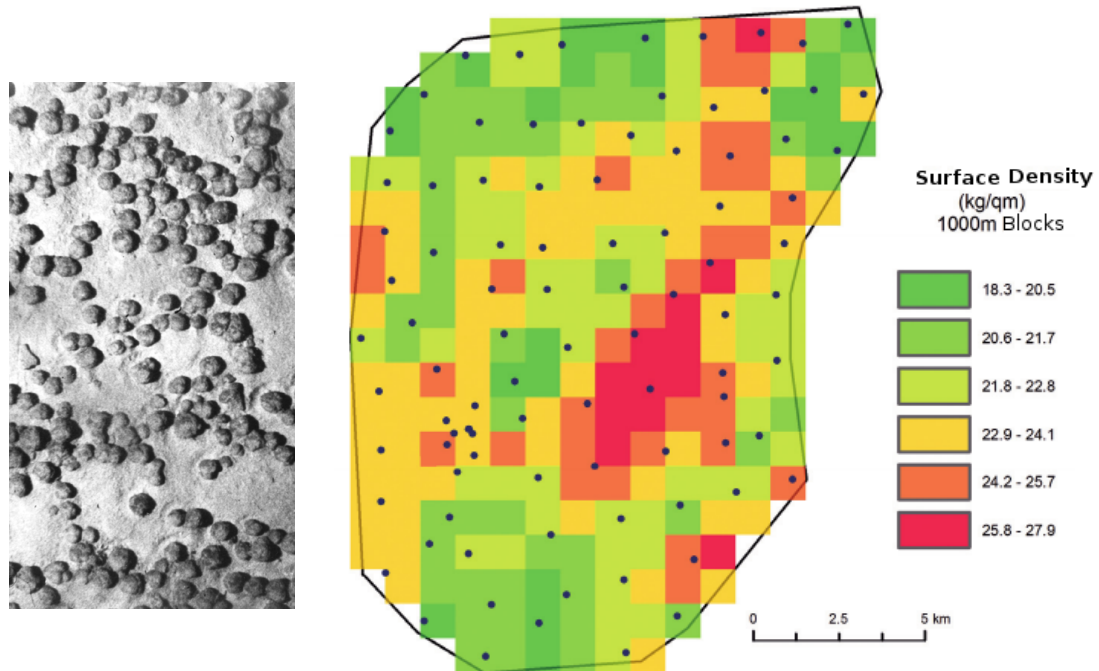
Figure 1.1.: Left: Image of manganese nodule field taken with a submersible [3]. Right: Density grid of manganese nodules in an area covered by the German licence. Grid spacing is 1.000m x 1.000m. Measurements have been made at the black dots by submerging a box corer from a vessel [1].

1.2. Subsea Monitoring via Intelligent Swarms

The research project Subsea Monitoring via Intelligent Swarms (SMIS) was founded by the German Federal Ministry of Economic Affairs and Energy in 2013. Focus of the project was to design and build a prototypic system of multiple autonomous vehicles that cooperatively monitor a large scale underwater environment in up to 6000m depth. SMIS has been proposed as a system fit for large scale monitoring tasks like the deposit assessment and impact monitoring mentioned in the previous chapter. This section will first highlight the challenges and solution approaches in this project and then introduce the research partners and their respective responsibilities.

1.2.1. Project Outline

In SMIS a team of cooperative autonomous vehicles is proposed for the task of large scale deep-sea monitoring and observation. A SMIS team consists of three different vehicle types shown in figure 1.2.
 The underwater vehicle will be supported by an unmanned surface vehicle (USV).
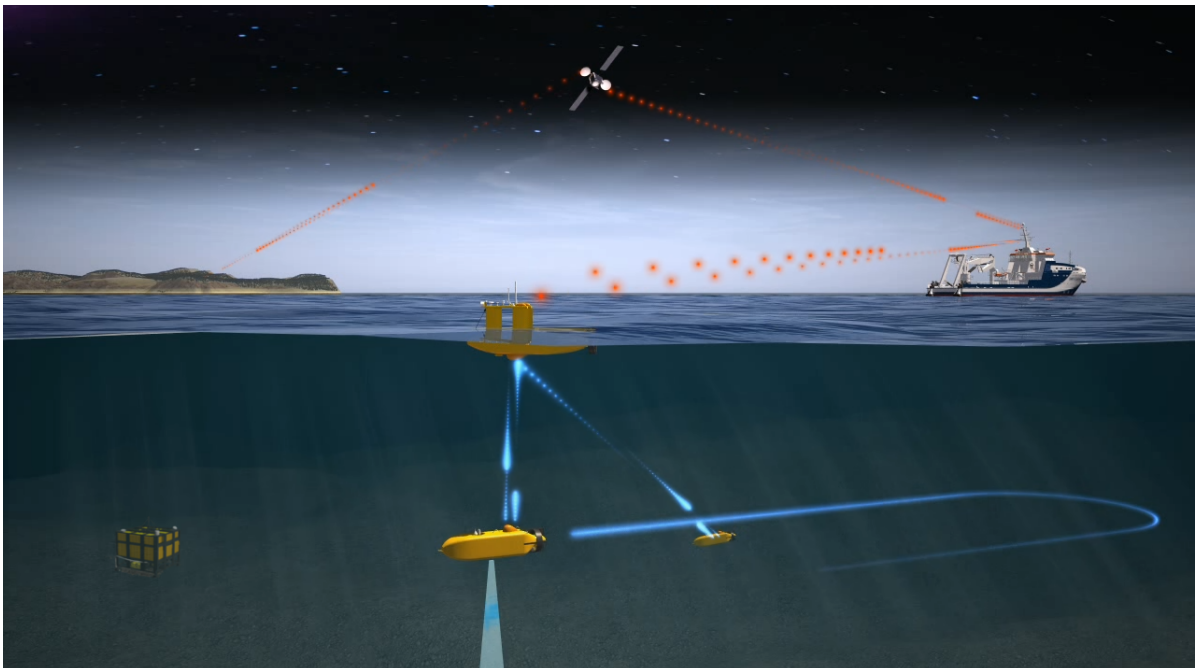
Figure 1.2.: Participants of a typical SMIS network with unmanned surface vehicle, sea-bed station and autonomous underwater vehicles. Communication with the surface vehicle is possible over a nearby research vessel or over satellite.

1. Introduction

These are small autonomous ocean going crafts that can withstand the harsh condition of the open ocean and serve as a communication relay between the underwater vehicles and the operators on the surface. The operators can communicate with the whole system over the USV from a ship in radar range or even from a land based station over satellite link. Another function of the USV is to provide geo-reference for the submersibles. Each USV is equipped with a global satellite navigation system as well as an acoustic modem for the communication with the underwater vehicles. Over the acoustic link, an USV can propagate its current global location, which can be used by the submersed vehicles to determine their own position.

The second vehicle type is the sea bed station (SBS). When deployed, the SBS passively sinks to the ground with an antecedent weight and observes the sea bottom at its landing site from several meter above the ground. If the surface is appropriate for landing, the SBS can pull itself in and attach itself to the ground with a mechanical fastening apparatus. When the current site is not suitable for landing, it can lift off with its thrusters and try at another spot nearby until it finds an appropriate landing site. Once the SBS is properly attached to the ground it uses its acoustic modem to initiate a calibration sequence with the USV on the surface. With the help of the USV, the SBS can determine its geo-position and function as another reference node for the navigation of the other underwater vehicles. Furthermore the SBS carries additional batteries that can be used to charge the other submersibles and thus extend the mission duration.

Autonomous underwater vehicle (AUV) will carry out the area-covering monitoring in relative proximity to the sea bed. They can be equipped with a range of payload sensors from sonar sensors to obtain a bathymetric map of the mission site to cameras for optical imaging and chemical sensors to measure the concentration of certain substances. Each AUV is equipped with a sensor suit for navigation and is supported by the USV and SBS with geo-reference. With its acoustic modem for inter vehicle communication, a group of AUVs can perform complex cooperative tasks and once the AUV batteries are nearly depleted it can dock at the SBS and recharge.

Once the mission is completed or all the batteries are depleted, the SBS detaches itself from the ground and floats to the surface together with the AUVs where the whole system can be retrieved by an operation vessel. On the vessel, the data can be downloaded from the vehicles for further use. According to an analysis, current monitoring systems suffer from high costs due to their dependence on the large operation vessel for the whole duration of their deployment. In SMIS an operation vessel is only required for the launch and then again at the retrieval. The SMIS system is designed to operate on a depth of up to 6000m autonomously for several days, setting the operation vessel free to perform other tasks in the meantime.

Throughout the project runtime, trials have been performed in an experimental canal in Berlin, in several lakes, the Baltic Sea and the Middle Atlantic Ocean to test different modules of the system. The final test of the SMIS system was performed in the lake constance where a team with one vehicle of each type was successfully deployed to demonstrate their interactive capabilities (see figure 1.3).

Figure 1.3.: SMIS vehicles during the final tests in lake constance.
Left AUV, center USV, right SBS

1.2.2. Project Partners

SMIS was proposed and carried out by a team of research partners from industry and academia. In alphabetical order those are:

- Energietechnik-Elektronik GmbH (ENI)
- IMPaC Offshore Engineering GmbH (IMP)
- Karlsruhe Institute of Technology (KIT)
- Leibniz-Institute for Baltic Sea Research, Warnemuende (IOW)
- Technical University of Berlin (TUB)
- University of Rostock (URO)

With their experience from previous research projects in the field, ENI was responsible for the energy management of all vehicles as they provided the pressure neutral electronics, batteries and battery management systems. Furthermore they were in charge of constructing and equipping two AUVs for the SMIS system.

IMP took over the project coordination and with their long expertise in the offshore business they helped to assemble an advisory board with many experts from the field. In addition IMP provided helpful fluid dynamics analysis for all vehicles.

With their background in multi robot systems, KIT was tasked with the navigation, communication and cooperation of the SMIS vehicles. In order to test the software independently from the actual vehicles, the creation of a simulator was also part of the project specifications.

As a marine research institute, IOW defined the scientific goals of the sea trials and was responsible for the scientific staff on-board the research vessels. Furthermore

IOW organized ship times for offshore experiments and the transport of equipment to the target harbours.

TUB has a long experience in naval architecture and ocean engineering and thus supported the construction of all SMIS vehicles with their practical expertise. Furthermore TUB was tasked with the construction of a SBS. Due to the special requirements, the design of the SBS yields several novelties like the attachment system, the variable ballast system and passive landing system that have been well documented in [4], [5]. As an institute for naval architecture they also provided an experimental station where the vehicles could be tested.

With their expertise in control theory for naval systems, URO was in charge of the low level control of the SMIS vehicles. In cooperation with TUB they also designed and constructed the ocean going USV which can supports the submerged SMIS vehicles with geo-reference and function as a communication relay with the operator. In their publications [6], [7] the authors elaborate on the design process of the sophisticate unmanned surface craft.

Throughout the project duration, the SMIS team has been in close exchange with possible users of this technology from industry and academia, to align the design process on their practical needs. These inputs have contributed greatly to steer the development of the project toward the successful and well thought out SMIS system design.

2. Fundamentals

Cooperative localization can be seen as an extension to single agent navigation. Therefore, it is important to understand the restrictions of the available navigation technologies and the impact they might have on a cooperative localization solution. This chapter will introduce some of the basic principles that are required to understand underwater navigation in general. Based on the foundation laid out here, cooperative localization will be discussed in the next chapter. The first section of this chapter covers the sensor equipment that is commonly used for underwater localization tasks and outlines the measurement principles as well as typical error bounds and limitations. In the second section the theoretical foundations and some variations of two of the most popular sensor fusion techniques will be presented. The fusion techniques mentioned here will later be used to integrate a single agent navigation with the cooperative localization approach that was developed in this work.

2.1. Underwater Localization Techniques

Most applications for underwater sensor networks require knowledge of the sensors position, since the location of sensed data is necessary for a meaningful interpretation of the measurements. Mobile nodes like AUVs need to navigate in the water and thus need to know their pose continuously and accurately.

Nowadays many AUVs apply a mix of proprioceptive sensors that measure the vehicles internal properties like velocity, turn rate and orientation in combination with an exteroceptive system which provides a global reference at a lower rate. The proprioceptive sensors are used to calculate the current vehicle state based on the previous determined positions and integration of the measured velocity and orientation over time, this is known as dead reckoning (DR). A common implementation for DR in AUVs uses a combination of an Inertial Navigation System (INS) and a Doppler Velocity Log (DVL). Independently of the quality of the sensors used, the error in the position estimate based on dead-reckoning information grows without bound [8]. Navigation errors based on such a dead-reckoning solution depend on the quality of the INS and are usually stated in relation to the distance travelled. Typical middle-class INS reach errors between 0.5% and 2% while expensive high-class INS can approach navigation errors of around 0.1% of distance travelled. Nevertheless the position estimation error grows over time and needs to be bounded by periodic global references. On the surface, AUVs can incorporate Global Navigation Satellite Systems to fix their

position estimate, however surfacing is impossible (beneath ice) or unacceptable for many applications. Because of the channel properties of water, the most feasible solution for exteroceptive underwater localization is based on acoustics [9].

In the remainder of this section, we will first examine common navigation sensors in more detail and then give an introduction to the acoustic localization techniques that are available.

2.1.1. Common Underwater Navigation Sensors

This section gives an overview of common available sensor systems that are used for the navigation of mobile underwater vehicle. Since AUVs are deployed in a wide range of deep and shallow water environments, the combination of equipped sensors may vary from mission to mission. However, most AUVs will use a subset of the sensor systems listed in this section.

2.1.1.1. Global Navigation Satellite System

Global Navigation Satellite Systems (GNSS) have become the dominating technology when it comes to outdoor localization. They offer a very high precision of less than one meter when supported by reference stations on the ground. On the open oceans however, there are often no reference stations in range so that the achievable precision drops to several dozen meters, which is still sufficient for most navigation applications on water. Currently there are three GNSS with a global coverage, which are the Unitet States' GPS, the Russian GLONASS and the European Galileo. The Chinese BeiDou system will reach global coverage in 2020.

With precision ranges from $15m$ (GPS without reference stations) to one meter (Galileo) they already have good individual performances. New GNSS sensors can further enhance the precision by combining satellites from different systems. Li et al. [10] analysed the combination of GPS, GLONASS, Galileo and BeiDou to get a sub meter accuracy for GNSS only localization. While GNSS yield excellent performances, they can only be used on the surface.

2.1.1.2. Inertial Measurement Unit

Inertial Measurement Units (IMU) have become a wide spread technology that has found its way into our daily live with applications in many sectors, from entertainment to robotics and spacecraft navigation. An IMU measures the acceleration and the turn rate applied to the sensor frame and often also outputs an orientation estimate. In a Micro Electro Mechanical Systems (MEMS) base IMU this is typically done by a set-up of three accelerometers and three gyroscopes which are aligned on the orthogonal sensor axis (see fig.2.1). Sometimes also magnetometers are integrated to
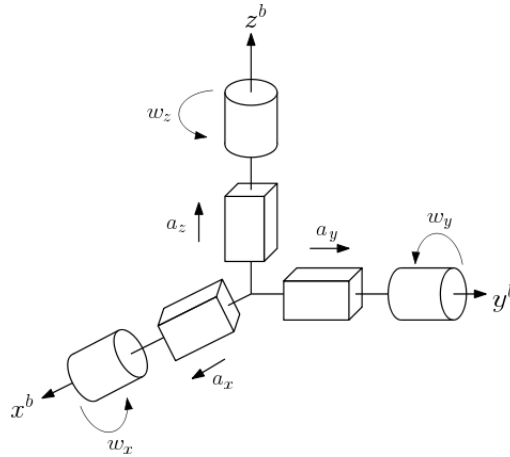
Figure 2.1.: MEMS based IMU frame with three gyroscopes and three accelerometers aligned to the x, y and z axis of the sensor.

measure the surrounding magnetic field.

Gyroscopes measure the angular rotation rate which is the change of orientation over time. By integrating the measurements it is possible to determine the orientation of the sensor. Since measurements are intrinsically noisy, the orientation estimation error will grow over time. There are many different measuring principles for gyroscopes and the quality of an IMU largely depends on the quality of its gyroscope. While MEMS based gyroscopes are cheap in production, they suffer from a bigger measurement noise which leads to a faster growing error in the orientation estimate. Optical gyroscopes on the other hand can be very precise but are also much more expensive. Both gyroscope types will experience an additional offset that is caused by the Coriolis force of earth rotation. With knowledge of the global position, this offset can be corrected however.

Accelerometer based on MEMS commonly have a proof mass that is placed between two parallel plates and held by a ring frame. When acceleration is applied, the proof mass moves between the plates, creating a change in capacitance which is proportional to the acceleration. During acceleration free periods the sensor will still measure the Earth's gravitational acceleration. This can be used to determine if the IMU is in an upright position and provides to possibility to correct the tilt (roll and pitch). In practice, it is not trivial to accurately differentiate between gravitational acceleration and body acceleration. Especially during transient accelerations the influence of gravity can be hard to distinguish which leads to errors in the roll and pitch estimations.

Magnetometers measure the surrounding magnetic field. In IMU settings they are

US/UK World Magnetic Model -- Epoch 2010.0
Main Field Declination (D)
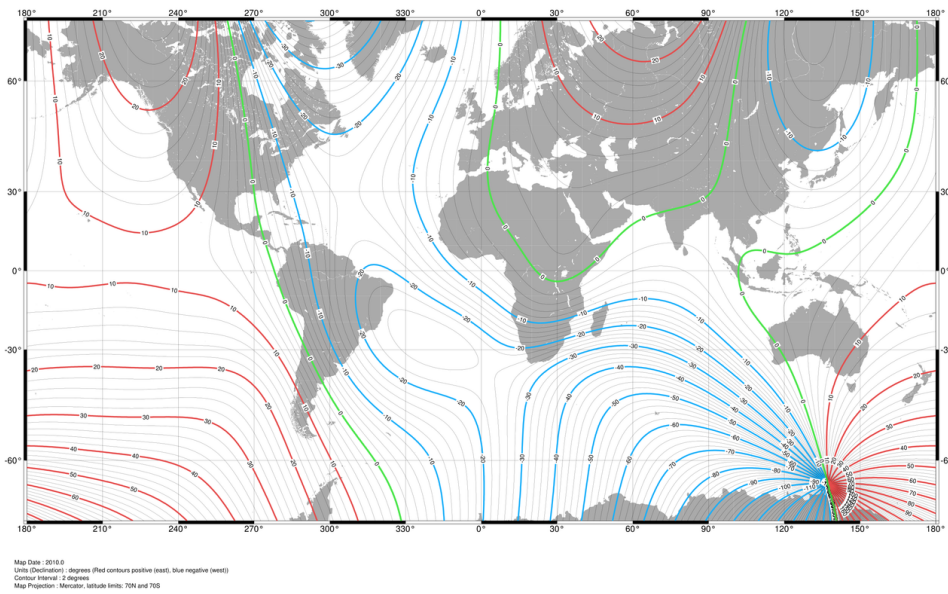
Figure 2.2.: World map of magnetic declination from the year 2010.

mostly used like a compass to detect the magnetic north in order to bind the heading error of the drifting gyroscope estimation. In practice, magnetometers are subject to many distortions. The earth magnetic field is altered by ferromagnetic materials, permanent magnets or strong currents of several amperes. When the magnetometer is placed close to an object that produces such distortions, the error in heading can become quite large. In AUVs, magnetic distortions can be caused by thrusters, power electronics and ferromagnetic material in the vehicle structure. By careful calibration, these influences can be filtered out to a large extent.

Another error source is the magnetic declination, which is the misalignment between the geographic north and the magnetic north (see Fig. 2.2). Earth's magnetic field is drifting constantly and this will also affect the measurements of a magnetometer. By consulting an up to date declination map and knowledge of the global position, the declination error can be corrected.

2.1.1.3. Pressure Sensor

Pressure sensors belong to the basic equipment in many maritime devices. Due to the relative incompressibility of water they can determine the depth reliably to several centimetres which is sufficient for most underwater navigation scenarios. Hence, most underwater positioning schemes can be reduced to a 2D problem by equipping a relatively inexpensive and small pressure sensor.

Pressure in water can be obtained by

$$P = \rho g h \tag{2.1}$$

where ρ is the density of the fluid, g is the gravity and h is the depth. Density varies between sea water and sweet water, gravity also differs slightly from region to region. A common way to measure the pressure in a fluid is to use a strain-gauge. Here the ambient-temperature may effect the accuracy because the measuring components are thermally connected [11]. Modern sensors already apply a temperature correction on-board for their specified temperature range.

2.1.1.4. Doppler Velocity Log

Doppler Velocity Logs (DVL) are acoustic sensors that utilize the Doppler effect to measure the velocity over ground as well as the distance to the ground. They are a cornerstone of underwater navigation and almost all AUV systems comprise a DVL in their localization solution. In order to work, a DVL must be in range to the ground. The maximum range can vary between $10m$ and $1000m$, depending on the utilized frequency band, whereby an increased range also means an increased size, weight and power consumption of the sensor. DVLs make use of multiple piezoelectric transducers that can transmit and receive sound signals. The travel time of a signal reflection gives the distance to ground while the frequency shift of an echo is proportional to the velocity over ground. In order to measure a 3D velocity, three or more transducers are required. Transducers are usually tilted so that their beams are pointing in different directions to cover all three axis (see fig. 2.3). Since the sensor requires an echo from the ground, ragged surfaces can lead to errors or absence of measurements when the reflected signal is redirected and misses the sensor. The same problem can occur at steeper slopes and cliffs.

2.1.1.5. Imaging Sonar

Acoustic imaging sensors like side-scan or multi-beam sonar are commonly seen as payload sensors in underwater vehicles. They have rarely been used for navigation until the breakthrough of simultaneous localization and mapping (SLAM) at the beginning of the century. SLAM has demonstrated to provide great accuracies in the terrestrial sector, where it is used in navigation for drones and self driving cars. Recent work in underwater SLAM shows that this class of algorithms can also be applied for acoustic imaging, where images are effected by high noise and acoustic distortions [12]. The required computational capacities of SLAM increase with the surveyed area, which often makes it impractical for large scale monitoring. Improvements in the acoustic image processing, as well as optimizations of the computational cost and the rise in computational power have lately led to promising solutions in this area of research [13].
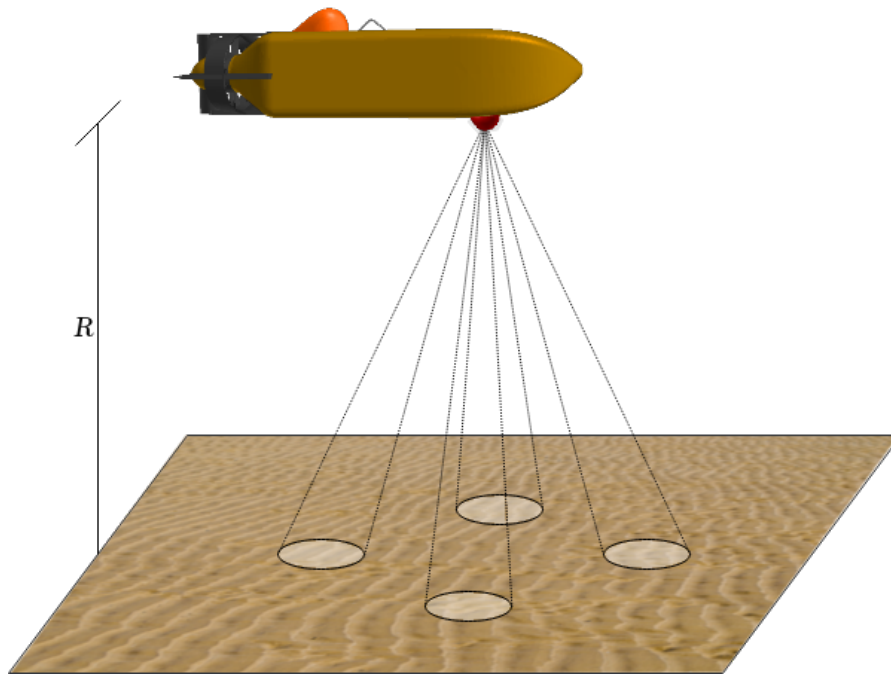
Figure 2.3.: DVL with four beams that are tilted at 30 degree to the vertical axis.

2.1.1.6. Optical Sensors

Optical imaging sensors like video cameras belong to the standard equipment for Remotely Operated Vehicle (ROV), where it can also be used in combination with SLAM for navigational purposes [14]. ROVs are usually connected with a tether to a ship, which provides the vehicle with power and a high bandwidth data link, so that the computational heavy SLAM can run on potent machines at the ship. For AUVs, optical sensors are mostly applied in shallow water, where sunlight provides the required illumination. In deep-sea scenarios optical sensors are not so widely used because of the absence of natural light and the high energy consumption that is required for the artificial illumination. Furthermore, turbidity may limit the range of view and render optical sensors mostly impractical for deep-sea navigation.

2.1.2. Acoustic Localization Systems

Acoustic localization systems are the backbone of AUV navigation. In absence of satellite navigation underwater, they can provide the vitally needed geographic references for the underwater vehicles over long distances. The basic principle of acoustic underwater localization is to measure the relative position to one or more reference transponders. Commercial systems can be broadly categorized by the baseline length between theses reference transponders into Long-Baseline (LBL), Short-Baseline (SBL) and Ultra-Short-Baseline (USBL) [15]. This section will first describe

| Long Base Line | Short Base Line | Ultra Short Base Line |
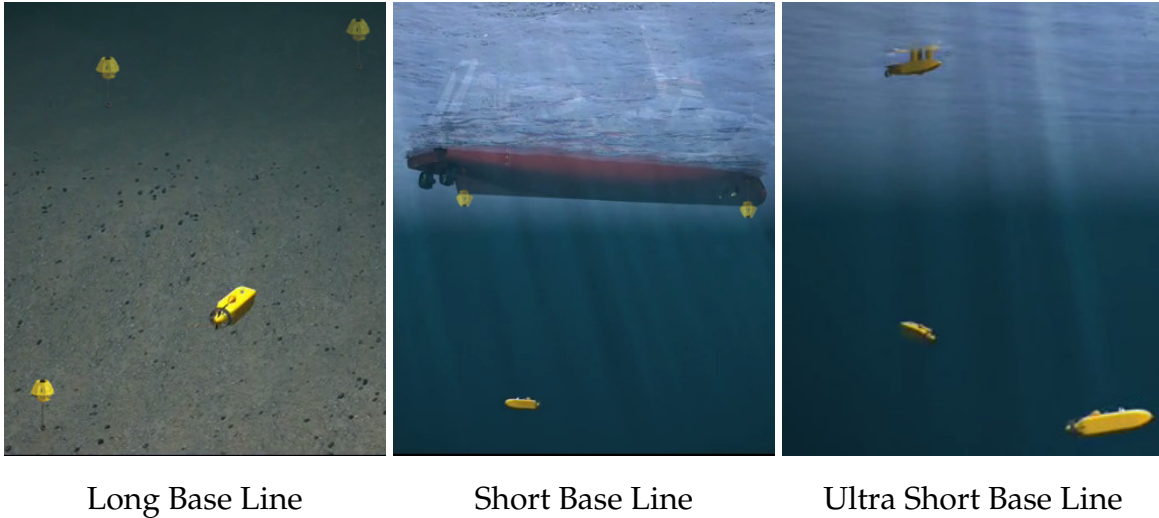
Figure 2.4.: Illustration of acoustic localization systems divided by the base line they use.

Table 2.1.: Acoustic localization systems categorized by their baseline.

System Type	Baseline Length
Long Baseline (LBL)	$50m \sim 6000m$
Short Baseline (SBL)	$10m \sim 50m$
Ultra Short Baseline (USBL)	$< 20cm$

the working principles of each type and then outline some issues that are common in acoustic underwater localization.

2.1.2.1. Long Baseline

In LBL systems the localization of a target vehicle is achieved by measuring the distances between vehicle and multiple static nodes, called anchor nodes, that need to be deployed at the sea floor of the working site. The spacing between anchor nodes is usually $50m \sim 2000m$ and their position needs to be known precisely. A transceiver is mounted on the vehicle and the anchor nodes are equipped with transponders. Now the target vehicle sends a ping to each transponder. Upon reception of the ping, each transponder will reply with an acknowledgement signal which will be received by the target. The target measures the round trip time (RTT) between sending the ping and receiving the acknowledgement. By knowledge of the sound velocity at the site and the RTT it is possible to determine the distance between the target and a transponder. Once the distances to all transponders have been obtained, the point where all distances intersect can be computed, either by trilateration ((see fig. **??**) or by the hyperbola curves method [16] (see fig. **??**). The determined point is the position of the target. Depending on the operating frequency LBL systems have good
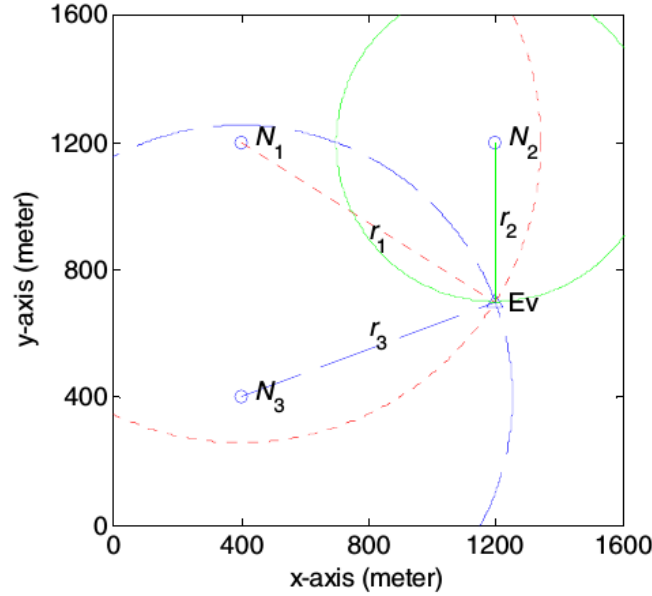
The location of an event Ev can be determined by trilateralation if at least three nodes N have a range measurement r to the event by finding the intersection point of three circles, where the center of the circles is at the position of the nodes and the radii correspond to the respective range measurements to the event [16].
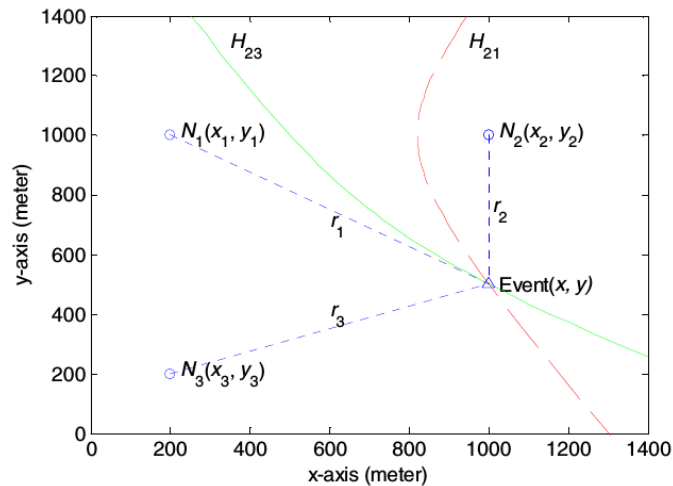
As with trilateration the hyperbola curve method requires range measurements r from at least three nodes N to identify the location of an event. Instead of circle intersections the method utilizes hyperbola curves intersection to identify the position of the event where each curve is a function of two node positions and their respective range measurements to the event [16].

precision abilities with an absolute position accuracy from $5m$ of up to $0.05m$. Higher frequencies result in better accuracy for the cost of limited range.

2.1.2.2. Short Baseline

Short Baseline systems can be applied when a submersible target needs to be located in respect to a ship or a surface platform. Here three or more transceivers are installed at the surface platform or the ship while the submersible is equipped with a transponder. One of the transceivers sends a ping and the transponder responds with an acknowledgement, which is in turn received by all transceivers. Like in LBL, the range from the target to each transceiver is used to compute the targets position. It is to mention that the approach is not suitable for AUV navigation in this form, since the position information is only present at the ship/surface platform and not on the vehicle, where it is needed. Also the localization accuracy improves with the distance between the transceivers. This means that SBL can have poor results on small ships/platforms, however this method does not require the deployment of anchor nodes like in the LBL approach. Since the ship or surface platform is in constant movement, the transducers position and orientation will be subject to variations. This needs to be corrected with additional sensors like GNSS and IMU in order to obtain a reliable global position estimate.

2.1.2.3. Ultra Short Baseline

In Ultra Short Baseline systems, an array of transceiver hydrophones is arranged in a small space with a baseline length of less than $20cm$. By measuring the Time Difference of Arrival (TDOA) at hydrophone pairs the Direction of Arrival (DoA) of an incoming acoustic signal can be determined with $\vec{z}_{DoA}$ as an unit vector pointing to the source of the incoming signal. Often the direction is expressed in spherical coordinates as azimuth angle θ and elevation angle φ. In this form it is called Angle of Arrival (AoA). As in LBL and SBL the range to the source can be obtained by the round trip time, resulting in a measurement of the relative position to the source. Because of the compact size, USBL does not require large ships or surface platforms but can operate on small vehicles as well. This enables applications in mobile underwater networks, where several vehicle need to be located. In such scenarios each target can be equipped with an USBL sensor to measure the relative position to other network nodes and update their own localization accordingly.

An important assumption is that the incoming acoustic wave front is planar at the transceiver array (see fig.2.5). This allows for the simple translation from the time differences measured by the hydrophones to the direction of arrival, utilizing knowledge about the sound speed and the hydrophone positions in the sensor frame. The planar wave approximation leads to a minor systematic error. However an analysis has shown that this error can be neglected [17]. A major drawback of USBL systems is that their precision decreases with the distance to the source and is therefore usually denoted as percentage of slant range. Furthermore, the transceivers configuration has a big influence on the performance. For 3D positioning at least four transceiver are required. Sometimes the exact sound speed at the transceivers is unknown which
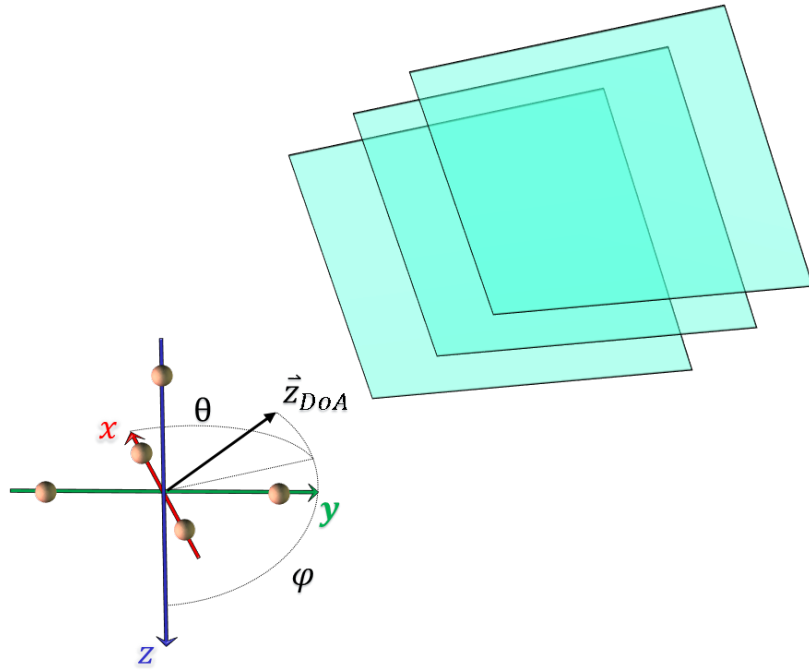
Figure 2.5.: Planar wave front approaching hydrophone array of a USBL sensor. The direction of the wave front will be measured by comparing the time difference at which the front will arrive at the hydrophones (spheres).

will result in an erroneous direction estimate. This can be dealt with by employing a configuration of at least five hydrophones which makes the AoA calculation over-determined so that the sound velocity can be excluded. The resolution of the AoA is mainly given by the clock resolution of the signal processing computer, since this limits the TDOA measurements. A typical clock resolution of one nanosecond together with a baseline length between $10cm$ and $20cm$ will therefore result in a AoA resolution of roughly $0.1 - 0.2$ degrees, also depending on the hydrophone configuration. When putting the angle resolution into relation to the slant range, this translates to a position resolution of $0.17\% - 0.35\%$ of the slant range. This value is often stated as the accuracy in the specifications of USBL systems, although it can not represent the actual localization performance. In reality, USBL measurements can be strongly distorted by the medium and it is necessary to distinguish between different types of accuracy. The following section will capture some of the issues.

2.1.2.4. Common Issues

Acoustic localization systems are associated with some major challenges regarding positioning accuracy and system complexity. The inhomogeneity of the acoustic underwater channel introduces performance impairing phenomena that are hard to predict and model like refraction effects due to sound velocity variation and multipath

propagation.

Sound velocity in water is a function of salinity, temperature and depth and changes throughout the water column and also differs from one body of water to another. Hence the signal path of an acoustic signal is not linear but undergoes refraction and sometimes even gets reflected due to thermoclines in the water. Most underwater acoustic localization techniques use time-of-flight measurements to compute distances based on the sound velocity. The time-of-flight is often determined by the round-trip-time (RTT) of an acoustic signal. This RTT is measured by a sender and describes the time that passes between the emission of a signal and the reception of an acknowledgement from the targeted node. When exact time synchronization between the nodes can be established (e.g. by atomic clocks [18]) the two way communication can be replaced by a single transmission. In this case the one-way-travel-time (OWTT) to the sender can be measured by every node that overhears a transmission. In both cases refraction effects will impair the distance measurements as the real distance is shorter than the curved travel path of the signal. Also the direction estimate in USBL is affected by refraction since the signal will arrive from a different angle at the hydrophone array. To cope with this error an up to date sound velocity profile of the current working site can be used in combination with a sophisticated acoustic channel model. In many cases however, a sound velocity profile is not always available and sensors will simply assume a constant sound velocity.

Another factor that is impairing underwater localization is multipath propagation. Reflections from the water surface, the bottom or any other flat object that is big enough can cause echoes that arrive at the transmitters at different times and angles. Because of the strong coherency, multipath interference with the direct signal path can even cause total destructive interference. Multipath arrivals can produce localization outliers that are persistent for that specific location which makes them hard to predict and detect.

Acoustic sensors are naturally affected by acoustic noise. Often a certain amount of background noise can not be avoided, e.g. noise from wind and waves or ship motors in a harbour environment and a high signal loss can be the result. All these factors make the performance of an acoustic localization difficult to characterize as it is highly dependent on the technology used and the circumstances in which it will be applied.

2.2. Sensor Fusion Algorithms

Each sensor mentioned in the previous section, measures a part of a nodes state and has its own advantages and drawbacks. In order to obtain an exhaustive picture of the node, sensor fusion algorithms can be used to consolidate many different information sources into one state estimation that is more robust and complete than each sensor separately. This Section gives an introduction to some of the most popular techniques for sensor fusion which have been used in this work.

2.2.1. Kalman Filter

The Kalman filter is widely used in navigation and control applications. It was first published in 1960 by Rudolf E. Kalman and has been used in numerous real world applications like the control system of the Apollo space craft and many others. It belongs to the family of Bayesian inference filters, which use the Bayes theorem to evaluate the probability of a hypothesis whenever new informations are available. So the Kalman filter does not only estimate a state but also gives a measure of how probable this estimate is believed to be. Unlike traditional filter for time-series analysis it distinguishes between the dynamic of the system state and the action of measuring it.

States are usually described by a multidimensional state vector X_k that hold all the important information of the system at a time t_k. The transition of the state from time t_{k-1} to $t_k = t_{k-1} + \Delta t$ is modelled as a time discrete linear difference equation, the state transition model

$$X_k = F_{k-1}X_{k-1} + B_{k-1}u_{k-1} + w_{k-1} \tag{2.2}$$

where F_{k-1} describes the transition from a prior state to the new one. Additionally the equation describes external influences on the state with the remaining terms. B_{k-1} is the control-input model which describes how the control input vector u_{k-1} affects the state and w_{k-1} is the process noise which describes natural noise in the system and is usually assumed to be white Gaussian noise with zero mean $w_k \sim \mathcal{N}(0, Q_k)$. Similarly observations Z_k of the state are modelled by

$$Z_k = H_k X_k + v_k \tag{2.3}$$

with H_k describing how the real state X_k gets observed and the observation noise vector with observation covariance R_k in the form $v_k \sim \mathcal{N}(0, R_k)$. Since the state transition model and the observation model depend only on the last state and the input values and both contain stochastic parts this is a special stochastic process known as hidden Markov model.

The aim of the Kalman filter is now to estimate the most probable state $\hat{x}_k$ and its covariance $\hat{P}_k$ as $\hat{X}_k \sim \mathcal{N}(\hat{x}_k, \hat{P}_k)$ based solely on the last state prediction as well as current observations. The prediction can be written as

$$\hat{x}_{k|k-1} = F_{k-1}\hat{x}_{k-1} + B_{k-1}u_{k-1} \tag{2.4}$$

and

$$\hat{P}_{k|k-1} = F_{k-1}\hat{P}_{k-1}F_{k-1}^T + Q_{k-1} \tag{2.5}$$

where Q_{k-1} is the covariance matrix of the process noise. In a second step the prediction, which in Bayes terms is an a priory estimation of the state, gets corrected by the observations to receive an a posteriori state estimation with

$$\hat{x}_k = \hat{x}_{k|k-1} + K_k\tilde{y}_k \tag{2.6}$$

$$\hat{P}_k = \hat{P}_{k|k-1} - K_k S_k K_k^T \tag{2.7}$$

Here $\tilde{y}_k$ is called the innovation and describes how good the predicted state vector matches with the observations. A big innovation indicates that the prediction does not closely represent the observed state while a small innovation means that prediction and observation are in accordance. The size of the innovation and the innovation covariance S_k is proportional to the correction that is applied to the prediction state.

$$\tilde{y}_k = z_k - H_k \hat{x}_{k|k-1} \tag{2.8}$$

$$S_k = H_k \hat{P}_{k|k-1} H_k^T + R_k \tag{2.9}$$

K_k is called the Kalman gain and, in simple terms, describes the ratio between the uncertainty of the prediction and the uncertainty of the observation.

$$K_k = \hat{P}_{k|k-1} H_k^T S_k^{-1} = \hat{P}_k H_k^T R_k^{-1} \tag{2.10}$$

The Kalman filter is a consistent and optimal linear filter because it will converge to the real mean and variance when the models are correct. However, the assumption of a linear system does not represent many real world applications. Also the noise in numerous operations is not adequately described by the assumed Gaussian distribution. Several advancements have been proposed for the original Kalman filter that try to overcome these limitations. Two of the most common adoptions are the Extended Kalman filter (EKF) and the Unscented Kalman (UKF) filter.

2.2.1.1. Extended Kalman Filter

In EKF the linear state transition F_k and the observation model H_k are replaced by non-linear functions f and h. While the functions can be used to estimate the state it is not possible to apply the covariance through the function directly. Instead a partial derivative of the covariance, the Jacobian, is computed at every time step and applied to evaluate the state estimate. The result of this procedure corresponds to a linearisation around the current state estimate. A well known drawback of EKF is its performance with highly non-linear functions where the linearisation leads to incorrect probability distributions.

2.2.1.2. Unscented Kalman Filter

Where EKF handles non-linearities with an analytic approach, the unscented Kalman filter applies a stochastic technique known as unscented transformation described in [19]. Here a set of so called sigma points are defined around the mean of the estimate. These sigma points are selected in a way that represents the covariance before the non-linear transformation. Now the mean and the sigma points are propagated through the non-linear functions f and h respectively. From the resulting points a

new estimation and covariance is formed. UKF has the advantage that the Jacobian does not need to be computed. The Jacobian can be hard to derive in complex cases or even impossible if the function is not differentiable.

For the unscented transformation the first step is to select a set of $2M+1$ sigma points $s_i = \{\tilde{x}_i, w_i\}$ with the rules

$$\tilde{x}_0 = \hat{x} \qquad\qquad w_0 = 1 - \frac{M}{c} \qquad\qquad i = 0 \qquad (2.11)$$

$$\tilde{x}_i = \hat{x} + \Delta x_i \qquad\qquad w_i = \frac{M}{2c} \qquad\qquad i = 1, ..., 2M \qquad (2.12)$$

$$\Delta x_i = (\sqrt{c\hat{P}_x})_i \qquad\qquad\qquad i = 1, ..., M \qquad (2.13)$$

$$\Delta x_{M+i} = -(\sqrt{c\hat{P}_x})_i \qquad\qquad\qquad i = 1, ..., M \qquad (2.14)$$

where M is the dimension of the state vector and c is a scaling factor. $\sqrt{c\hat{P}_x}$ is the matrix square root of the scaled covariance matrix $\hat{P}_x$ and $(\sqrt{c\hat{P}_x})_i$ is the ith column of $\sqrt{c\hat{P}_x}$. That way the sigma points represent the mean and covariance of the state estimate without the covariance matrix $\hat{P}_x$ that is difficult to pass through a non-linear function f. After propagating the sigma points through the non-linear function by

$$\tilde{y}_i = f(\tilde{x}_i) \qquad (2.15)$$

we can now compute the mean and covariance after the non-linear transform by

$$\hat{y} = \sum_{i=0}^{2M} w_i \tilde{y}_i \qquad (2.16)$$

$$\hat{P}_y = \sum_{i=0}^{2M} w_i (\tilde{y}_i - \hat{y})(\tilde{y}_i - \hat{y})^T \qquad (2.17)$$

The UKF has been applied to many recent non-linear problems and is considered to achieve consistently better performances than the EKF [20]. However, it still assumes Gaussian probability distribution which is not given for all applications. A filter strategy that does not rely on this assumption and has gained much attention in the last decade is the particle filter, which will be presented in the next section.

2.2.1.3. Covariance intersection

Besides Gaussian distributed probabilities and linear systems, the original Kalman filter, as explained above, makes another assumption that is not always true. When fusing the uncertainties of prediction $\hat{P}_{k|k-1}$ and observation R_k, the covariance matrices are assumed to have no cross-correlation. While this assumption is often true when the observation is made by a sensor, the observation can also originate from
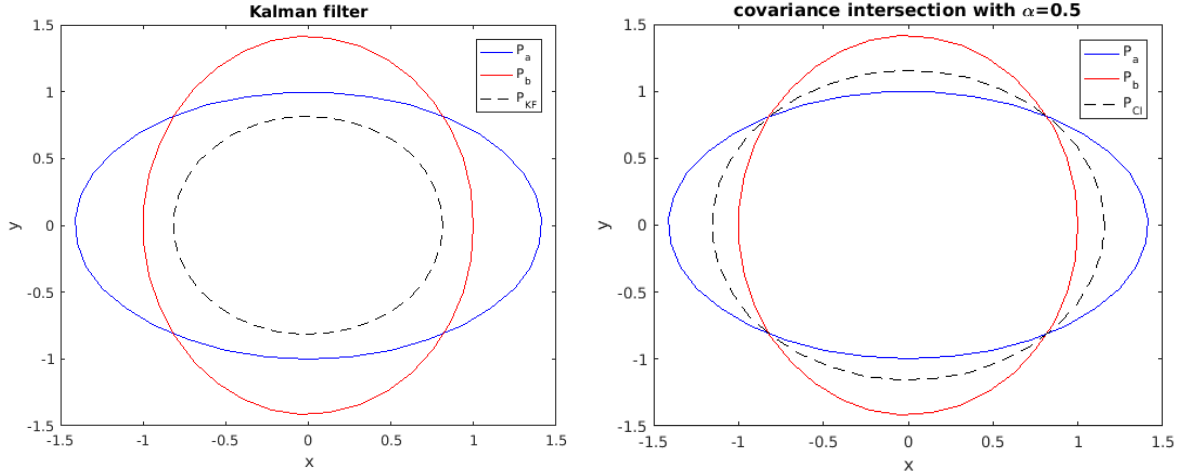
Figure 2.6.: Example of covariance fusion with Kalman filter (left) and covariance intersection (right). The covariance estimation of the kalman filter P_{KF} is smaller but does not include the whole area of intersection between P_A and P_B while the CI estimation P_{CI} does include the whole intersection region and is also guaranteed to produce a consistent estimate.

another filter that incorporates the current state estimate and possibly some sensor information. In that case, there is a cross-correlation which is not accounted for by the standard Kalman filter and is often hard to identify.

Covariance Intersection (CI) can be used in place of the conventional Kalman update to ensure that the merged covariance includes any possible but unknown cross-correlations between the two estimates that are fused. It does so by introducing a scaling parameter α to the Kalman Gain

$$K_{CI} = \alpha \hat{P}_{k|k-1} H_k^T (\alpha H_k \hat{P}_{k|k-1} H_k^T + (1-\alpha) R_k)^{-1} \tag{2.18}$$

The merged mean and covariance are then computed with

$$\hat{P}_k = (1-\alpha)^{-1} \hat{P}_{k|k-1} - K_{CI} H R_k \tag{2.19}$$

$$\hat{x}_k = \hat{x}_{k|k-1} + K_{CI} \tilde{y}_k \tag{2.20}$$

Figure 2.6 illustrates the differences between the original Kalman update and the covariance intersection method. The KF solution produces a smaller covariance estimation that does not include the whole intersection between both estimates. A CI solution on the other hand does include the whole intersection region and is also guaranteed to produce a consistent estimate where the fused accuracy outperforms each separate estimate.

2.2.2. Particle Filter

With the recent advancements in processing power a rise in simulation based approaches for non linear filter problems could be observed. Particle Filter (PF) also known as Sequential Monte Carlo (SMC) methods, belong to this kind of stochastic filters. Like in the Kalman filter, PF assumes that the system can be described as a Markov process where the hidden system state X_k is recursively determined by the last state X_{k-1} and an observation process Y_k, starting with a known initial state X_0. While the KF works with a single estimated mean value and the corresponding covariance, PF applies a swarm of so called particles, where each particle represents a weighted estimation in the state space. The resulting mean and covariance can now be drawn from the distributed particles. This approach has the advantage that the particle swarm can represent complex probability density functions with multiple clusters instead of the single Gaussian distribution assumed in KF. Furthermore it can be applied to highly non-linear functions since only the particles need to be propagated through the transfer function and the covariance is drawn form the particles themselves. Although the principle idea of sequential Monte Carlo filtering was already introduced in the 1950s, a lack of computation power and problems with degeneracy at that time have made it impractical. SMC reappeared in the 1990s when the performance was improved by methods like the bootstrap filter [21] as well as better sampling algorithms like the sequential importance sampling and sampling importance resampling [22]. After outlining the general idea of the particle filter, the working principles will be discussed in more detail.

The particle filter aims to estimate the state X_k and the posterior density of the state variables $p(x_k|y_{1:k})$ given the values of the observation process $Y_{1:k}$. For this purpose, a set of N weighted samples, the so-called particles labelled as $\{\hat{\xi}_k^i : i \in \{1, ..., N\}\}$, are drawn from the posterior distribution. Each particle consists of a state estimate and the corresponding weight $\{\hat{x}_k^{(i)}, w_k^{(i)}\}$. The posterior distribution can be described as

$$\hat{p}(x_k|y_{1:k}) = \frac{1}{N} \sum_{i=1}^{N} \delta_{\hat{\xi}_k^i}(x_k) \tag{2.21}$$

where $\delta(d)$ denotes the Dirac measure function. Assume $h(x)$ an observation function of x. The expected value of $h(x)$ can be approximated as a discrete sum using Equation 2.21

$$\mathbb{E}(h(x_k)) = \frac{1}{N} \sum_{i=1}^{N} h(\hat{\xi}_k^i) \tag{2.22}$$

In order for the approximation to hold, the drawn particles are assumed to be independent and identically distributed. In other words, by drawing a sufficient finite number of samples from the posterior distribution, the expected value of a random variable can be approximated.

The expectation $\mathbb{E}(h(x_k))$ can be approximated by the sampling method shown above. However, it is not always possible to directly sample from the posterior distribution

function, as it is often unknown. This problem can be avoided by choosing an appropriate known distribution, the so-called proposal distribution $q(x_k|y_{1:k})$ and using it for the sampling instead of the posterior distribution. The proposal distribution can be approximated by the weights of each particle, which is known as importance sampling. By employing the Bayes theorem we get the conditional probability of observing the true value given the proposal probability

$$w_k = \frac{p(y_{1:k}|x_k)p(x_k)}{q(x_k|y_{1:k})} \tag{2.23}$$

We call w_k the importance weight. The expected value can now be approximated, even without the knowledge of the posterior distribution of the random variable. After normalizing the importance weights, the following equation can be deduced:

$$\mathbb{E}(h(x_k)) = \sum_{i=1}^{N} h(\hat{\xi}_k^i)\tilde{w}_k(\hat{\xi}_k^i) \tag{2.24}$$

with $\tilde{w}_k^{(i)}$ the normalized importance weights

$$\tilde{w}_k^{(i)} = \frac{w_k^{(i)}}{\sum_{j=1}^{N} w_k^{(j)}} \tag{2.25}$$

After the importance sampling an additional resampling step is introduced that multiply or eliminate particles according to their weights. Particles with heigh weights are more likely to represent the true state and therefore will be multiplied while samples with low weights are less relevant and can be deleted from the filter. By continuously resampling the particles around the current estimate a better long-term performance can be achieved. Several resampling strategies have been proposed like systematic sampling, multinomial sampling, stratified sampling and residual sampling. The systematic sampling maps the Dirac measures $\{\hat{x}_k^{(i)}, \tilde{w}_k^{(i)}\}$ into an equally weighted random measure $\{\hat{x}_k^{(i)}, \frac{1}{N}\}$. This task can be done by a uniform sampling from the discrete set $\{\hat{x}_k^{(i)} : i = 1, ..., N\}$ with the corresponding weights as probabilities $\{\tilde{w}_k^{(i)} : i = 1, ..., N\}$. Figure 2.7 illustrates how the different stages affect each particle.

$i = 1, ..., N = 10 \; particles$

$\{\hat{x}_{k-1}^{(i)}, N^{-1}\}$

Importance Sampling

$\{\hat{x}_{k-1}^{(i)}, \widetilde{w}_{k-1}^{(i)}\}$

Resampling

$\{x_{k-1}^{(i)}, N^{-1}\}$

Prediction

$\{\hat{x}_{k}^{(i)}, N^{-1}\}$

Importance Sampling

$\{\hat{x}_{k}^{(i)}, \widetilde{w}_{k}^{(i)}\}$
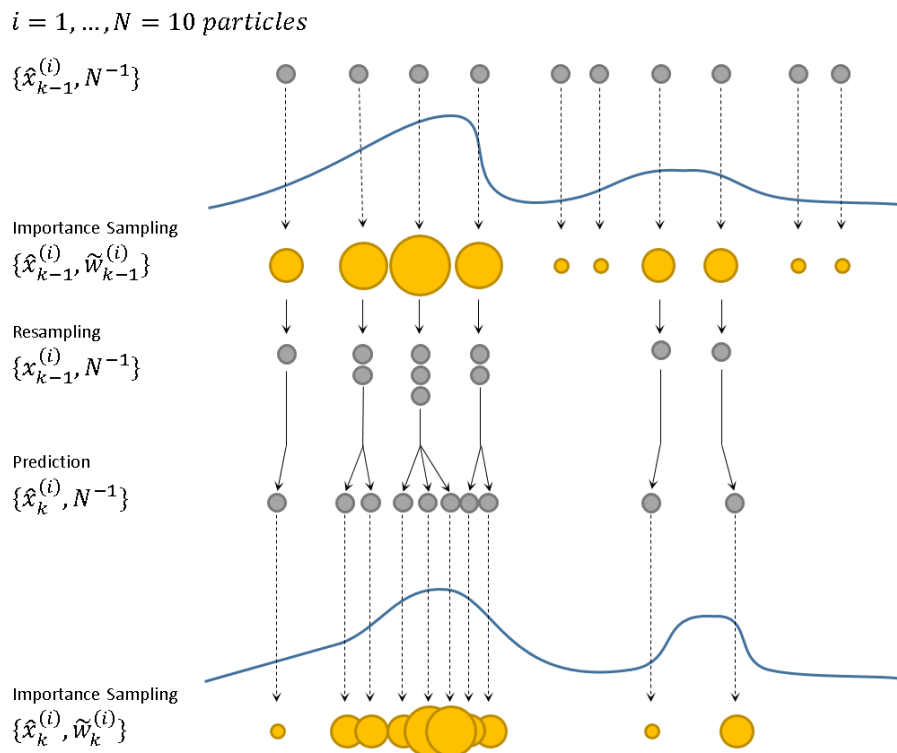
Figure 2.7.: Propagation of weighted particles .

3. Cooperative Localization in Multi Agent Systems

This chapter captures several aspects of cooperative localization (CL) in underwater acoustic sensor networks. First a detailed analysis of the challenges in this field is conducted and desirable properties are defined. Afterwards the related work is discussed in the light of these properties and open problems are highlighted. In conclusion, the objectives of this thesis will be elaborated.

3.1. Challenges and Desirable Properties

Cooperation, in general, requires two or more participants that pursue the same goal for a mutual benefit. In CL the objective is to establish or enhance the ability of self-localization for each participant. Often but not necessarily, cooperation includes the exchange of information between partners, either active, by transmitting own information, or passive, by observing others and how they effect the environment. Because of the high attenuation of most electromagnetic radiation, including light and most radio waves, acoustics is the preferred communication form in water. This poses some challenges on the cooperation of underwater systems. As mentioned in the previous chapter, the acoustic underwater channel imposes harsh conditions for communication and acoustic localization. High latency, small bandwidth and multipath interference are just some of the characteristics that need to be considered.

Apart from channel restrictions there is also a lack of infrastructure for underwater technology. While terrestrial sensor networks have recourse to a power grid and a radio network in many parts of the world, this is not given for the underwater space. Here static infrastructure is hard to establish and often economically prohibitive. As a result the whole sensor network needs to be shipped to the deployment site. Also the sensors are usually powered by battery, which is limiting their operation time and calls for an energy efficient design. From an operational aspect it is difficult to launch and recover the gear in the presence of wind and waves. Especially during the recovery, the risk of damaging the apparatus is very high, so that it should be avoided to deploy any additional equipment where possible. While all maritime technology developments ought to keep that in mind, a localization system should not increase the risk by adding more equipment.

The field of cooperative localization comprises a variety of other research areas ranging from sensor fusion to protocol development and cooperative navigation, each of which brings its own challenges and implications. The following list is an extension to the lists contributed by [23] and [24] and tries to capture some properties that are generally desired when designing a cooperative localization algorithm for acoustic underwater networks:

High Accuracy The purpose of a localization algorithm is to minimize the difference between predicted position and the true location. Accurate estimations are of major importance for the interpretation of the collected payload data and they are essential for underwater navigation as well.

Low Communication Cost Communication in the network is ought to be minimized as far as possible due to several reasons. Energy in underwater MAS is usually scarce because of limited battery power and every saved transmission will extend a nodes lifetime. The shared acoustic channel will lead to signal collisions, depending on the number of nodes and the transmissions per node. Reduced communication will also decrease interference with acoustic (payload) sensors like sonar and the disruption of marine animals.

Resilient Performance Sensors and state estimators are subject to noise and outliers and can sometimes fail. Robustness against inaccurate and faulty informations should be an integral characteristic of the cooperative localization. This means that e.g. measurement outlier can not impair the localization performance of the whole network.

Good Scalability High signal latency poses a challenge on the scalability of acoustic networks, because it limits the media accessibility. A CL algorithm should rely on as few nodes as possible but consolidate as many as available. Furthermore the algorithm complexity should not increase with network size.

Fast Convergence In a mobile network, nodes are constantly in motion and need position updates on a frequent basis in order to navigate properly. Therefore the localization procedure should report the actual location when data is sensed and can not defer the output until more information is available.

Wide Coverage A cooperative localization approach often fosters the interconnectedness of nodes in the network. However it should be ensured that nodes which have only few direct neighbours can also be localized.

Facile Deployment Some localization schemes rely on the deployment of additional equipment like anchor nodes, which are often used in acoustic underwater localization. The static anchor nodes need to be deployed and configured before the system can operate, which makes the localization inflexible and often more expensive.

Extensive Consistency Cooperative localization approaches often develop correlations between node estimates because they exchange informations in a network and sometimes nodes receive the same piece of information from two different nodes. This correlation needs to be accounted for or the localization will be inconsistent i.e. overconfident.

Reliable Uncertainty A state estimation should not only keep track of the state variables, but also evaluate the quality of the estimation. Having a reliable uncertainty measure that represents the scale of the real error can significantly improve the overall result.

This list, which might not be exhaustive, can help to guide the design process of the localization approach presented in this work. Furthermore it will serve as an orientation for the following reflection on the state of the art.

3.2. Related Work

Some of the early works on cooperative localization is done by Romeliotis, Rekleitis and Mourikis. In [25] Romeliotis et al. elaborate a formal framework on which they investigate the upper bound on the position uncertainty for a group of N robots on a plane. In their simulation each robot estimates its own state by means of a Kalman filter. The position is measured by optometry and the orientation by a compass, both with a predefined additive white Gaussian noise. A cooperative localization is accomplished by each robots cyclic noisy measurements of the relative position of all other robots. Under the assumption that each robot knows its initial state and all robots share the same proprioceptive and exteroceptive capabilities, the authors where able to prove the following.

> "Lemma: For a group of N robots with the same level of uncertainty for their proprioceptive and exteroceptive measurements, when they perform cooperative localization their covariance at steady state grows, on the average, linearly with time." [25]

By the term steady state, they refer to the convergence for $lim_{t \to \infty}$ of a subset of the covariance matrix that does not accumulate over time. Further they show that under their assumptions the rate of the uncertainty increase at steady state is inversely proportional to the number N of robots and proportional to the odometric and orientation uncertainty and does not depend on the accuracy of the relative position measurement. These results could later be verified in [26] and [27] for a small group of mobile robots.
Mourikis et al. [28] takes the framework from above and investigates the uncertainty

evolution for cooperative localization with time varying topologies. For that he introduces the relative position measurement graph (RPMG) which is a weighted directed graph that describes the robot-to-robot measurement capability in the network. Nodes represent robots and edges stand for the interconnectedness or visibility of a pair of robots. In their simulations, the authors examine the upper bounds of the position uncertainty and how changes in the topology influence the uncertainty increase throughout the network. The remarkable results of their investigations is that, the growths of the maximum uncertainty, is independent of both the topology of the RPMG and of the precision of the exteroceptive measurements. They conclude that this quantity depends solely on the number of robots in the network, and the accuracy of each robots dead reckoning capabilities. The interpretation of this conclusion is that the primary factor determining the uncertainty growth is the rate at which uncertainty is injected in the unobservable subspace of the system. Under their assumptions the number, or the accuracy, of the relative position measurements does not alter this subspace. Hence they expect no change in the rate of uncertainty increase, as a result of changes in the information contributed by the exteroceptive measurements. Figure 3.1 shows an excerpt of a simulated experiment conducted by
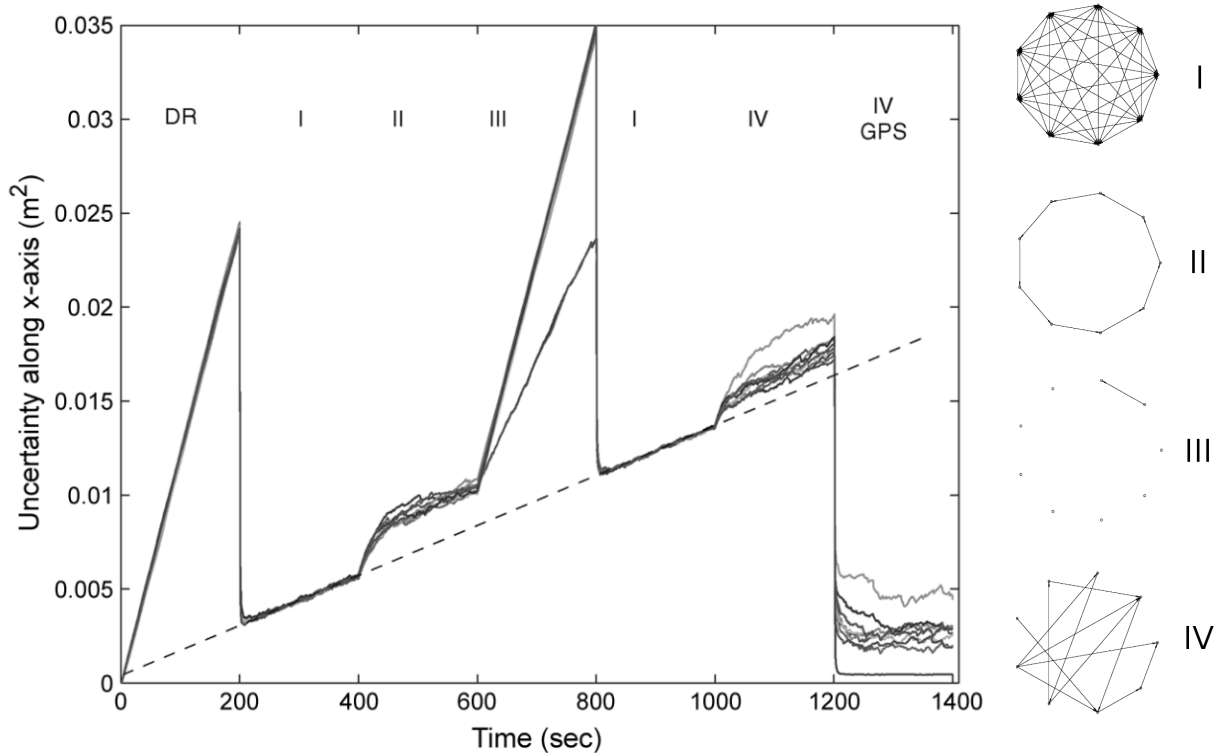
Figure 3.1.: Covariance evolution for nine robots performing CL with changing network topologies. Full lines represent each robots covariance and the superimposed dotted line represents the uncertainty evolution with a fully meshed network for comparison. The network topology indicated with Roman letters is visualized on the right hand side [28]

Mourikis et al. with a network of nine robots. Each robot starts at a known location and executes a random walk while trying to localize its position based on dead reckoning and relative position measurements to the other robots in the scene. The graph shows the upper bounds of the position uncertainty along the x-axis for each robot. Over time the network topology changes to investigate uncertainty growth during the different different phases. The phase is indicated in the upper part of the diagram and the experiment starts with independent dead reckoning (DR) followed by a sequence of different network topologies which are visualized on the right hand side by the RPMG graphs. In the last phase the network is fully meshed and one of the robots starts receiving absolute (GPS) measurements. From the uncertainty evolution it can be seen how transitions to spares topologies result in higher uncertainty increase while transition to a more interconnected topology will recover the uncertainty growth. Superimposed with the dotted line is the expected uncertainty growth for a fully meshed network for comparison. The intriguing work of Romeliotis et al. and Mourikis et al. shows several important characteristics of cooperative localization by analytically investigating the maximum expected uncertainty. The key properties can be summarized as:

- The uncertainty of a group of robots that perform cooperative localization will in average grow linearly.

- The uncertainty growth depends on the number N of robots and the uncertainty growth of the DR of each robot.

- The number and accuracy of relative position measurements affects only the constant term of the covariance while the rate of uncertainty increase remains the same.

- The topology of the network directly affects the amount of uncertainty increase.

- When an absolute position is available to at least one of the network members, the uncertainty will be bound for all robots that are connected directly or indirectly to this member.

The implications of this properties should be considered in the design of a cooperative localization strategies.

It is important to note that the implementation of the above work can not be translated directly to the underwater environment, mainly due to the many limitations of the acoustic underwater channel. Depending on the available sensor equipment it might be not possible to observe the relative position to another member in the underwater network directly. Historically range measurement have been the only observable property of the relative location, until the appearance of USBL sensors. In the literature on underwater CL two branches can be observed with only few cross references between both. On the one side there is the research on stationary networks, that are networks in which the target nodes are not moving e.g. mooring stations or static underwater facilities. The other branch handles mobile networks in which the

target nodes are usually mobile submersibles like glider, ROV or AUVs. Since this work focuses on mobile underwater networks, the former will not be discussed here. The interested reader is referred to [23], [29] and [30] which give detailed overviews of available acoustic localization systems for static UASN.

The field of CL in mobile underwater networks has received growing attention in the last decade, when prices for AUVs decreased. For a long time, teams of autonomous underwater vehicles where economically prohibitive and could only be investigated through simulations. With the emergence of cheaper AUVs we now see increasing numbers of cooperative unmanned crafts. This trend is likely to accelerate with the growing demand on underwater exploration and monitoring in science and industry. As a consequence thereof, new strategies for underwater localization need to be developed, that allow the efficient deployment of multiple submersibles in a scalable manner. Cooperative localization yields a promising approach towards this goal. In the following some of the major contributions on this field will be discussed.

Cheng et al. [31] proposes a silent Underwater Positioning Scheme (UPS) where anchor nodes periodically exchange timing information with each other. The target or sensor nodes needs to be in reach of all anchor nodes to read the messages but require no time synchronization. Each sensor nodes is able to derive its position solely from overheard transactions between the anchor nodes. Due to its silent property the number of sensor nodes that can localize themselves is only restricted by the area which is spanned by the anchor nodes. In their simulations the localization performance is dependent on anchor positions and will degrade when nodes are too close or too far away from any of the anchor nodes. Further they analyse that the position error is correlated with the arrival rate of messages at the sensor node.

[32] Soares et al. treat the network localization as a optimization problem by formalizing an approximation of the problem that can be applied as a distributed implementation. The concept is based on inter-vehicle range measurements and range measurements to static acoustic anchors with known positions. They incorporate a simple motion model for the nodes that assumes a constant velocity in order to better estimate moving vehicles. In their simulations they compare the method against an linear Kalman-Filter and static localization for scenarios with different trajectories and multiple vehicles. In an companion publication ferreira et al. [33] introduce bearing measurements to remote vehicles and anchor nodes into the problem formulation, however the optimization needs to be solved on a central node. Unfortunately, the authors fail to elaborate any advantages to LBL system and their localization error greatly exceeds that of common LBL.

Both of the above mentioned methods require several anchor nodes for their operation. Dependence on anchor nodes limits the mobility of the network and the tedious calibration process complicates the deployment of the whole system. Like discussed in the previous section, anchor nodes are undesirable for mobile underwater networks and should be avoided when possible.

31
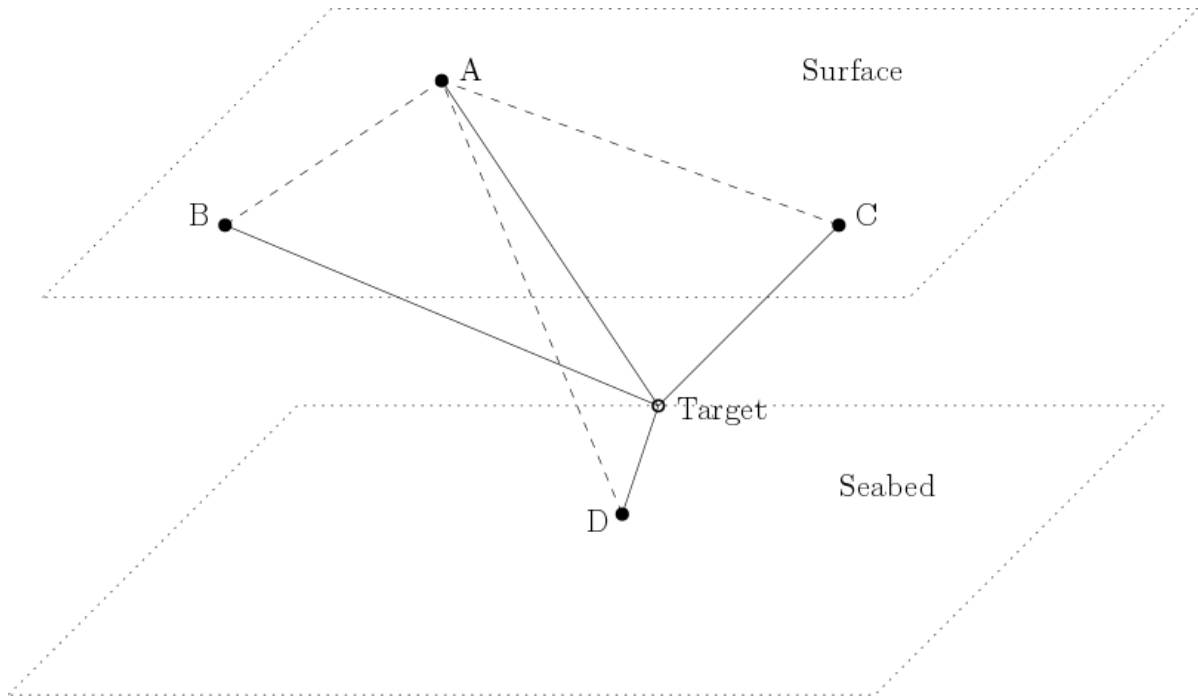
Figure 3.2.: Sketch of a UPS network with four anchor nodes and a target node.

Palomera at al. [34] shows an implementation of a fully mobile team with one surface vehicle that follows and supports an AUV using standard USBL measurements (with Evologics Modem). For that, the surface vehicle measures the AUV via USBLLONG ping-pong style and sends the measured position to the AUV on the next ping via acoustic link. On the AUV, the information is fed into an EKF together with IMU, DVL and pressure sensor readings to estimate its state. This procedure introduces significant delays between USBL measurement and reception of that measurement on the AUV (stated as $2 - 10$ seconds) which need to be accounted for. The algorithm was tested in a real world scenario where the AUV executed an bathymetric scan of a harbour environment. An quality statement of the localization precision was only given by an visual comparison between the captured bathymetric map against an previously captured map with RTK GPS of the same area. Although not exceptional elaborated, the work presents a common approach in nowadays underwater localization which is sufficient for the purpose of shallow water localization and only few vehicles. An important property of the presented approach is its mobility since no anchor nodes are required to be deployed in the mission area.

With the recent success of simultaneous localization and mapping (SLAM) techniques, these methods also found their way into the domain of cooperative localization. As it turns out SLAM and CL can be described with the same formalism when the remote nodes in CL are viewed as features for the SLAM. Here we will briefly describe pose graphs, which are on of the possible representations utilized for both, CL and SLAM. Pose graphs are often used where proprioceptive and exteroceptive informations are combined. Every node in the graph represents an vehicle state. An edge between

two nodes corresponds to a spacial measurement between the nodes. Edges can be either represent a proprioceptive measurement u or a exteroceptive measurement z. Proprioceptive measurements can e.g. come from dead reckoning and indicate the propagation of one vehicle in time so that

$$x_{t+1}^A = f(x_t^A, u_t^A) \tag{3.1}$$

while exteroceptive measurements convey the spacial relation between two different vehicles or more generally a vehicle and the location of a feature so that

$$x_t^B = f(x_t^A, z_t^{AB}) \tag{3.2}$$

Now the pose graph is a representation of the propagation of states and the relations between those states. Usually the edges also contain information on how accurate the measurement is in form of a covariance matrix or the inverse of it, the information matrix. Figure 3.3 gives a visual interpretation of the concept. We can see that pose graphs convey the same information that is used by KF and PF. This notation gives rise to some graph based techniques that have been used extensively in the field of simultaneous localization and mapping [35]. Cooperative localization and SLAM share many properties and both problems can be formulated in terms of pose graphs. While originally SLAM was used in single robot scenarios, Kim et al. [36] and Cunningham et al. [37] formulated an extension for online multi-robot mapping. In their implementation each vehicle sends its full pose graph to all neighbouring vehicle and in turn collects their transmitted pose graphs. During a pose estimation phase each vehicle optimizes over all available graphs. The authors are able to reach a consistent estimate that matches a centralized omniscient approach to the expense of high communication cost, which grows with the size of the local graph. Clearly this approach is not applicable to the underwater domain because of the limitations in the acoustic channel. However there have been several works that apply pose graphs for the underwater setting.

Bahr et al. [38] utilize time synchronized acoustic modems to obtain ranging information between nodes by OWTT in combination with INS/DVL sensors for dead reckoning. In their set-up surface vehicles periodically send a time stamp and their position and position covariance to AUVs in the water. Upon reception of a message, the AUVs have a OWTT range measurement to the surface craft as well as its position. Each submersible keeps track of previously received position-range pairs and for every new pair computes its likeliest position by optimizing a cost function over all pairs. The authors evaluate their method against and EKF and PF implementation on several sea trails and conclude that their solution is better suited than the other two in the presence of outliers. However, they state that outliers are easily detectable and that PF can reach comparable accuracy with sufficient number of particles. Also the required storage quickly increases with network size due to their bookkeeping strategy. In terms of complexity a single localization is stated as $O(q^3)$ with q being the number of past measurements taken into account.

A similar approach was proposed by [39] for a team of two AUVs. Here the vehicles
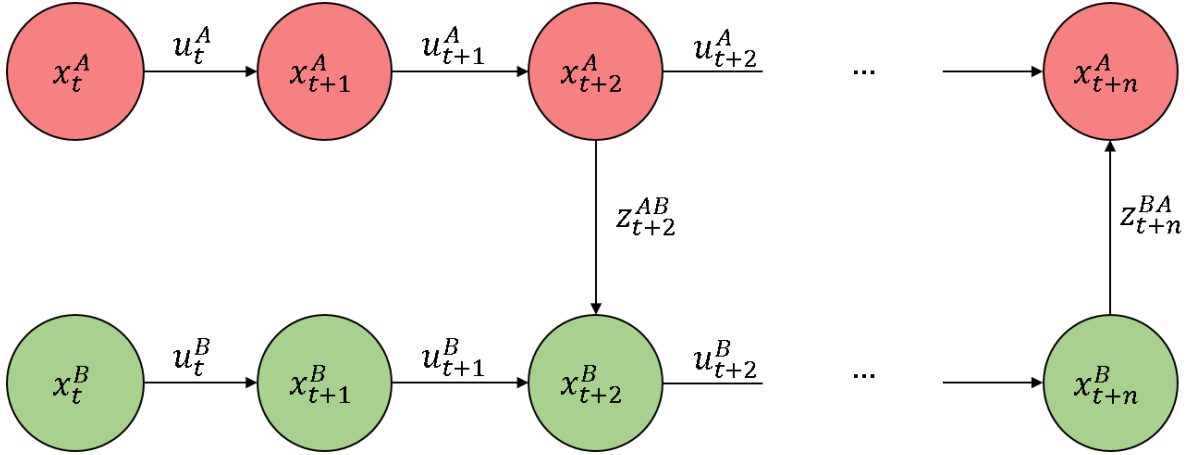
Figure 3.3.: Example of a pose graph of two vehicles A and B. Vertices denote vehicle states and edges represent proprioceptive and exteroceptive measurements.

also incorporate their dead reckoning with inter vehicle range measurements based on synchronised clocks. Instead of sending a single position and covariances however the vehicles send parts of their internal pose graph. They utilize the method of [35] to filter over the whole vehicle trajectory in order to reduce the uncertainty even further. In the results they compare the uncertainty of the approach for different transmission drop-out rates. The required data throughput of the proposed method increases linearly with the network size.

In [40] Webster et al. propose a decentralized information filter (DEIF) for a single beacon cooperative localization in a server client set-up. In single beacon CL, state and ranging information from a single reference source on the surface (the server) are used by the underwater vehicles (the clients) to improve their localization. Ranging is acquired on the submersibles by synchronised clocks and OWTT measurements and the server state is broadcasted via acoustic modem. Clients use the server state and ranging to improve their dead reckoning state estimation. By storing previously received state information of the server, the client is also able to estimate its smooth trajectory. A comparison of the approach with a omniscient centralized information filter as well as two comparable methods from the literature is given for simulation and field experiments with one surface vehicle and two AUVs. The authors show that the DEIF reproduces the same results as the centralized approach in a loss free channel assumption. In this version the packets that need to be transmitted are to big (180 bytes) for a single transmission with the utilized modem and need to be splitted. This makes the approach vulnerable to transmission loss, which is a common problem in underwater communication.

Walls et al. [41] extended the DEIF to be applicable under the faulty underwater channel environment. This is achieved by reducing the state space and sending not only the current server state but a fraction of the servers pose graph. With the redundant information a client can reconstruct its pose estimation even if a transmission was

lost. They evaluate the approach with several real world shallow water experiments and compare the results with their previous work as well as a EKF and SLAM implementation. In [42] the authors further decreased the required packet size by using factor graphs and extend the formulation to allow n server to m client topologies. The DEIF approach has shown remarkable results under real conditions and marks the current state of the art in cooperative underwater localization.

The following works, although not related to underwater CL, are nevertheless notable because of their interesting properties. Ribeiro et al. [43] applies a noteworthy approach to cooperative navigation in which they transmit just a single bit per measurement representing the sign-of-innovations. While reducing the overall bandwidth, the algorithm requires 100% packet reception, which is unrealistic for the faulty underwater channels.

In [44] Bailey et al. proposes a central fusion center where pose graphs transmitted by terrestrial vehicles are fused with relative-pose observations to estimate full joint distribution over all vehicles poses. The innovation of this work is that the method estimates not only the position but also the heading of the vehicle.

While most localization methods assume Gaussian uncertainty distributions for the position estimates, Spetzler et al. [45] uses polygons to describe uncertainty bounds on the 2d vehicle positions in an terrestrial CL framework.

3.3. Open Problems

Some of the open problems in the field of underwater CL descent from the difficult communication channel at hand. The experiments in most of the available literature take place in relatively small areas and shallow depths of less than $100m$. Here the impact of the sound speed variation is insignificant. For deep-sea networks at several thousand meter depth that span over kilometres and have agents operating on different depths, sound speed variations in the water column cause refraction effects that can severely impair acoustic measurements. Despite the impact, this is rarely accounted for in present works in the field of CL.

Another issue that arises from the high latency, low bandwidth channel is the impact of media access control (MAC) strategies on the localization. While there is a lot of recent research on MAC techniques for the underwater environment, the interplay with CL is barely investigated. Especially when networks grow bigger and denser, arbitrary information exchange between nodes gets restricted by the available channel, thereby constraining the cooperative localization algorithms.

When observing current commercial underwater navigation solutions, USBL technology takes an increasingly important role. In the literature on underwater CL however the most common approaches use range only measurements in the form of OWTT

with synchronized clocks. Atomic clocks can provide highly precise time measurements with sufficient long term stability [46]. In combination with USBL devices, reliable relative position measurements are possible in 3D, rather than 1D range only measurements. This state of the art technology has not yet been exploited in underwater CL.

Furthermore the orientation of the vehicles is not considered by any of the localization schemes in the maritime domain, although orientation information can be derived in some cases from the shown localization schemes like [44] does for terrestrial robots. The orientation is of major importance for the navigation of mobile submersibles. Especially the heading is often prone to error accumulation in IMU sensors since the drift of the heading tends to be higher than the drift in roll and pitch, due to different correction techniques.

3.4. Scope of this Thesis

Only recently the combination of underwater communication and underwater localization seem to grow joint interest in the research community where they had only few points of contact in the past. Integrated communication and navigation solutions are needed to cope with the challenges of future underwater sensor networks.

> "While path planning for robotic sensors has been active research area, very few works have explicitly considered the joint optimization and integration with communication. Given the severe restrictions of underwater acoustic channels (delay, data rate, transmission range), joint communication and navigation designs are needed." [47]

This thesis aims to elaborate and validate a cooperative localization scheme for deep-sea environments, that takes into account the desired properties which have been worked out in this chapter.

Observations in the maritime sector indicate that more efficient systems are desired to explore the vast territories under the seas. The current state of technology allows only a very narrow glimpse into this world. In the last decades, development in several related fields lead to the first prototypes of mobile underwater systems comprised of several cooperative robots. In order to monitor spacious underwater areas efficiently, bigger fleets of autonomous underwater vehicles are desired and the cost for each AUV needs to be reduced further. On way to achieve this is to reduce the spending on sensors. Here the gyroscope comes directly into mind as the high accuracy laser gyroscope is substantially more expensive than a MEMS based IMU sensors. Hence, an important part of this thesis will be to investigate if it is possible to achieve the localization performances of current commercial systems with a combination of low cost IMU and cooperative localization. Because of the fast drift of DR with low quality IMU measurements, it is crucial to fix the position frequently. Also bigger orientation errors contribute more to the position uncertainty. In this regard it could

be advantageous to increase the confidence in orientation estimates e.g. within the cooperative localization process. This has been missed in current developments on underwater CL and will be another subject of this work.

4. Design of a Cooperative Underwater Localization Strategy

The previous chapters have illuminated several aspects of the field of cooperative localization (CL) in the underwater domain and highlighted where extended research is required. This chapter is meant to give a systematic approach towards an CL design which incorporates the findings of the previous chapter. First, all constraints and requirements are summarized in order to derive a solution concept thereon afterwards.

4.1. Requirements

In this section the requirements for an underwater cooperative localization scheme will be formulated. The requirements in this section will be derived from the open problems discovered in the scientific literature as well as from the demand of potential end users of this technology. Naturally, this only reflects the author's interpretation of the demands, which has developed from several conversations with users of maritime technology with scientific and industrial background. The aim of the requirements is to provide a set of high level, non-technical properties to guide the development process of the cooperative localization strategy. Moreover, the requirements serve as concrete indications on which the developed concept can later be evaluated on.

The overall goal is a scalable CL approach for a network of vehicle that is capable of monitoring spatially extended underwater areas in deep-sea environments. Given the remote target areas, there is typically no infrastructure available in the form of reference anchor stations, so that CL is ought to work in a fully mobile network like the one illustrated in Figure 4.1. As a consequence the network can be subject to constantly changing topology and a direct communication link between all vehicles can not be guaranteed. In this context, sophisticated communication protocols on the medium access and routing levels might be required, which in turn could influence the layout of a CL procedure.

Independent from its connectivity, each mobile agent in the network must be able to localize itself with a quality that is equal or better than its dead reckoning capability. Here the precondition is, that each vehicle continuously estimates its location with DR and that the CL approach does not deteriorate this estimate.

Further more, the results of the cooperative localization should be usable by the agents for online navigation. This requires that the necessary operations can be computed by each agent and makes centralized approaches particularly unsuitable for this application. When considering future underwater networks with growing vehicle counts, the scalability of the approach is crucial. On the one hand, complexity should not increase with the number of nodes in the network. On the other hand, CL has the potential to increase the performance when more nodes are involved. Both are important properties that are required for a truly scalable cooperative localization.

While exact knowledge of its state is desirable for every underwater vehicle, the practical purpose of localization in a sensor network is merely to support the actual payload sensors with state informations. In the underwater environment these are often acoustic sensors like sonar, which can be impaired by the acoustic inter-vehicle communication commonly used in underwater CL. Therefore, it is an important design goal to reduce the communication to a minimum in order to prevent interference with payload sensors.

From the above we can compile a list of concrete high-level goals on which the co-
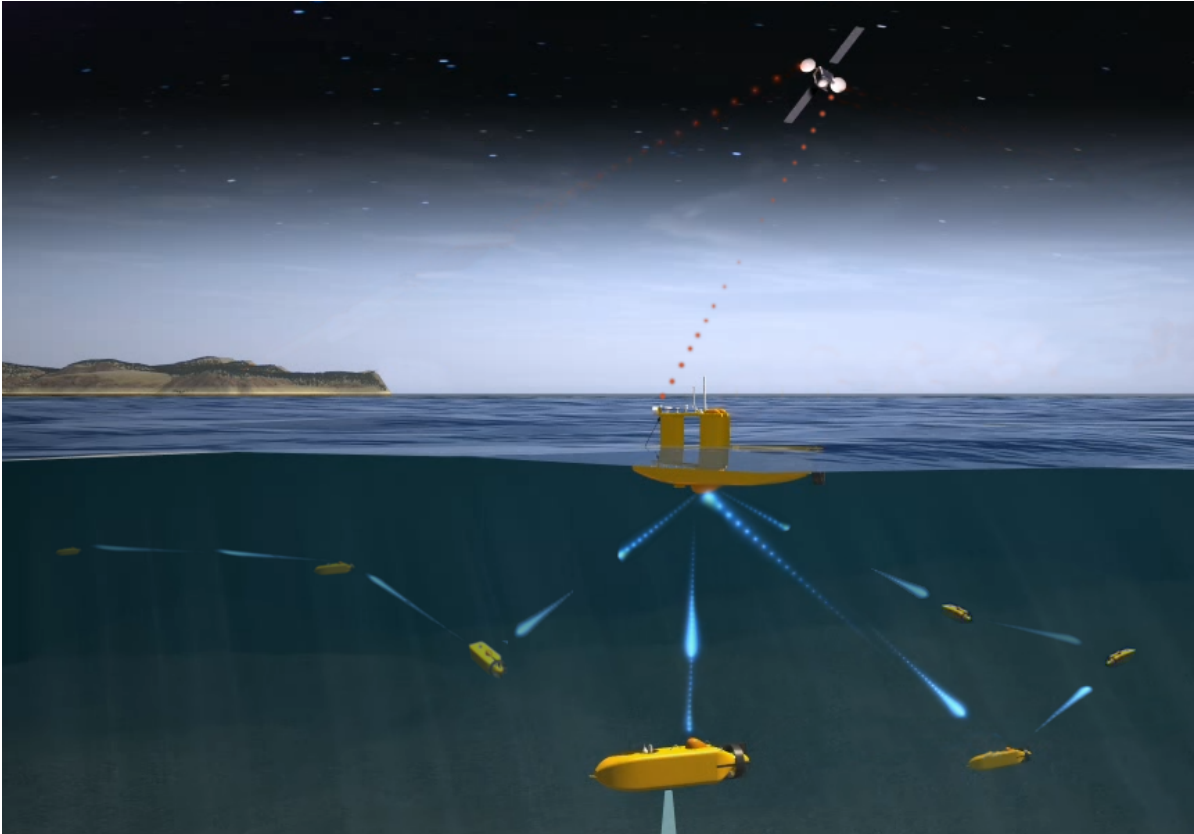
Figure 4.1.: Concept of a fully mobile underwater network, consisting of several AUVs that perform measurement tasks and an unmanned surface vessel that provides geo-reference for the underwater members.

operative localization approach can be evaluated on:

- Localization is supported for fully mobile networks

- Procedure does not rely on a particular network topology or communication protocol

- Every agent can use CL to self-localize

- Computation complexity remains the same, independent from network size

- Localization performance improves with network size

- When CL is performed by an agent, the localization quality is better than its dead reckoning capability

- Acoustic interference with payload sensors should be avoided

4.2. Deep-Sea Network Localization

After specifying the goals in the previous section, the cooperative localization approach, which is the core of this thesis, will be elaborated in this section. Referring to the target environment and the cross-linked nature of cooperative localization, the algorithm will be named *Deep-Sea Network Localization* or DNL for short. The section will start with a concretization of technical design choices that arise from the requirements. Based on that, the basic idea behind the DNL algorithm will be outlined, followed by a deeper explanation of the underlying methods that have been used to derive a reliable measure of the estimation quality. The section is concluded by a description of the data packet layout that is used for the cooperative localization algorithm throughout the network.

4.2.1. Design Choices

By choosing the deep-sea as target environment, we can already derive some design principles that arise thereof. When operating in deep-sea areas with a fully mobile network and thus no anchor nodes to reference to, at least one vehicle needs to provide the necessary geo-references from the surface to the submerged part of the network. Regular surfacing with one AUV to obtain GNSS measurements might be applicable in some mid-depth scenarios, however this approach gets more and more infeasible with increasing depth. Another, more viable option, is to have dedicated surface vehicles that serve as mobile reference nodes for the network. The inherently big distances between nodes further limits the already low data rate that can be achieved, as only low frequency, low data rate, acoustic modems provide the necessary communication range. Associated with the long distances as well is the

long propagation time of acoustic signals. For a node at a distance of $6000m$ from the sender, a sound wave takes around three seconds to reach the target and an additional three seconds until the response returns to the interrogator. This makes any approach based on a round-trip-time or hand-shake method very time intensive and even impractical when multiple nodes share the same medium. In general, a method that requires a sequence of multiple communication packets to be delivered successfully in order work is highly error-prone, considering the high signal loss ration in acoustic underwater communication. Hence the designed CL should avoid such concepts and rather take inspiration from passive methods that incorporate acoustic localization and communication like the UPS proposed from Cheng et al. [31] and explained in the previous chapter. This would also facilitate to reach the goal of minimal acoustic inference, since network nodes can obtain position information without the need to trigger an acoustic transmission that potentially disturbs the payload sensors.

The importance of a distributed solution was described already in the former section. With the aim of providing a scalable approach, the interchangeability of network agents becomes another desirable feature. More concrete this means that vehicles roles should not be preassigned as e.g. in server-client set-ups. For a big network, where the topology can change over time, it is advantageous to treat every vehicle equally. By following this concept, the localization layer becomes more flexible as it is independent from the vehicle types that the network is comprised of. Considering the practical fact that commercial autonomous vehicles usually come with their proprietary navigation solution, it would be impractical to replace every navigation software with one unified solution. Instead the cooperative localization should be designed as a service layer on top of the proprietary navigation solution and connected via an universal interface. In this way the integration of arbitrary vehicle types can be realized with relatively small overhead.

Most of the current cooperative localization algorithms provide solely position information for the network members. In many applications however the orientation also plays an important role. Systematic errors like magnetic declination or drift in the gyro-sensors impair the position estimate through the orientation uncertainty, especially when the system is deployed over a long time period. Here occasional references of the absolute orientation could help to mitigate the long term deviations in the orientation estimate. That it is possible to integrate heading estimates into a CL framework was shown already for terrestrial systems, e.g. in [44], but was not yet seen in underwater CL. Hence one of the design goals for the DNL algorithm will be to provide estimates of position and orientation.

Apart from the algorithmic design choices, there is also the question of which technology is best suited for the exteroceptive measurements. For the given circumstances there are only two possibilities, range-based sensors or direction-based sensors like USBL. The majority of the related work on underwater CL applies acoustic sensors that determine the range to the source of a transmission, e.g. with accurate, synchronized clocks. In contrast USBL measures the direction to the source. To the author's knowledge there has been no approach for a scalable cooperative localization based on USBL sensors in the literature up to date, despite the fact that USBL measures the

relative location in two dimension (azimuth and elevation in spherical coordinates) while the range only consist of one dimension. Furthermore, USBL are also capable of measuring the range when equipped with synchronized, high precision clocks, so that they can provide a 3D measurement of a relative position to the source of a transmission. One of the reasons why these sensors have not been used to a greater extend in CL might be the cost factor. Nevertheless, this work will be based on USBL modems since it is scientifically and practically compelling to investigate the capability of USBL for cooperative localization. Since high precision clocks add additional costs to the already relatively high-priced sensor, we will assume unsynchronized USBL as default case for the development of the algorithm, while also incorporating range measurements from synchronized or two-way range measurements when available. With the design goals defined, we can proceed to outline the deep-sea network localization algorithm.

4.2.2. Outline

The posed requirements and design goals focus the development process by discarding many possible design pathways. For example the goal to avoid hand-shake based methods and, at the same time, assume that clock synchronization is not available greatly restricts the amount of information that can be used for localization. This led to reconsider the data that is generally available on a vehicle and narrow down what information is minimally required in addition for a cooperative localization.
The technology of choice is USBL, hence the measurements of this sensor will play an integral part in the CL approach. A standard measuring process for USBL with and without clock synchronization is depicted in Figure 4.2. For both cases the round trip time (RTT) and the one way travel time (OWTT) respectively provide the slant range measurement. By choosing to avoid hand-shake based methods and clock synchronization, we are restricted to measure the angle of arrival only.
  Alongside the direction measurements, a second source of information is available for node B in the diagram: the data packet transmitted from the sender A. What is conveyed in this data can be decided by the user of the system. From the viewpoint of localization, the global position of the transmitting node is of high interest. By combining the position of the source in a global frame and the relative location measurement of the source in the body frame of the observer, the observer is able to compute its own global position. Given accurate relative measurements and an exact global position of the sender, this would already suffice for the self-localization of every observer that overhears the message of the sender. Due to the assumption of unsynchronized sensors however, the measurement contains only the direction and not the range. The question now is, if its possible to work out the full relative location with the given informations. We will assume that each vehicle tracks its state by means of its proprioceptive sensors and therefore has a rough estimation of its own pose, composed of position and orientation, as well as the uncertainty of this estima-

measuring process
without clock sync.

measuring process
with clock sync.
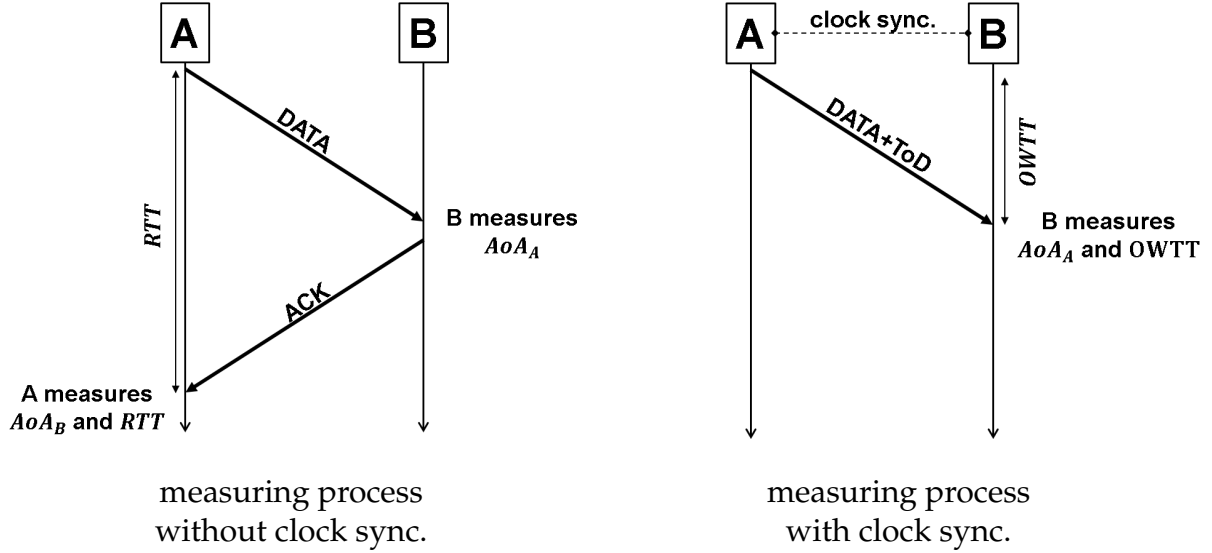
Figure 4.2.: Common USBL measuring process for 3D relative position measurements. The direction to the transmission source (AoA) is measurable with an one way transmission only, while the slant range measurement requires either a hand-shake based method (left) or synchronized clocks (right).

tion. The observer now can calculate the range between his global position beliefs and the position transmitted by the sender.

Naturally, any measurement or estimate is subject to noise and inaccuracy and thus the resulting range will be as well. With increasing distance however, the uncertainty in the position will have less effect on the slant range, so that the estimation error is bound. A first investigation on the influence of such range an estimation to the localization capabilities of single vehicle was made in [48]. In this work, the sender transmitted its global position together with its position uncertainty. The uncertainty was used to calculate confidence intervals for the range estimation.

A common way to represent uncertainty is the covariance matrix. For a 3D position, the covariance matrix is a 3x3-matrix, representing the variance in each dimension on its diagonal components and the covariance between dimensions on the non-diagonal components. Although there are also other forms of uncertainty representations, covariance matrices can be thought of as a common denominator since the majority of today's underwater navigation solutions can be expressed that way, be it Kalman filter, information filter or particle filter. Hence, it makes sense to choose this representation as interface between the cooperative localization layer and the vehicle navigation.

Figure 4.3 summarizes the interaction of the different elements that play a role in this cooperative localization approach. The process starts with a network node A that broadcasts its own position belief and uncertainty, designated as $[\vec{p}_n^A, \Sigma_{p_n^A}]$, via acoustic link. The subscript n here denotes that the variable refers to a common nav-

$$\begin{pmatrix} \widehat{\vec{p}}_n^{\,O}, \widehat{\Sigma}_p^O \\ \widehat{\psi}^O, \widehat{\sigma}_\psi^O \end{pmatrix}$$

vehicle
navigation

$$\begin{pmatrix} \vec{p}_n^{\,O}, \Sigma_p^O \\ \vec{q}^{\,O}, \Sigma_q^O \end{pmatrix}$$

exteroceptive
sensor

$(\vec{z}_b, [r])$

cooperative
localization

communication

$(\vec{p}_n^{\,A}, \Sigma_p^A)$
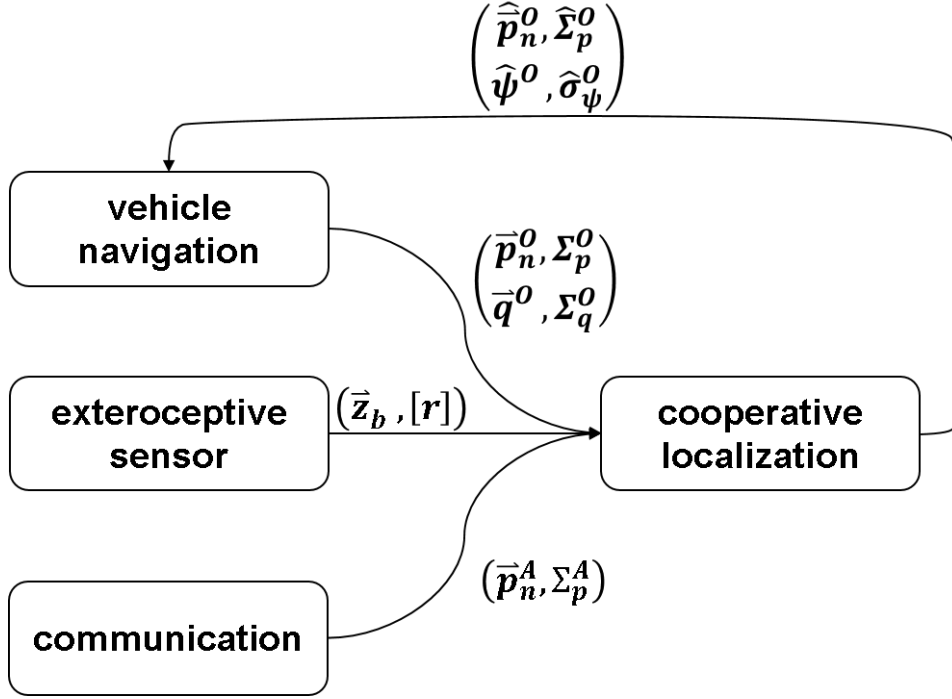
Figure 4.3.: Information flow of the DNL algorithm.

igation frame that is the same for every member in the network. When the broadcast is received by an observing node O, the USBL sensor on the observer will measure the direction of the incoming signal in the reference frame of the observer as the euclidean unit vector $[\vec{z}_b]$ with the subscript b for body frame. Simultaneously the position information of the broadcaster will be extracted from the transmitted data packet. In combination with the observers own current position belief, $[\vec{p}_n^{\,O}, \Sigma_{p_n^O}]$ it is possible to estimate the distance r between O and A as well as the uncertainty of this estimate. By assembling range and direction measurement, we now have a 3D vector of the relative location of node A in the body frame of the observer. Since each node also keeps track of its orientation q, the observer can transform the relative location vector into the navigation frame and from there compute its position in the navigation frame with the simple vector subtraction

$$\hat{\vec{p}}_n^{\,O} = \vec{p}_n^{\,A} - r\vec{z}_n \tag{4.1}$$

The process uses the noisy vehicle orientation for the transformation into the navigation frame. As a consequence, inaccuracies in the orientation will have a big impact on the position estimation $\hat{\vec{p}}_n^{\,O}$, especially when the distance between observer and transmitter is large.

As defined in the design goals, we want to utilize the available informations also for estimating the orientation and thereby enhancing the accuracy of the orientation belief. Because the heading is in particular error-prone in IMU based dead reckoning, the focus will be to establish a more reliable heading estimation. Figure 4.4 outlines

the basic idea behind this concept, which was published earlier in [49]. Let α_n be the angle spanned between the north axis of the navigation frame and the vector $\vec{z}_n^p$ that is obtained by the position difference of observer $\vec{p}_n^O$ and transmitter $\vec{p}_n^A$. Further let α_b be the azimuth component of the USBL direction measurement in the body frame of the vehicle. Then the heading ψ can be calculated with

$$\psi = \alpha_n - \alpha_b \tag{4.2}$$

However, this simple formula can only be used when the vehicle is aligned to the horizontal plane, meaning that roll and pitch are zero. In real systems, this assumption is not met. The solution is to project the direction measurement onto the horizontal plane, while keeping the azimuth angle in the body frame. This can be achieved by modifying the vehicle orientation q, so that rotations around the Down-axis are neglected. When q is represented as Euler angles, this is accomplished straight forward by setting the yaw angle to zero.

So far the basic concept to derive the desired quantities 'position' and 'heading'
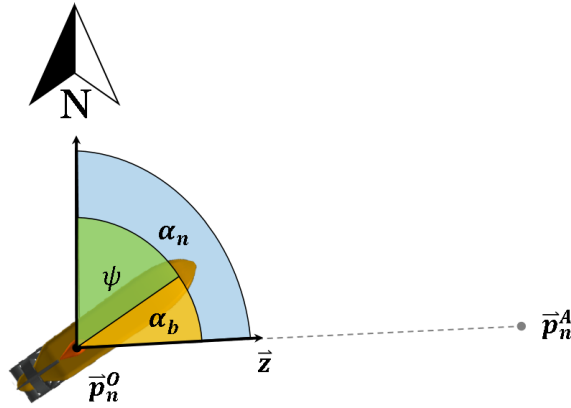
Figure 4.4.: The heading ψ of a vehicle can be obtained when the direction vector $\vec{z}$ to an arbitrary point is known in the body frame of the vehicle as well as in the global navigation frame.

have been explained without considering the involved measurement noise and estimation uncertainties. A general solution needs to incorporate those factors as well. The general procedure of the proposed deep-sea network localization can be seen in Algorithm 1. How to integrate the uncertainties into the solution will be subject of the following subsection.

input :

        $[\vec{p}_n^A, \Sigma_{p_n^A}]$ position and position covariance of transmitter

        $[\vec{p}_n^O, \Sigma_{p_n^O}]$ position and position covariance of observer

        $[\vec{q}, \Sigma_q]$ orientation and orientation covariance of observer

        $\vec{z}_b$ direction of arrival measurement of USBL

        r optional range measurement of USBL

output:

        $[\hat{\vec{p}}_n^O, \hat{\Sigma}_{p_n^O}]$ position and position covariance estimate of observer

        $[\hat{\psi}, \hat{\sigma}_\psi^2]$ heading and heading variance of observer

$[\vec{z}_n^p, \Sigma_{z_n^p}] \leftarrow zFromPositions([\vec{p}_n^A, \Sigma_{p_n^A}], [\vec{p}_n^O, \Sigma_{p_n^O}]);$

if *r was measured* **then**   `// range measurement of USBL is available`

    $\Sigma_{z_b} \leftarrow covarianceFromUSBLSample(r\vec{z}_b);$

end

else

    $r \leftarrow |\vec{z}_n^p|;$

    $\Sigma_{z_b} \leftarrow covarianceFromUSBLSample(r\vec{z}_b, \Sigma_{z_n^p});$

end

```
/* Transform direction measurement and include orientation
   uncertainty                                            */
```

$[\vec{z}_n, \Sigma_{z_n}] \leftarrow zToNavigationFrame([\vec{z}_b, \Sigma_{z_b}], [\vec{q}, \Sigma_q]);$

$[\vec{z}_h, \Sigma_{z_h}] \leftarrow zToHorizontalPlane([\vec{z}_b, \Sigma_{z_b}], [\vec{q}, \Sigma_q]);$

```
/* Merge direction and position estimates to get final
   position and heading                                   */
```

$[\hat{\vec{p}}_n^O, \hat{\Sigma}_{p_n^O}] \leftarrow mergeForPosition([r\vec{z}_n, \Sigma_{z_n}], [\vec{p}_n^A, \Sigma_{p_n^A}]);$

$[\hat{\psi}, \hat{\sigma}_\psi^2] \leftarrow mergeForHeading([\vec{z}_h, \Sigma_{z_h}], [\vec{z}_n^p, \Sigma_{z_n^p}]);$

Algorithm 1: Deep-Sea Network Localization (DNL) main algorithm

4.2.3. Incorporating Uncertainty

There is a series of uncertainties that play into the estimation of $\hat{\vec{p}}_n^O$ and ψ. For both cases, noise in position, orientation and direction measurement add up, so that the resulting estimation uncertainty is a result of those three error sources. Noise has not been considered in the naive approach described above. To obtain the probability distribution for the final estimation, all error sources have to be accumulated.

When the uncertainties, in the form of covariance matrices, are independent from each other and describe the dispersion of the same variables they can simply be added element wise. This is only true for the position uncertainties of the observer $\Sigma_{p_n^O}$ and transmitter $\Sigma_{p_n^A}$, because both describe the dispersion of the position in the

same North-East-Down navigation frame.

The dispersion of the direction measurement is described in the sensor frame. Without loss of generality, we will assume the sensor frame to be aligned with the body frame of the vehicle. Nevertheless, the covariance matrix of the USBL measurement Σ_{z_b} has to be transformed into the navigation frame before it can be merged with the others, which is not trivial. Also, Σ_{z_b} has to take different forms for the position estimation and the heading estimation. In the heading estimation case, we are interested in the spherical deviation of the azimuth angle, projected onto the horizontal plane. While for the position estimation, a representation in Cartesian coordinates is desirable. In general, the error distribution of USBL sensors has not yet been studied thoroughly. Since a reliable statement of the uncertainty distribution is required, the USBL localization quality has been investigated in this work and will be discussed in section 5.2.

Contrary to the spatial uncertainty, noise in the orientation works on a completely different set of variables, but needs to be merged with the spacial dimensions. Here the question arises: How is it possible to combine all those different uncertainty representations.

A transformation between different coordinate systems can be seen as a non-linear
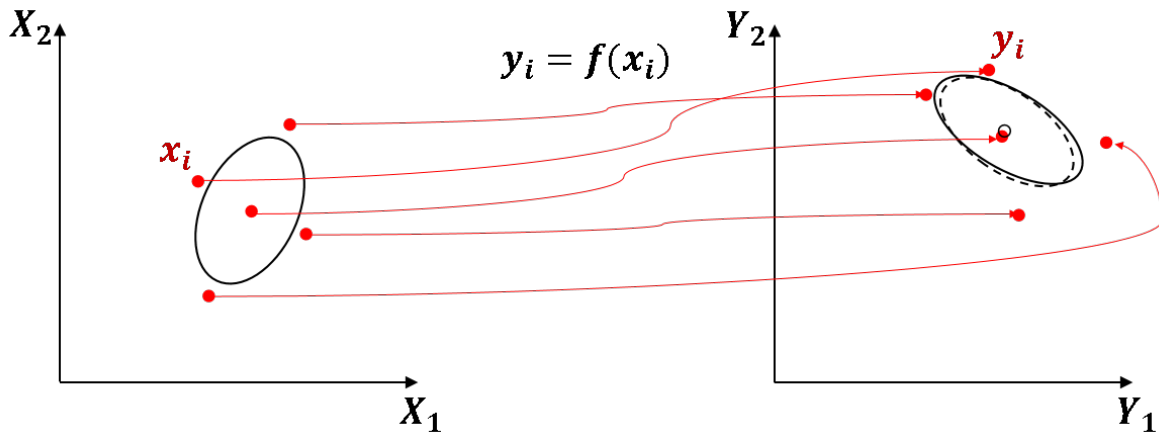
Figure 4.5.: The unscented transformation chooses a set of sigma points (red dots) from a distribution in the original space X, shown as a 1σ border ellipse on the left. Those sigma points are propagated through the non-linear function f and can then be used to approximate the distribution in the transformed space Y. The approximated distribution is shown as dotted ellipse and the true distribution as full ellipse on the right.

function, e.g. in form of a rigid transformation from one Cartesian frame to another or as conversion between Cartesian and spherical coordinates. In section 2.2, a brief introduction to fusion techniques was given, which also deals with the propagation of covariance matrices through non-linear functions. It was pointed out, that for non-linear state estimation problems, the unscented Kalman filter consistently achieves better performances than the extended Kalman filter [20]. Therefore we are particu-

lar interested how the unscented transformation technique can be used to incorporate the different uncertainty sources.

The general idea behind the unscented transformation (UT) is to break down the co-variance matrix into a set of points, the so called sigma points, which adequately describe the distribution. Now, instead of a matrix, the sigma points will be propagated through the non-linear function f. After the transformation, the sigma points can then be used to reconstruct a covariance matrix. The UT process is illustrated in Figure 4.5.

Algorithm 2 gives one example, where the direction measurement of the USBL is transformed from the vehicles body frame into the navigation frame, while also including the contribution of noise in the orientation estimation. Usually this would require two separate UT operations, one for the transformation and another one to combine spacial and orientational uncertainties. In the example both operations have been queued up to operate on the sigma points directly. First the sigma points for the direction measurement and the orientation uncertainty are calculated separately. Then, for each direction sigma point $x^{(z_b)}$ we rotate around each orientation sigma point $x^{(q)}$.

The result is a new set of sigma points $x^{(z_n)}$, where each point describes a possible solution of the direction measurement in navigation frame. From this population we can draw the weighted mean and construct a covariance matrix which will represent the distribution. An example of the sigma point distribution for this function can be seen in Figure 4.6.

Similar to the above example, other transformations in the DNL algorithm are handled with the UT technique to get the probability distribution for a measurement variable as well as a more informed mean value that is drawn from that probability. The DNL algorithm makes uses of UT to:

- Transform covariance matrices between spherical and Cartesian space

- Merge spacial and orientational uncertainties

- Combine multiple uncertainties of the same kind to get a more informed estimate
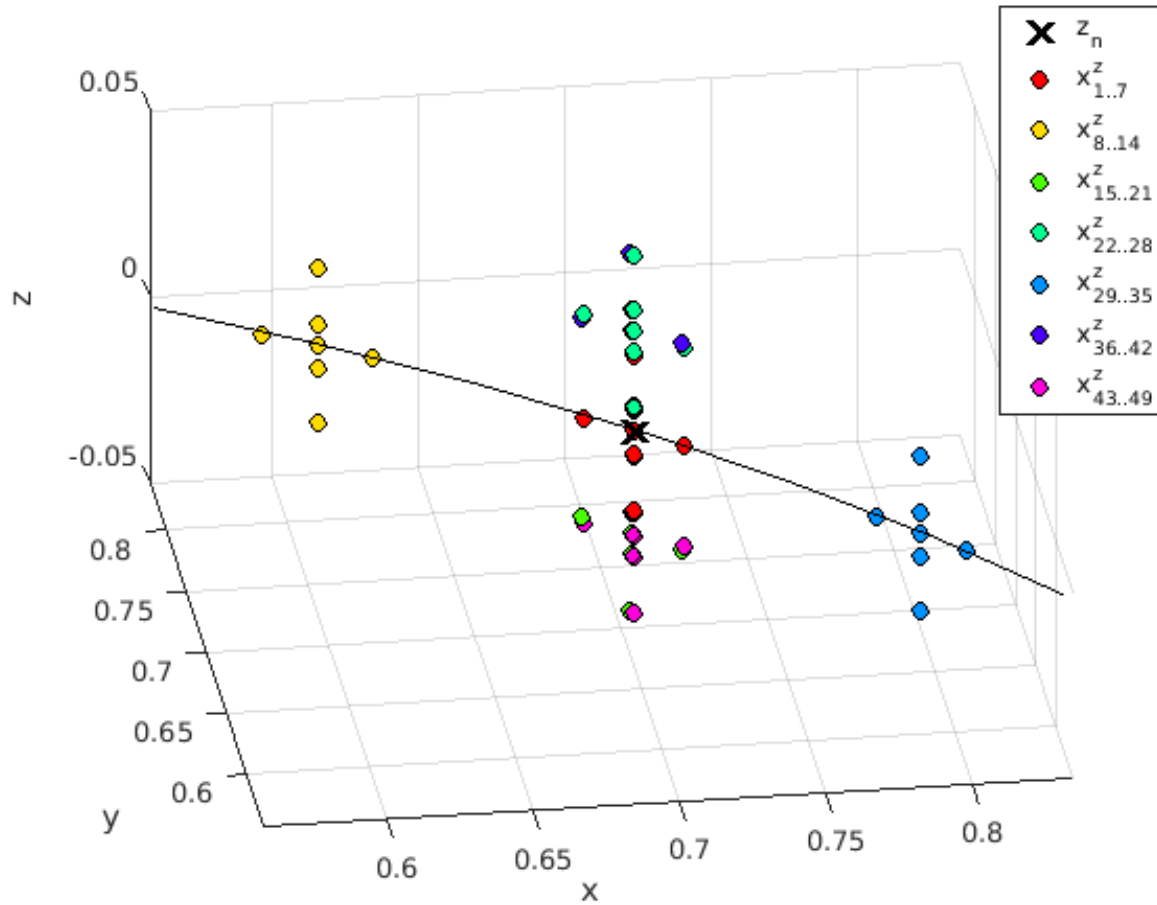
Figure 4.6.: Example of sigma points for a transformation of direction measurements. Each point represents the end point of a direction vector on the unit sphere. Red points correspond to unrotated direction sigma points while the other color groups represent the red group rotated around different orientation sigma points. The estimated mean direction of the population is denoted by the cross and the line shows a segment of the unit circle on the XY-Plane.

input :

$[\vec{z}_b, \Sigma_{z_b}]$ direction measurement and covariance in vehicles body frame

$[\vec{q}, \Sigma_q]$ orientation and orientation covariance of observer

output:

$\vec{z}_n$ direction measurement in navigation frame

$\hat{\Sigma}_{z_n}$ covariance in Cartesian space including orientation

```
/* set-up parameter & weights for scaled UT                    */
```
$M \leftarrow 2size(\vec{z}_b) + 1;$

$L \leftarrow 2size(\vec{q}_b) + 1;$

$\kappa \leftarrow 20;$

$\alpha \leftarrow 1;$

$\beta \leftarrow 2;$

$\lambda \leftarrow \alpha^2(ML + \kappa) - ML;$

$w_0^{(m)} \leftarrow \frac{\lambda}{ML+\lambda};$

$w_i^{(m)} \leftarrow \frac{1}{2(M+\lambda)};$ `/* i = 1, ..., M      */`

$w_i^{(m)} \leftarrow \frac{1}{2((M-1)L+\lambda)};$ `/* i = M + 1, ..., L */`

$w_0^{(c)} \leftarrow w_0^{(m)} + (1 + \alpha^2 + \beta);$

$w_i^{(c)} \leftarrow w_i^{(m)};$ `/* i = 1, ...ML      */`

```
/* determine sigma points of direction covariance          */
```
$\Delta x^{z_b} \leftarrow \sqrt{(M + \lambda)\Sigma_{z_b}};$

$x_0^{(z_b)} \leftarrow \vec{z}_n;$

$x_i^{(z_b)} \leftarrow \frac{\vec{z}_n + \Delta x^{z_b}}{|\vec{z}_n + \Delta x^{z_b}|};$ `/* i = 1, ..., M/2      */`

$x_i^{(z_b)} \leftarrow \frac{\vec{z}_n - \Delta x^{z_b}}{|\vec{z}_n - \Delta x^{z_b}|};$ `/* i = M/2 + 1, ..., M */`

```
/* determine sigma points of orientation covariance        */
```
$\Delta x^{(q)} \leftarrow \sqrt{(L + \lambda)\Sigma_q};$

$x_0^{(q)} \leftarrow \vec{q};$

$x_j^{(q)} \leftarrow quatnormalize(\vec{q} + \Delta x^q);$ `/* j = 1, ..., L/2      */`

$x_j^{(q)} \leftarrow quatnormalize(\vec{q} - \Delta x^q);$ `/* j = L/2 + 1, ..., L */`

```
/* combine spacial and orientation sigma points            */
```
for $i = 0$ **to** M **do**

    for $j = 0$ **to** L **do**

        $k = iM + j;$

        `/* rotates vector ` $x_i^{(z_b)}$ ` around quaternion ` $x_j^{(q)}$ `*/`

        $x_k^{(z_n)} \leftarrow rotate(x_i^{(z_b)}, x_j^{(q)})$

    end

end

```
/* get mean and covariance from combined sigma points   */
```
$\vec{z}_n \leftarrow \sum_{i=0}^{LM} w_i^{(m)} x_i^{(z_n)};$

$\Sigma_{z_n} \leftarrow \sum_{i=0}^{LM} w_i^{(c)} (x_i^{(z_n)} - \vec{z}_n)(x_i^{(z_n)} - \vec{z}_n)^T;$

Algorithm 2: DNL function $zToNavigationFrame$

4.2.4. DNL Data Packet Layout

Communication is an integral part of the DNL approach, since each agent must be able to broadcast its position and position uncertainty belief to the network. However, the bandwidth of underwater communication is very limited and depends on the utilized frequency, especially for long range communication where low frequencies are required. While it is technically possible to transfer data chunks of arbitrary size, big data packets are more likely to suffer a transmission failure. Hence it is advisable to limit the packet length and some acoustic modems will support a transmission mode based on short messages with a size between $32Byte$ and $256Byte$ per message. Keeping this restrictions in mind, an efficient data representation for position and uncertainty is demanded. The position is comprised of a latitude, longitude and depth value while the covariance for the position is a positive semi-definite matrix of 3x3 elements. Assuming a single precision resolution ($4Byte$) for all values, this would result in a packet size of $12x4Byte = 48Byte$. The size can be reduced by lowering the resolution of some variables. To allow for a precise geo-reference the latitude and longitude should remain in full resolution, however the depth and covariance resolution can be adjusted without losing to much information.
A depth resolution of around $0.15m$ is sufficient for the cooperative localization task and can be achieved with $2Byte$ unsigned integer and a proper scaling value of $11000m$. The scaling value refers to the deepest known point on earth of approx. $11000m$ depth at the Mariana Trench, so that the full possible depth is covered.
Covariance matrices are composed of variances, the square of standard deviation. Hence the values of the matrix change quadratically when the deviation changes, which is not ideal for the scaling. Furthermore, the positive semi-definite structure yields some redundancies. A feasible way to avoid the quadratic changes and redundancies is to break down the matrix with a Cholesky decomposition. The method will decompose the covariance matrix into the product of a triangular matrix T and its conjugate transpose, so that

$$\Sigma = TT^* \tag{4.3}$$

Instead of sending the full 3x3 covariance matrix, the same information can conveyed by sending the non-zero part (six elements instead of nine) of the decomposition T and reconstruct the covariance matrix at the receiver. The decomposed matrix also does not scale quadratically with changes in the deviation, which makes it easier to define a proper resolution. Elements in T denote standard deviations for the position estimate as well as the correlated deviation between dimensions. We define an upper limit for the position standard deviation of $100m$. In this way, with the biggest possible uncertainty, the real position has a 99% probability of being within a sphere with radius $300m$ around the conveyed mean. This would be a rather vague guess and vehicles should in any case provide more precise estimates, since it is hardly possible to navigate with such a high inaccuracy. If one element value in the matrix is greater than this upper bound, the position estimate is treated as if the probability density is unknown. Elements of T can have positive and negative values so that we define

Table 4.1.: Components of the DNL header packet

Variable	Size	Data type	Range	Resolution
Longitude	4 Byte	Int32	$-180° - 180°$	$\sim 8.4°10^{-8}$ ($\sim 1mm$ at equator)
Latitude	4 Byte	Int32	$-180° - 180°$	$\sim 8.4°10^{-8}$ ($\sim 1mm$ at equator)
Depth	2 Byte	uInt16	$0m - 11000m$	$\sim 0.15m$
T_{0-5}	6x2 Byte	Int16	$-100m - 100m$	$\sim 0.0031m$
Total	22 Byte			

the scaling factor as $200m$. When each element of T is encoded as a signed integer with $2Bytes$ this yields a resolution of $0.0031m$, which is sufficiently accurate for the cooperative underwater localization.

With the adjustments it is now possible to transmit the necessary data with a footprint of only 22 Byte, which is small enough to fit into one transmission packet, even for the most restrictive long range USBL devices on the market. Table 4.1 shows the components of the DNL header and their respective range and resolution. The small footprint increases the transmission robustness since shorter data packets are less likely to get distorted by the acoustic channel. Also it allows to include other relevant data into the same packet if necessary, like navigation data and mission updates that might be used to coordinate the behaviour of vehicles in the network.

5. Implementation

The focus of this chapter is to give an insight into the software framework that will be used to evaluate the proposed cooperative localization approach described in the previous chapter. First an introduction to the simulation framework will be given, including the software architecture, motion and sensor models as well as the simulation mechanics which are relevant for this work. Since the USBL sensor model is of particular importance for the evaluation of the DNL algorithm and one of the core contributions of this thesis, it will be discussed in the following separate section. In the last section of this chapter, the sensor fusion framework of the simulated agents will be illuminated, including the integration of the DNL estimates.

The concepts, described in this chapter, will aid to comprehend the results of the experiments, which are described in the subsequent evaluation chapter.

5.1. Simulation Framework

At the core of the simulation framework is the SMIS Mission Simulator, a simulation tool that was developed for the research project Subsea Monitoring via Intelligent Swarms (see section 1.2). It was written in object oriented Matlab but offers ROS interfaces on many levels. The purpose of this tool is to allow the development and test of algorithms for the interaction of teams of autonomous underwater systems, like the SMIS system. The foundation of the simulator is comprised of a variety of interface and control classes that describe agent entities and manage the simulation flow at a low level. In this section, some of the simulator components, which are relevant to this work, will be discussed.

5.1.1. Scene

The scene is an object that holds all the relevant informations of the environment in which the simulation takes place. Robots usually interact with the environment e.g. when they measure the distance to the ground, the temperature at their position or some other quantity outside of the robot itself. Here the scene class offers as a central storage to these kind of environmental informations. Furthermore, the class provides functions to efficiently access the stored informations around a given location. For example when a robot which is close to the seabed measures the distance to the ground,
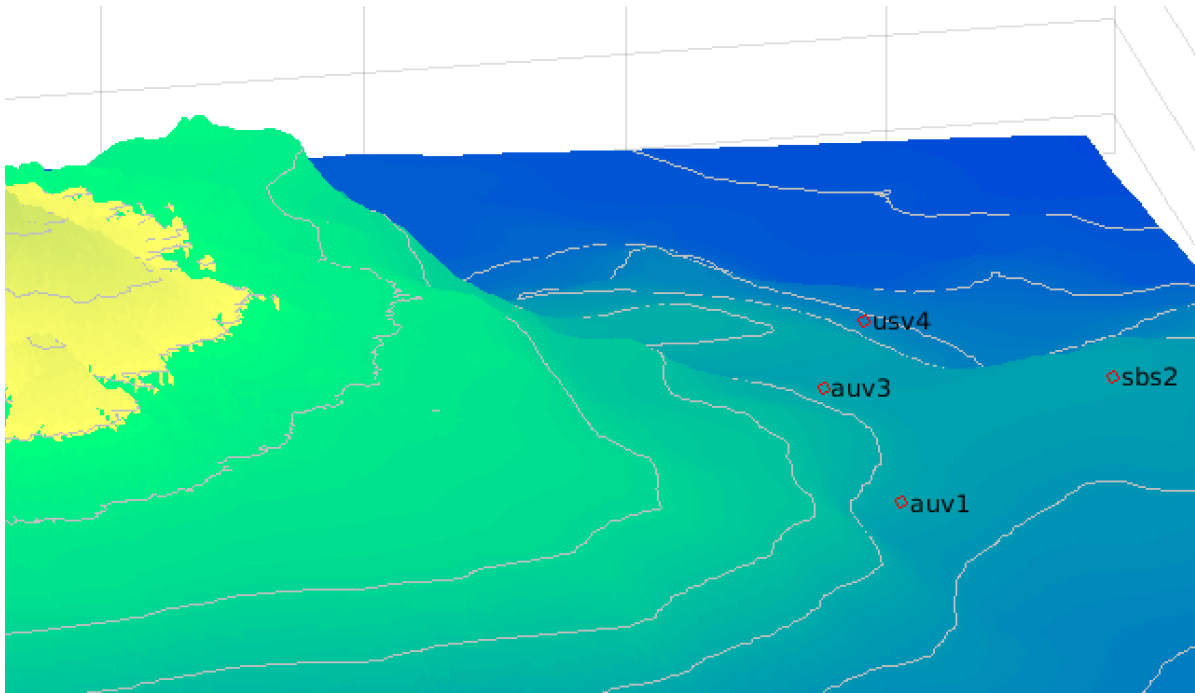
Figure 5.1.: Display of simulated scene with elevation map of the seabed east of the island Gran Canaria (yellow area) and a group of vehicles operating in the sea, marked as red circles.

only the terrain information of a specified volume around the robots location will be searched.

There are several, so called, overlays that define different properties of the environment. The most relevant overlays for this work are listed below.

Terrain The terrain overlay holds the surface of the seabed in form of an elevation map. Several of the common formats for geographic information systems are supported.

Sound Velocity Profile A sound velocity profile defines the sound speed in different areas of the scene. Usually sound speed changes in the horizontal direction are negligible and the profile defines only the change over depth. The sound speed is an important factor for many acoustic sensors and communication devices like the USBL.

Magnetic Declination Magnetic declination defines the angle deviation between the magnetic and the geographic north direction. This deviation comes into play when sensors like the magnetometer in an IMU are applied. The declination can either be a single value that takes effect on the whole scene or it can be an field of values changing between different areas of the scene.

5.1.2. Vehicles

The vehicle class is the base representation for all robots in the simulation. It comprises the physical state of the robot in the scene (position, orientation, velocity etc.) as well as its hardware and software components.

Hardware components are divided into sensors and actors and can be added to a vehicle instance modularly. Each hardware component itself is stored with the relative pose to the vehicles body frame.

Apart from the hardware components, a vehicle instance also holds an instance of the agent interface, which represents the software that runs on the vehicle and is responsible for the control of this vehicle. A vehicle can be configured to have any amount and kind of sensor and actor but only one software agent. Since the amount of possible configurations is limitless, a helper class was developed which guides the generation of vehicle instances. This so called vehicle factory will parse a XML-file in the Unified Robot Description Format (URDF) and construct a valid vehicle instance thereof. An example of such a URDF document can be seen in listing 5.1.

```
1  <robot name="AUV">
       <!-- description of the robots structure -->
3      <link name="base_link">
           <origin xyz="0 0 0" ypr="0 0 0"/>
5      </link>
       <!-- motion model by wich the robot moves through the world -->
7      <motion_model class="AUVMotionModel"/>
       <!-- software agent that is controlling the robot -->
9      <agent class="AUVAgent">
       <observer>
11        <fusion class="AUVParticleFilter"/>
       </observer>
13     <ctrl>
           <controller class="BehaviorController"/>
15     </ctrl>
       </agent>
17     <!-- sensors installed on the robot -->
       <sensor class="IMUSensor" name="MTI-G-700" update_rate="100">
19         <parent link="base_link"/>
           <origin xyz="4.2 0 0.15" ypr="90 0 90"/>
21     </sensor>
       <sensor class="DVLSensor" name="WHN 600" update_rate="2">
23         <parent link="base_link"/>
           <origin xyz="3.5 0 0.25" ypr="0 0 180"/>
25     </sensor>
       <sensor class="PressureSensor" update_rate="16">
27         <parent link="base_link"/>
           <origin xyz="0 0 0" ypr="0 0 0"/>
29     </sensor>
       <sensor class="USBLModem" name="S2CR 7/17 USBL">
31         <parent link="base_link"/>
           <origin xyz="1.5 0 -0.3" ypr="0 0 0"/>
33         <sonar minRange="0" maxRange="6000" beamAngle="190"/>
       </sensor>
35  </robot>
```

Listing 5.1: Example of an URDF description of an AUV

5.1.3. Motion Models

A motion models describe the locomotion capabilities of a robot. In the simulation, the motion model is an interface that takes as input the robots previous state and a set of command values that are ought to be executed by the robot. The output is the new robot state after the commands where executed for a given period of time. This general formulation allows to use the same interface for robots with different locomotion types like AUVs, surface vehicles, glider or even crawling robots.

For the AUVs in the simulated experiments a simple motion model was used, which is based on the drive configuration of the Doris AUV. The basic configurations layout is similar to those of many long range AUV, with one thruster at the end of the submersible, followed by an elevator and a steering rudder in the wake field. This model expects three control commands, one for the thrusters revolutions per minute and the other two for the deflection of elevator and rudder. In this simple model, mass and buoyancy is neglected. Thruster RPM will be translated linearly into vehicle speed and deflections of elevator and rudder will be translated directly into differences in pitch and yaw angle respectively.

5.1.4. Sensor Models

Vehicles navigate based on the sensory input they get from the sensors they are equipped with. In simulation these sensor values will be replicated by sensor models. For each sensor in the vehicle there is also a sensor model. Since one goal of this thesis is to investigate the impact of cooperative localization on the navigation capabilities of underwater vehicle, it is crucial that the sensor models mimic the real sensors as close as possible.

The sensory equipment of the simulated AUVs will be based on those sensors which are installed on the Doris AUV from the SMIS project. Figure 5.2 gives an overview of all the sensors that are utilized for navigation. In the following, the mathematical models of each sensor will be discussed in more detail.

5.1.4.1. IMU

An inertial measurement unit is composed of a gyroscope, an accelerometer and a magnetometer, integrated into one device as described in section 2.1.1.2. It is used to measure the orientation of the vehicle and its accelerations, both linear and rotational.

Magnetometer measure the Earth's magnetic field to determine the magnetic north direction, similar to a compass. Instead of simulating complex magnetic field components, the sensor model will access the real north direction, known by the simulator
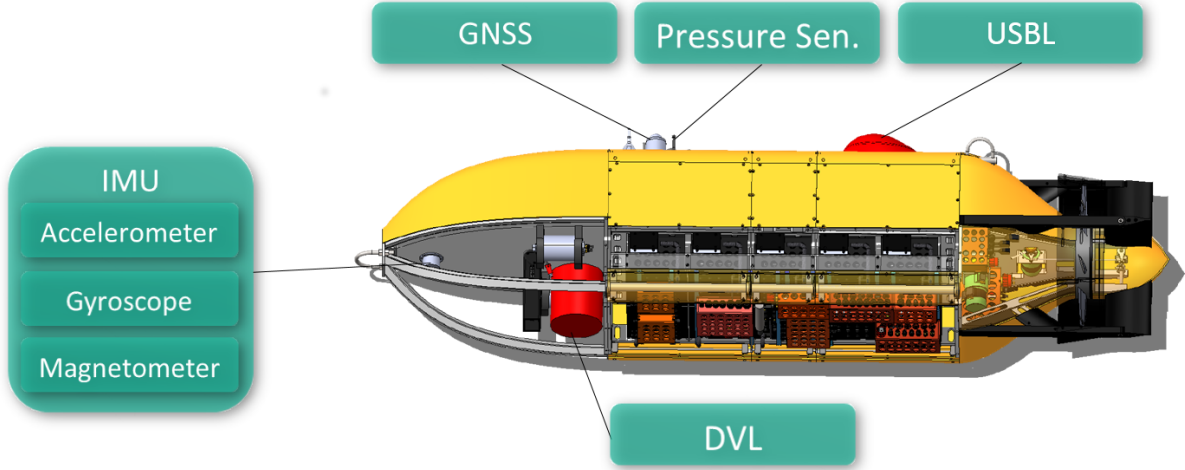
Figure 5.2.: AUV sensors.

and generate a distorted measurement according to

$$\widetilde{\psi}_{mag} = \psi + \varepsilon_{mag} + \eta_{mag} \tag{5.1}$$

where ψ denotes the yaw angle of the vehicle, $\eta_{mag} \sim \mathcal{N}(0, \sigma_{mag}^2)$ is a noise term and ε_{mag} is the magnetic declination at the sensor position as given by the simulation. Distortions of the magnetic field resulting from soft-iron and hard-iron influence will be neglected, since they can be calibrated in real sensors.

The accelerometer measures the linear acceleration $a \in \mathbf{R}^3$ on the three orthogonal axis of the sensor. Due to Earth's gravitation, the sensor will always experience an acceleration a_g towards the down direction. Furthermore, the measurement is subject to noise η_{acc} and will also experience a drift b_{acc} over time so that the actual measurement value $\widetilde{a}$ is modelled as

$$\widetilde{a} = a + a_g + b_{acc} + \eta_{acc} \tag{5.2}$$

with a_g as the gravity vector pointing downwards with constant magnitude $9.81 m/s^2$, $\eta_{acc} \sim \mathcal{N}(0, \sigma_{acc}^2)$ and b_{acc} as the in-run bias. The acceleration bias error can change over time due to temperature changes and mechanical stress. However the sensors internal filter is able to correct the bias during stationary phases, so that it does not grow without bounds. When the magnitude of a_g and $\widetilde{a}$ are equal, the sensor only experiences the acceleration by the gravity and the bias can be estimated reliably. When the measured acceleration is much greater than the gravitational acceleration alone, the estimation becomes less reliable. In the model this is implemented via a reliability factor

$$\rho_g = 1 - |1 - \frac{|a_g|}{|\widetilde{a}|}|. \tag{5.3}$$

Here ρ_g equals one when the bias can be estimated reliably and drops when the measured acceleration increases.

The gyroscope measures the turning rate $w \in \mathbf{R}^3$ on the three orthogonal axis of the sensor. Like the acceleration, this measurement is subject to noise η_{gyr} and will also experience a drift b_{gyr} over time so that the actual measurement value $\widetilde{w}$ is modelled as

$$\widetilde{w} = w + b_{gyr} + \eta_{gyr} \tag{5.4}$$

for the implementation with $\eta_{gyr} \sim \mathcal{N}(0, \sigma_{gyr}^2)$. The drift b_{gyr} is modelled as random walk and depends on the quality of the gyroscope. Optical gyroscopes can have a drift of 0.0035 degree per hour while cheaper MEMS based sensors have up to 70 degree per hour. The Doris AUV is equipped with a sensor that is specified with a drift of 10 degree per hour and and this value will also be used in the model. The Coriolis force of Earth's rotation is also measured by the real gyroscopes. Since this influence will be automatically corrected by the sensor when the approximate global location is known, we assume that it can be neglected in this sensor model. By Tailor expansion we get the orientation

$$\hat{\theta}(t + \Delta t) = \hat{\theta}(t) + \dot{\hat{\theta}}(t)\Delta t \tag{5.5}$$

with Δt as the inverse of the sensors sample frequency, $\dot{\theta}$ as $\widetilde{w}$ and $\hat{\theta}(t)$ as the orientation estimation from the last time step. The orientation error increases over time and needs to be corrected. Correction is done by means of Earth's gravitational field for roll and pitch angle and magnetic field for yaw angle (strap down) inside the real sensor. The roll and pitch correction in the model is based on the previously used reliability factor so that

$$\theta_{cor} = \rho_g(\theta(t + \Delta t) - \hat{\theta}(t + \Delta t)) \tag{5.6}$$

with $\theta(t + \Delta t)$ being the real orientation known from the simulation.
For the yaw correction, the magnetic north is used

$$\psi_{cor} = \widetilde{\psi}_{mag} - \widetilde{\psi}. \tag{5.7}$$

The correction terms are then added to the estimated orientation to yield the final orientation output of the sensor. By adjusting the noise terms and measurement resolution appropriately, this IMU model generates measurements that are in accordance with the performance specifications of the reference sensor (Xsense MTI-g 700).

5.1.4.2. DVL

Doppler Velocity Logs are acoustic sensors that utilize the Doppler effect to measure the velocity over ground as well as the distance to the ground, as described in section 2.1.1.4. In order to work, a DVL needs bottom lock, meaning the sea ground must be in range of the sensory apparatus. To verify if this is given in the DVL model, the scene class can be queried for the terrain map in the close proximity of the sensors

current position. If there is no terrain in range of the sensor, no measurement will be triggered since the sensor is not close enough to the ground. When a measurement is triggered, the terrain data is transformed into the sensor frame of the DVL and the unit normal vectors v_n of the terrains triangulation vertexes will be computed. A DVL usually consists of several individual transducers (in this case four) which are tilted so that their beams are pointing in different directions. Now only the vertex normal vectors are selected which lay within one of the beam cones, given by the beam direction v_b and its opening angle. Subsequently the bearing angle between each remaining vertex normal vector and the beam directions are computed, in order to figure out the reflection path per vertex. When the bearing angle is greater than a threshold, the reflected beam does not reach the sensor and therefore it can not be used for the measurement. When the at least one bearing angle is smaller than this threshold, the respective transceiver receives a reflection and is able calculate the range to the ground and contribute to a velocity measurement. At least three of the transceivers must contribute to the velocity measurement or the sensor is unable to determine the velocity.

When this condition is satisfied the velocity is measure with

$$\widetilde{v} = v + \eta_{dvl} \tag{5.8}$$

where v denotes the true velocity in the sensor frame and $\eta_{dvl} \sim \mathcal{N}(0, \sigma_{dvl}^2)$ is the measurement noise term. For the final distance to ground measurement, we take the median of the four transceiver measurements. Noise, range and transducer parameters are take from the reference sensor which is Teledyne's WHN 600.

5.1.4.3. Pressure Sensor

A pressure sensor provides an inexpensive way to accurately measure the depth of a vehicle. The comparably simple measurement approach allows for a equally simple sensor model.

$$\widetilde{d} = d + \eta_{prs} \tag{5.9}$$

with d as the real depth and $\eta_{prs} \sim \mathcal{N}(0, \sigma_{prs}^2)$ a noise term. The noise parameter has been selected so that it reflects the precision of the reference sensor (SBE 50 from Sea-Bird Electronics). While pressure sensors are affected by ambient temperature drift and a static bias, these influences can be calibrated and therefore have not been considered in this model.

5.1.4.4. GNSS

For underwater navigation, global navigation satellite systems are not accessible directly and play only a subordinated role in the cooperative localization. Therefore,

this sensor model is not very sophisticated. The GNSS measurement will be composed only of the horizontal position

$$\widetilde{p}_{ne} = p_{ne} + \eta_{gnss} \tag{5.10}$$

with p_{ne} as true horizontal position and $\eta_{gnss} \sim \mathcal{N}(0, \sigma_{gnss}^2)$ as noise term. In the experiments σ_{gnss} is set to $3m$, which is a trade-off between the higher accuracies that are possible with DGPS and the slightly worse precision at the open ocean where DPGS is not available.

5.1.4.5. USBL

As mention in the introduction of this chapter, the USBL sensor model is treated in the following section 5.2 separately, due to its importance for this work.

5.1.5. Software Agent

An agent is the software system that governs a robots actions from the perceptual processing over decision making to the coordination of the scheduled actions. The complexity of software agents usually increases with the degree of autonomy. To discuss the details of the internal mechanism used for the AUV agents would be out of the scope of this work. Instead, only some of the key features, which where used in the experiments, will be mentioned here.

5.1.5.1. World Model

The world model is a software module that is responsible for combining the perceptual input of all sensors into a coherent representation of the robot and its environment. This information can then be accessed by other modules e.g. to adjust the course to a target location or follow a chemical trace measured by a sensor.
In this work, the vehicle state is defined as a vector $\vec{x}$ composed of position $\vec{p}$, velocity $\vec{v}$, orientation $\vec{q}$, acceleration $\vec{a}$ and turn-rate $\vec{w}$ as well as a $15\mathrm{x}15$ covariance matrix P. While the world model also contains additional information about the environment, like the distance to ground or maps of the seabed, the focus of this work is based solely on the vehicles own state.
One of the sub-modules of the world model is the state observer which handles the fusion of all perceptual data regarding the vehicle state. The sensor fusion framework will be discussed in more detail in section 5.3.

5.1.5.2. Locomotion Behaviour

Locomotion behaviours can be assigned to an agent as motion tasks. Different behaviours have been implemented such as approach target, path following, pursuit of another vehicle, region evasion and many more.
Most of the more complex task require knowledge about the own vehicle state and sometimes also the location of features or other vehicle states. Since the main objective of this work is to investigate the localization capability of a vehicle, the execution of such tasks could mutually interact with the state estimation quality. In order to prevent such effects in the evaluation, only the wander locomotion behaviour has been used in the experiments, which does not require information about the vehicle state and hence is independent from the localization precision. When the wander locomotion behaviour is active, the agent executes a random walk in the north-east-plain while keeping its depth. This is done by frequently changing to a new random course after a predefined time interval.

5.1.5.3. Communication Schemes

Communication schemes can be assigned to an agent as proactive or responsive communication instruction. A scheme consist of a trigger condition, a message type as well as optional fields that further specify the message content, e.g. the recipient of the message if it is not a broadcast. Two different types of conditions can be selected when creating a communication scheme. Time triggered schemes will initiate the proactive transmission of a message at a predefined start time and may include a cyclic repetition of the transmission until a set end time is reached. Action triggered schemes on the other hand initiate message transmissions as a response to a measured value, a internal state or to a previously received message. The mechanism of communication schemes allows to flexibly define communication patterns in network, which will be applied in the experiments.

5.2. USBL Modem Model

A USBL modem is a sensor and a transceiver in one device, as it is able to transmit and receive messages and also can measure the direction and relative position to another USBL modem. Consequently both functionalities need to be considered in the simulated model. The USBL model deserves particular considerations and fine tuning, since it is the most crucial sensor for the cooperative localization experiments that will follow. Even though the cooperative localization described in section 3 does not rely on the specific USBL localization technique, the localization performance improves when the uncertainty of the proprioceptive sensors are known accurately. Accordingly, it makes sense to closer investigate an actual device, and thereby getting

an insight on the performance and limitations of this technology. While the fundamentals of USBL localization is given already in section 2, this section focuses on the mathematical and programmatic implementation of the USBL model in the simulation. There are different influences to measurements and communication which need to be taken into account, in order to have a reliable model of this complex device. A substantial amount of time has been invested to adapt the USBL model to best match the performance of the real device, narrowing the gap between simulation and reality as much as possible. This section will start with an introduction to the reference USBL modem that is going to be emulated by the USBL model, followed by a section about the effects on localization that have been considered in the model. Conclusively, the integration into the simulator will be explained.

5.2.1. Reference USBL modem

Evologics S2CR 7/17 USBL Underwater Acoustic USBL modem is the physical reference Sensor that will be emulated by this model. It operates on the frequency band between 7 kHz and 17 kHz. The relatively low frequency allows for long range communication up to 10 km under good conditions [50]. As mentioned above, USBL modems are hybrid devices that fulfil two functions, communication and localization.
Communication between modems are realized in two modes, called burst mode and instant message mode. The Burst mode is used for point to point transmission with higher data rates. In this mode the modem utilizes its sweep spectrum carrier technology to analyse parameters of the current channel and optimize its modulation accordingly. The instant message mode is designed for network communication and operates without analysing the channel prior to the transmission. Instead the modem sends independent data packages with a maximal size of 64 Byte. While the burst mode has a much higher transmission rate, the instant message mode allows for better medium access control and flow control techniques, which are highly desired in a network. Because of the irrelevance of the burst mode to the this work, the focus will be on the instant message mode. In order to seamlessly switch from the real device to the model, a subset of the modems interface was implemented into the simulated model, allowing the use of the same commands for the real hardware and the model.

For localization, the USBL uses a set of five hydrophones. When a signal from another modem arrives at the device, it will arrive at each hydrophone at a slightly different time. Using the time difference of arrival (TDOA) between those hydrophones allows for the estimation of the direction $\vec{z}$ of the incoming signal and thus its source. The details of the localization algorithm are not publicly available due to commercial interests of the manufacturer, however some hints on the signal processing can be derived from the available information in the manual and from the interfaces of the device. For example the general layout of the hydrophone configuration, which is of

a) USBL reference frame   b) connectivity map
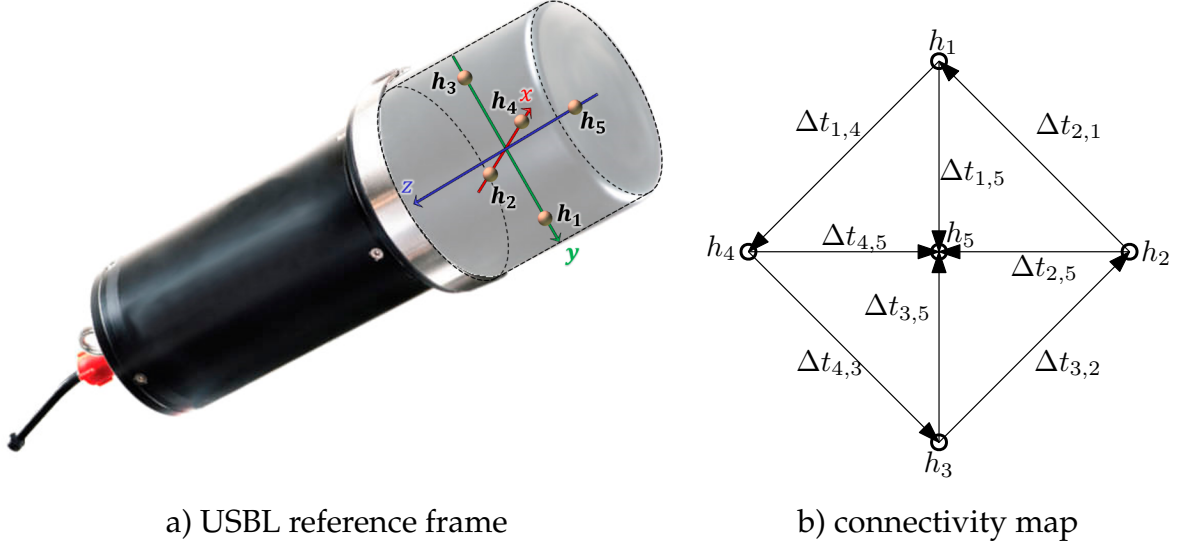
Figure 5.3.: Configuration of hydrophones in the USBL reference frame (a) and connectivity map (b) for used time difference of arrival measurements.

major importance for the localization performance, is mentioned in the manual [51], however the exact location of the hydrophones are not given. Furthermore, the device can be configured to output the time difference measurements that have been used for a direction estimation, as well as a set of six internal direction estimates. Based on these informations, it is possible to reverse engineer the internal signal processing algorithm for the purpose of the USBL model.

In figure 5.3 the hydrophone configuration is shown as well as the hydrophone pairs that are used for the TDOA measurements. Summarising the hydrophone pairs and respective position difference into matrix form yields

$$S = \begin{bmatrix} \vec{s}_{1,5}^{\mathsf{T}} \\ \vec{s}_{2,5}^{\mathsf{T}} \\ \vec{s}_{3,5}^{\mathsf{T}} \\ \vec{s}_{4,5}^{\mathsf{T}} \\ \vec{s}_{1,2}^{\mathsf{T}} \\ \vec{s}_{4,1}^{\mathsf{T}} \\ \vec{s}_{3,2}^{\mathsf{T}} \\ \vec{s}_{3,4}^{\mathsf{T}} \end{bmatrix} = \begin{bmatrix} x_1 - x_5 & y_1 - y_5 & z_1 - z_5 \\ x_2 - x_5 & y_2 - y_5 & z_2 - z_5 \\ x_3 - x_5 & y_3 - y_5 & z_3 - z_5 \\ x_4 - x_5 & y_4 - y_5 & z_4 - z_5 \\ x_1 - x_2 & y_1 - y_2 & z_1 - z_2 \\ x_4 - x_1 & y_4 - y_1 & z_4 - z_1 \\ x_3 - x_2 & y_3 - y_2 & z_3 - z_2 \\ x_3 - x_4 & y_3 - y_4 & z_3 - z_4 \end{bmatrix} \in \mathbb{R}^{8 \times 3} \tag{5.11}$$

with $\vec{s}_{i,j}$ denoting the vector from hydrophone i to hydrophone j. Respectively the time difference of arrivals can be written as

$$\Delta T = \begin{bmatrix} \Delta t_{1,5}, \Delta t_{2,5}, \Delta t_{3,5}, \Delta t_{4,5}, \Delta t_{1,2}, \Delta t_{4,1}, \Delta t_{3,2}, \Delta t_{3,4} \end{bmatrix}^{\mathsf{T}} \in \mathbb{R}^8 \tag{5.12}$$

Obtaining a direction estimate from ΔT can now be achieved by solving the linear equation system given by

$$\vec{z} = -cS^+ \Delta T \tag{5.13}$$

63

where $S^+ = (S^\mathsf{T}S)^{-1}S^\mathsf{T}$ is the pseudo-inverse of S and c is the sound velocity at the receivers location. The resulting unit vector $\vec{z}$ is then pointing towards the source of the signal. It is to mention that the distance to the source can not be derived from the vector length. As mentioned in chapter 2, there are several methods to measure the distance. The basic reference USBL uses the round trip time method to determine the distance, however it is possible to upgrade the devices with atomic clocks, which allows for the use of range estimations that are based one way travel time. If a range measurement is available, the device will output a so called $USBLLONG$ message, which holds the relative position to the source as a euclidean vector given by $r\vec{z}$ in the reference frame of the sensors. A $USBLANGLE$ message is outputted if only a direction estimate, without range measurement, is available. $USBLANGLE$ messages hold the direction estimate to the source in the form of azimuth and elevation angle, again in the reference frame of the sensor. In order to differentiate between the direction in Cartesian coordinates and spherical coordinates, spherical coordinate vectors will be marked as $\vec{z}^\circ = [\psi, \phi, r]^\mathsf{T}$.

An important property of equation 5.11 is, that it is independent of the sound velocity if matrix S is of rank three, which is given by the hydrophone configuration in figure 5.3. For every $USBLANGLE$ and $USBLLONG$ measurement, the device also outputs a $USBLPHYP$ message. This message holds a set of six direction estimates in Cartesian coordinates, where each estimate is computed independently, based on a hydrophone triplet as shown in table 5.1. By using three hydrophones, it is only possible to estimate the source direction in the plane that is spanned by these three hydrophones. For the given configuration that means, triplets $1-4$ can only measure the direction in the X-Y plane and triplets 5 and 6 can only detect the direction in the Y-Z plane and X-Z plane respectively. Also, by reducing the rank of S, the sound speed can not be neglected any more, which has an impact on the direction estimate if the correct sound speed at the sensors position is unknown. The manufacturer does not state how the $USBLPHYP$ message is used for $USBLANGLE$ or $USBLLONG$ estimations, however one possible use case is that those estimates are used only to detect if there are outliers in the ΔT measurements, caused by the channel or by a faulty hydrophone. While the simulation model could also represent the defect of a single hydrophone, it would go to far to recreate the internal outlier processing of the device. Therefore, the $USBLANGLE$ and $USBLLONG$ estimation in the model will be based on equation 5.11 with all five hydrophones intact.

5.2.2. Effects to USBL measurements

Acoustic localization techniques like USBL are known to have many possible influencing factors, which makes them difficult to model. Before an measurement is made at the device there are typically a sequence of actions that need to be considered. First an acoustic signal is send by one USBL device with a characteristic directivity. This

Table 5.1.: Hydrophone groups in a $USBLPHYP$ message with used hydrophones and ΔT measurements

Triplet No.	Hydrophones	Δt	Estimation Name
1	h_1, h_2, h_3	$\Delta t_{1,2}, \Delta t_{3,2}$	$\vec{z}_{p_1}$
2	h_4, h_3, h_2	$\Delta t_{3,2}, \Delta t_{3,4}$	$\vec{z}_{p_2}$
3	h_4, h_3, h_1	$\Delta t_{4,1}, \Delta t_{3,4}$	$\vec{z}_{p_3}$
4	h_4, h_1, h_2	$\Delta t_{1,2}, \Delta t_{4,1}$	$\vec{z}_{p_4}$
5	h_1, h_5, h_3	$\Delta t_{1,5}, \Delta t_{3,5}$	$\vec{z}_{p_5}$
6	h_2, h_5, h_4	$\Delta t_{2,5}, \Delta t_{4,5}$	$\vec{z}_{p_6}$

Table 5.2.: Stages of a modelled acoustic signal and the considered effects to the USBL measurments.

Stage	Influencing effect
Signal emission	Directivity sender
Signal propagation	Refraction effects Multipath arrivals Transmission loss
Signal detection	Directivity receiver Ambient noise Signal interference
Direction estimation	Sound velocity error Measuring noise Motion induced error

signal propagates through the acoustic channel which might absorb, deform and refract the signal. When the acoustic wave reaches another, receiving, USBL device, it might be detected, depending on the receivers orientation, directivity and the signal to noise ration at the receiver. If the signal reaches the device, a correlation processing will detect the time difference of arrival between the hydrophone pairs mentioned above. Based on these time difference measurements, the USBL device will estimate the signal direction as stated in the previous subsection.

The effects that have been investigated in this work are listed in table 5.2. In the Following there will be a short explanation to each effect as well as a description of the realization in this model.
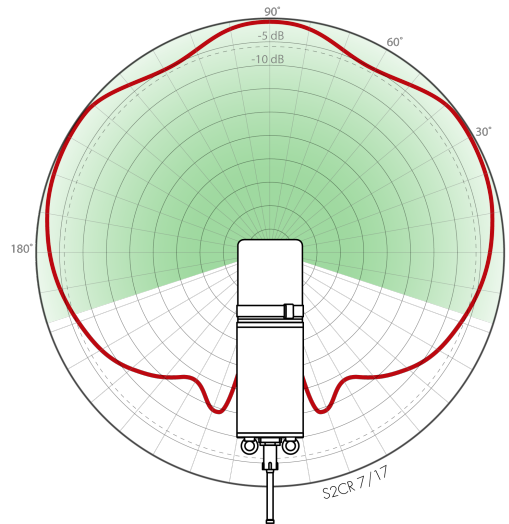
Figure 5.4.: Directivity pattern of a S2CR 7/17 USBL modem [52].

5.2.2.1. Directivity

Directivity plays a role in sending as well as receiving. For sending devices, directivity gives a measure of how strong an emitted signal is concentrated in comparison to an ideal isotropic radiator which emits in all directions uniformly. A strongly concentrated signal will cover a smaller area but has a higher range because it looses less energy on the way, due to the focus. Directivity applies also for receiving devices, where it represents the direction dependent sensibility of an antenna. According to the manufacturer, the reference USBL has an opening angle of around 210 degree. Sometimes the directivity of an antenna can be affected by the surrounding structures e.g. when the device is mounted on an ship or AUV, the hull of the vehicle will produce a signal shadow for certain directions, depending on the hull structure and the antenna position. Also baffles might be utilized during reception to cancel out directions that produce noise, e.g. for an USV the water surface is a big source of noise which can be damped by a baffle. In order to allow for an flexible adaptation of the directivity in the model, it is possible to specify the opening angle for each instance of the USBL model separately. The opening angle will be used to check if a receiving device is able to detect an signal from the incoming direction. When emitting a message, the directivity is used to find possible receivers that lie inside of the beam angle.

5.2.2.2. Refraction Effects and Multipath Arrivals

Refraction in acoustic underwater signals influences many aspects of underwater communication and acoustic localization. For the implementation of the model we will confine to three effects that are considered most influential to USBL which are

Distortion of the time of arrival:
> Depending on the sound velocity profile it is possible for a given acoustic signal to reach a target location faster, or with a higher energy, when it follows a curved path instead of a direct line from source to target. This has a consequence in the range estimation of the USBL as it uses the round trip time of a signal and computes the distance based on a fixed sound velocity. Also the underwater communication is affected if an exact time of arrival is required e.g. for synchronization between nodes.

Distortion of the angle of arrival:
> Similar to the ToA the angle of arrival is affected since the incoming signal direction differs form a straight line between source and target, leading to a measurement error that is dependent on the sound velocity profile.

Multipath propagation:
> This effect occurs mostly in shallow water and harbour scenarios but can also occur in deep water environments where reflected signals from the sea bed, the surface or underwater structures are perceived by the sensor. Such echoes can happen to be recognised as the predominant signal by the USBL and will produce entirely wrong measurements.

The refraction actually takes place in the channel and is therefore physically and logically independent from the USBL modem, however, it directly affects the USBLs performance and is therefore mentioned here. The field of acoustic field computation is generally used to model refraction effects in the underwater channel. It is a well studied field and many good model approaches exist of which two models have been integrated into the simulation for testing. First the Bellhop model, which is a very accurate model but computationally complex, and second a simpler ray tracing model which is not as powerful but less computational intensive. Both models will be described briefly here.

Bellhop:
> Among the most popular methods for acoustic field computation is the bellhop model, which originates from [53] and is used in many oceanographic and UWSN related research frameworks. Bellhop uses Gaussian beam tracing for the prediction of acoustic pressure fields and is well suited to model the above mentioned effects and more. For the integration into the simulator, the acoustic toolbox [54] for Matlab was used which already include wrappers to the bellhop binaries. The acoustic toolbox includes also other acoustic field models, however only the bellhop model has been tested with the simulation. For

each acoustic transaction the bellhop model takes an environmental file as input, with informations about the sound velocity profile, sea bed structure, the source location, radiation characteristics and sending frequency of the source as well as the receivers locations. There are several output modes of which one computes the arrival time and angles at the receivers locations.

Ray tracing:
The ray tracing algorithm takes as input a sound velocity profile, the depth of the source and a radiation angle. It then computes the path of the ray by assuming a piecewise linear sound velocity gradient and integrating the rays position until a given horizontal distance to the receiver is travelled or a maximal propagation time is reached [55]. Like the bellhop model, this method can give the arrival time and arrival angles as output. However it is not guaranteed that, for a given radiation angle, the ray will reach the receivers location. Therefore, the method was extended to follow an optimization process that tries several radiation angles to find one that minimizes the passing distance between ray and receiver. Despite the additional optimization process, this method is faster than the Bellhop model. In certain cases the optimization process may not find the global optimum, but a solution from a reflected signal. In this way, also multipath propagation is considered in this model.

The simulation uses the ray tracing as default channel model because it is generally faster, however the bellhop model can by applied if accuracy is desired.

5.2.2.3. Sound Velocity Error

In the reference USBL, the range between sender and receiver is estimated by either the round trip time or, if time synchronisation is available, by time stamps that are send along the normal data. Both methods require the knowledge of the sound velocity in the medium to adequately estimate the range. Since the USBL assumes a constant sound velocity throughout the signal path, the estimated range will differ from the real range based on the sound velocity profile in the water. Also refraction effects will have an influence on the signal path, leading to a longer propagation time and hence to an error in the range estimation. In the simulation, this effect is already taken into account by using a channel model, see point "Refraction Effects and Multipath Arrivals" above.

5.2.2.4. Transmission Loss

Transmission loss (TL) is a parameter that compares a signal intensity at a given range from a source to the intensity at e.g. one meter from the source. By looking at the

combination of TL and transmission source level (SL) we can determine the received source Level L_s in respect to the range from the source with

$$L_s = SL - TL = 10\log\frac{I(1m)}{I_{ref}} - 10\log\frac{I(1m)}{I(r)} \tag{5.14}$$

$$L_s = 10\log\frac{I(1m)}{I_{ref}} + 10\log\frac{I(r)}{I(1m)} \tag{5.15}$$

$$L_s = 10\log\frac{I(r)}{I_{ref}} \tag{5.16}$$

The received source level is the ratio between the reference signal Intensity and the actual intensity at range r in dB.

Since transmission loss occurs while the signal propagates through the channel, it should be taken care of by the channel model as well. In fact, transmission loss is inherently calculated in the bellhop model, which uses pressure fields for the beam tracing. The ray tracing channel model on the other hand does not natively calculate the transmission loss, so we need to implement our own TL method.

Transmission loss results from geometric loss due to signal spreading and attenuation due to absorption and signal scattering by the water

$$TL = TL_{sp} + TL_{at} \tag{5.17}$$

For the spreading loss we assume an ideal isotropic radiator that emits a signal in all directions equally, so that the intensity function is

$$I(r) = \frac{1}{4\pi r^2} \tag{5.18}$$

This yields the the ratio between the reference intensity at one meter and an arbitrary range

$$\frac{I(1)}{I(r)} = \frac{4\pi r^2}{4\pi 1^2} = r^2 \tag{5.19}$$

Inserting this into the TL formula yields the transmission loss due to signal spreading

$$TL_{sp} = 10\log(r^2) = 20\log(r) \tag{5.20}$$

Transmission loss to signal spreading is the most dominant factor, however the attenuation also needs to be considered.

A part of the signal energy will be absorbed by the sea water because of its dissipative nature. This attenuation loss is far more complex to model, because it depends on several parameters like signal frequency along with water properties like temperature, pressure and even chemical composition. In practice the attenuation is therefore modelled as

$$TL_{at} = \alpha(r)dB \tag{5.21}$$

where for α there exist lookup tables for different bodies of water, signal frequencies and so on. The simulation will use a α that corresponds to the $7 - 17kHz$ band of the USBL and water conditions that match typical middle Atlantic sea water. The interested reader is referred to [56] for a detailed explanation on the topic of transmission loss and underwater acoustic in general.

5.2.2.5. Ambient Noise

Ambient noise from waves, wind and ship traffic can greatly impair acoustic sensors that are close to the surface. The simulation allows to define ambient white noise sources as a tuple of position, reference source level and geometry, e.g. a plain for the water surface or a point sources for a ships propeller. This noise is subject to transmission loss (see above), but can lead to missed acoustic signals when the signal to noise ratio drops below a threshold at the USBLs position.

5.2.2.6. Signal Interference

Acoustic sensors are common in the underwater domain. As a result, interference between multiple acoustic device have to be considered. In addition to an acoustic communication device like the USBL modem, in many cases mobile sensor nodes are equipped with DVL for navigation and a side-scan sonar or a multi-beam sonar to execute the monitoring/surveillance task. Although these sensors might operate on different frequencies, interference is likely to impair their performance nevertheless. In order to reproduce these effects, every acoustic sensor has to be modelled and simulated in a common channel like the bellhop model mentioned above. While the bellhop model is theoretically capable to produce good results, it was not considered to implement this solution because of the computational burden for the simulation. Instead of modelling the acoustic pressure field, a computationally lighter method was used. Since the time of arrival of a given acoustic USBL signal is known for each recipient, this information can be used to detect packet collisions. Each recipient stores an incoming message in a acoustic buffer with timestamps that mark the begin of the reception of the message. When the amount of bytes in the message is known, it is possible to calculate the signals length. Timestamps and signal length form a time window. If there are two messages in the acoustic buffer with overlapping time windows, a collision occurred. This method is lightweight and can be implemented in the USBL model, instead of using a complex channel model. However it requires knowledge of the signal time and time of arrival which is currently only implemented for the USBL model. Therefore, interference with other sensors are not modelled here, but can be implemented with relative ease, if desired.

5.2.2.7. Measuring Noise

Like any sensor, USBL is also affected by measuring noise. In contrast to systematic errors, measuring noise follows a random process, which is mostly modelled by some kind of distribution function. The manufacturer states the root mean square error of the bearing angle to 0.25 degrees, however this does not account for an error that is dependent on the hydrophone configuration. In order to allow for a noise model that regards the measuring principle, measuring noise should be added where it occurs. For USBLs, measuring noise ultimately applies on the sensing elements, which are the hydrophones. Time measurements of the hydrophones are subject to several types of error, which are propagated to the direction and range calculation. On one hand the noise in the signal detection process, which highly depends on the signal structure and the correlation processing of the device and on the other hand noise in the hardware of the hydrophone as well as the analogue-digital-converter sampling might play a role. These noise sources are hard to model, especially when the underlying methods and hardware specifications are unknown. A common practice is therefore to empirically determine the noise, either by simulations or, where possible, by real experiments.

In [57] the authors examine noise for different USBL modems, however the results only give a rough estimation of the true distribution as there is no ground truth data for more precise analysis. Furthermore the deviation is also only specified as the quadratic mean deviation and it is unclear to which extend the effects mentioned here are considered in the paper. In [58] the authors evaluate USBL localization performance with a configuration of four hydrophones by utilizing a Monte Carlo simulation. The authors apply white Gaussian noise with zero-mean and standard deviation of $0.01/c$ s to the ΔT measurement and calculate mean error and standard deviation of azimuth and elevation over 1000 runs. By employing the same method, we can analyse how noise at the ΔT level effects the direction estimates, for our hydrophone configuration. An error analysis of the full spherical aperture was conducted, evaluating direction errors, when applying noise on the ΔT level according to

$$\Delta t_{i,j} = \frac{\vec{z} \cdot \vec{s}_{i,j}}{c} + \eta_{t,i} + \eta_{t,j} \tag{5.22}$$

with $\eta_t \sim \mathcal{N}(\mu_t, \sigma_t)$ being additive white Gaussian noise. Each η_t term represents noise at the time of arrival level of one hydrophone, expressing deviations induced by several sources like the correlation processing of the signal, the sampling frequency of the analogue-to-digital converters as well as noise at the hydrophones themselves. In figure 5.5 the mean bearing error and the bearing standard deviation is shown for $\eta_t \sim \mathcal{N}(0, 200ns)$. The bearing error is the angle that is spanned between the true arrival direction and the resulting arrival direction estimation according to equation 5.13 with noisy ΔT measurements.

A detailed discussion on how to find a good value for σ_t is given in the evaluation section 6. Here figure 5.5 is meant to give an impression on the impact of the noise to the direction estimation. The maximal mean bearing error of around 0.3 degree
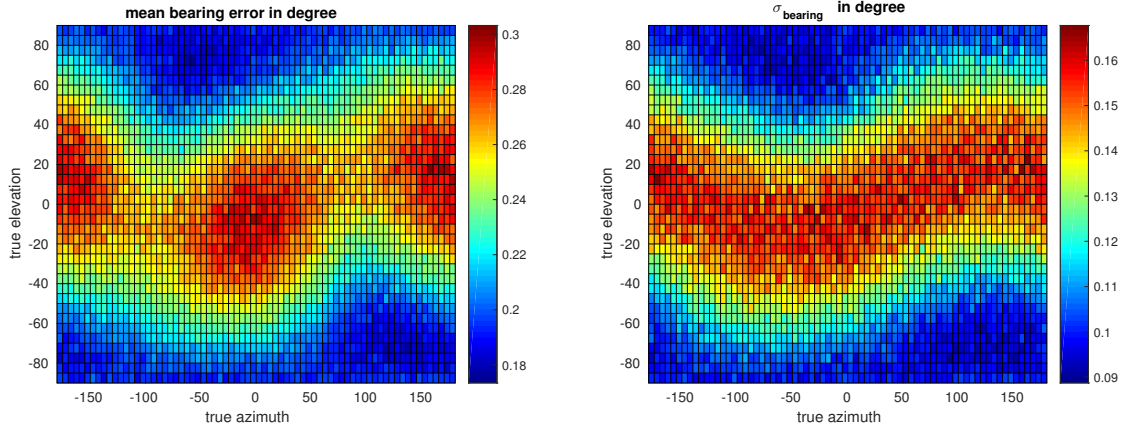
Figure 5.5.: Mean bearing error (left) and standard deviation (right) resulting from noise in ΔT for a full spherical spacial analysis with five degree steps for arrival direction and 1000 samples per arrival direction with $\eta_t \sim \mathcal{N}(0, 200ns)$.

results in an Euclidean error of about $26m$, assuming a slant range of $5000m$. Also the root mean square error over all bearing errors results in 0.268 degree, which is close to the value of 0.25 given by the manufacturer.

5.2.2.8. Motion Induced Error

When a receiver experiences a velocity during a signal reception, the motion may impair the localization performance. Due to the receivers velocity, the time at which each hydrophone will detect the signal may vary from the static case, causing an error in the angle of arrival. This effect, which is visualized in figure 5.6, will be called motion induced error.

In order to account for this effect, we need to find the time difference between t_b, the time at which hydrophone h_b would encounter the signal in a static case, and $t_{\tilde{b}}$, the time at which hydrophone b will detect the signal in the dynamic case. Due to the motion induced error the basic TDOA formula will have a additive error term Δt_{vel}, so that

$$\Delta t_{a,\tilde{b}} = \Delta t_{a,b} + \Delta t_{vel} \tag{5.23}$$

and

$$\Delta t_{vel} = \Delta t_{b,\tilde{b}} = \frac{\vec{z} \cdot \vec{v} \Delta t_{a,b}}{c} \tag{5.24}$$

with $\vec{v}$ as the receivers velocity in the sensor frame. Applying 5.24 to 5.23 yields the TDOA measurement including the motion induced error

$$\Delta t_{a,\tilde{b}} = \frac{\vec{z} \cdot \vec{s}_{a,b}}{c} + \frac{\vec{z} \cdot \vec{v} \Delta t_{a,b}}{c}. \tag{5.25}$$
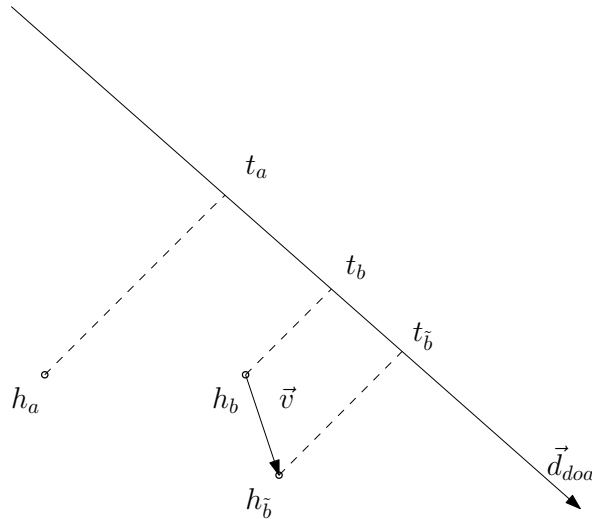
Figure 5.6.: A velocity during the reception of a signal will cause an error in the ΔT measurements.
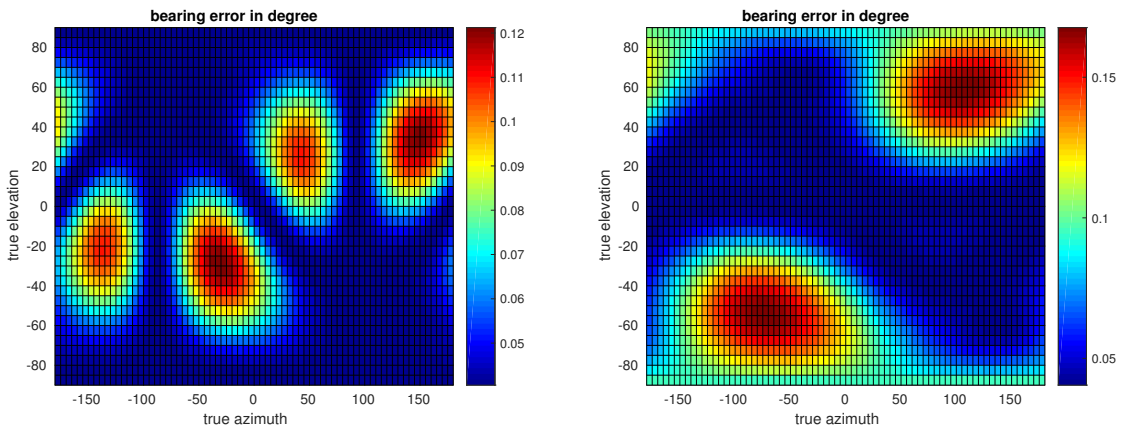
Figure 5.7.: Systematic, motion induced, bearing error for a receiver velocity of $4\,m/s$ in X direction (left) and in Z direction (right) of the sensor frame.

If the motion is orthogonal to the direction of arrival, the scalar product of the two vectors is zero and there is no effect. For slow moving vehicles the motion induced error is generally small, but can make a difference during high velocity surveys. Analysing the estimation error produced by the motion alone, shows that the biggest errors are to be expected when $\vec{z}$, $\vec{v}$ and $\vec{s}$ are aligned. Figure 5.7 shows the systematic bearing error that is produces by Δt_{vel}, assuming a relatively fast survey AUV with a velocity of $4\,m/s$. While a maximal bearing error of 0.12 degree does not appear to be a big issue, for a big slant range this can get significant. For example at $5000m$ this already translates into an deviation of around 10 meter, additional to the other distorting effects mentioned above.

5.2.3. Measurement Model

From the above effects, we can frame a measurement model. The input to the measurement model is the direction to the source $\vec{z}$ as given by the channel model as well as the true sound velocity c given by the sound velocity profile of the scene. Together with the model parameter for the hydrophone constellation S, the noise of the arrival time measurement of each hydrophone η_t and the sensors velocity we can compute the measured time difference of arrival for each hydrophone pair i and j as

$$\Delta t_{i,j} = \frac{\vec{z} \cdot \vec{s_{i,j}}}{c} + \eta_{t_{i,j}} + \eta_{t_{j,i}} + \Delta t_{vel_{i,j}}. \tag{5.26}$$

The USBL will usually use a local estimation of the sound velocity $\hat{c}$ in order to obtain the direction estimate with the differential equation given by equation 5.13.
A direction measurement is triggered when the modem received an transmission from a remote node and the signal to noise ratio (SNR) is above a fixed detection threshold. The signal to noise ratio is influenced by the senders source level and the transmission loss, constituted by the signals travel distance to the receiver. In addition, noise sources in the vicinity of the receiver reduce the SNR.
Apart from the direction, the range can be measured by the signal travel time by employing either a round-trip-time (RTT) or an one-way-travel-time (OWTT) when time synchronization between the modems is possible. The USBL model contains a switch which allows to toggle time synchronization of a sensor instance on or off with the default defined as deactivated. The USBL model calculates the range as

$$r = \frac{t_{RTT}}{2} \hat{c} \tag{5.27}$$

or respectively as

$$r = t_{OWTT} \hat{c}. \tag{5.28}$$

In the first cases the propagation time is measured by the interrogation device by stopping the time from sending a request to a remote node until the arrival of an acknowledgement from the this node. In the later case the message includes a time stamp of the time of departure, so that the propagation time can be computed at the receiver according to $t_{OWTT} = t_{TOA} - t_{TOD}$. For both cases, the acoustic signal and thus its propagation time may be subject to refraction effects, given that the simulated scene provides a sound velocity profile.
Refraction effects take place in the channel model and can not be accessed by the USBL model, so that effectively the direction and range measurements are impaired by the channel. Just like in the real USBL devices, these effects are hard to compensate. In order to reduce complexity and focus on the localization capabilities of the sensors, the simulated experiments in the evaluation section will assume a constant sound velocity throughout the water column.
Apart from emulating measurements, it is also possible to use the USBL model to

estimate the uncertainty of a given measurement. This can be achieved by permuting the ΔT measurements with the empirically determined noise of the arrival time detection. By computing several permuted sets of the arrival time pairs according to $\mathcal{N}(\Delta T, \sigma_t)$ and calculating the direction estimate for each of the sets, we gain knowledge about the probability distribution in direction space. From the multiple direction estimates a covariance matrix can be drawn which simplifies further processing. Figure 5.8 displays such a distribution in the spherical space, which follows a wrapped normal distribution and describes a ellipsoidal surface on the unit sphere. The probability distribution of an USBL measurement is an important characteristic value for the navigation and the proposed cooperative localization in particular.
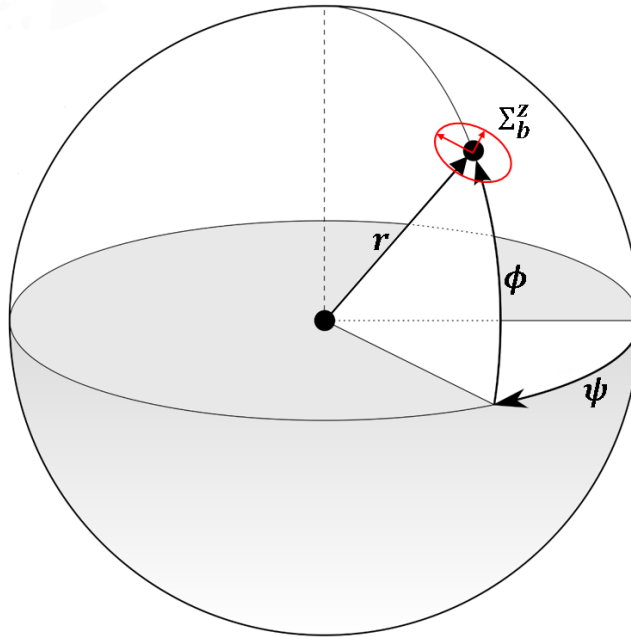
Figure 5.8.: Probability distribution model of USBL measurements in spherical coordinates. The red circle shows the 1σ border of the example distribution on the sphere shell and the red arrows indicate the Eigenvectors.

5.3. Sensor Fusion Framework

In this section the integration details of the multi sensor fusion framework will be explained. This framework was used in the simulated agents and thus in the simulated experiments of the subsequent chapter. For the sensor fusion a particle filter (PF) was implemented and tuned to the specific use case of underwater navigation. First we will outline the general layout of the particle filter and specify some of the tuning parameter that where found reasonable for the task. The subsequent sections

concentrate on the parts of the fusion chain that are related to the specific problem of AUV localization.

5.3.1. Particle Filter Implementation

The sensor fusion is a part of the vehicle agent's world model (see section 5.1.5). Like the other parts of the agent, the sensor fusion algorithm is written in Matlab. It extends Matlab's particle filter implementation by specific functions to handle the AUV sensor set-up. Section 2.2 already covers the general principle of particle filters. This section will therefore focus on the adoptions to the standard implementation of the PF. The control flow of the filter can be divided into three phases which are depict in figure 5.9. In each phase, a customized function will be called to execute the problem specific parts and the rest is handled by the parent class, which allows for a quick and easy implementation.

Among the first steps in designing a state estimation filter is to specify the filter layout. That is, which state parameters should the filter predict, based on which input data. In the case of AUVs the desired output state x is specified as the vehicles position, velocity and its orientation. As input we will assume the sensor set-up of the SMIS AUV with IMU, DVL and pressure Sensor aided by an USBL. The output frequency of the state estimation is set to 10 Hz, which is sufficient to control an AUV with the mass of the SMIS AUV and its consequent high inertia. Another important property of a PF is the number of particles used. During experiments it was found that 100 particles showed a good trade-off between accuracy and performance for this task.

Most of the implementation details of the PF is taken care of by the parent class provided by Matlab. The problem specific parts of the estimation problem are the motion model and the observation model which will be explained here.

5.3.2. Motion Model

The motion model takes the state and the steering command from the previous time stamp to predict the current state. Unlike in Kalman filters, a precise motion model has shown to produce bad results in particle filter estimations. This counter-intuitive behaviour can be explained by the different representations of probability density in Kalman filters and particle filters. In KF the probability density is given by a distribution, often Gaussian, with the predicted state in the center, while in particle filters the density is represented by the distribution of the particle in state space. Consequently, the purpose of the motion model in PF is not to accurately model a state transition but rather the evolution of the probability distribution in the system. Having a very accurate model with little variance results in the particles quickly congregating to a
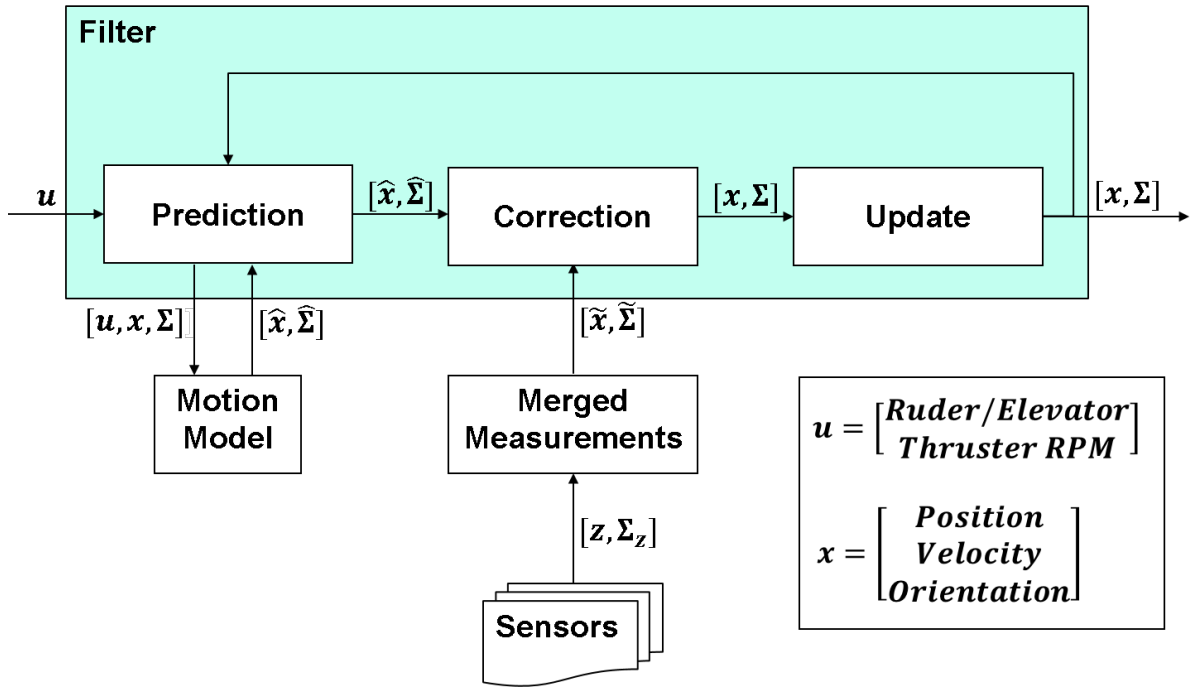
Figure 5.9.: Fusion flow.

few states. Especially with uninformative measurement updates, the PF tends to converge into a single state, which gives a false sense of certainty.

Bearing that in mind, the motion model used in this work doesn't incorporate the vehicles control signals at all. Instead, for each particle a random Gaussian noise is added to the current turn rate and acceleration. Those noised terms will then be used to predict the change in orientation and velocity which in turn are used to predict the change in position. This cascaded approach ensures a plausible, jerk free, trajectory for each predicted particle and a smooth diffusion of the particle swarm as a whole.

5.3.3. Observation Model

Since each sensor operates with a different update rate, their output need to be collected and synchronized before feeding them into the filter. Furthermore the measured properties might not directly represent the desired state parameter, so that preprocessing is required for the measurement values as well. This is done in the observation model. The observation model takes the sensor readings z and Σ_z as input and generates a measurement state $\tilde{x}$ as well as the corresponding covariance matrix $\tilde{\Sigma}$ which are aligned with the estimated state dimensions of x. Matrix Σ_z is either gathered from the data sheet of the specific sensor or it is computed by a sensor model as in the case of DNL.

The pressure sensor supplies an accurate depth measurement with an output frequency of 16 Hz. Measurements in between a state estimation cycle will be buffered and the mean value gets processed further.

A non drifting velocity over ground is measured by the DVL. The DVL is configured with a ping frequency of 2 Hz, however, the output frequency might slightly vary, due to variance in sound velocity and distance to ground. In between DVL measurements and when the sensor does not acquire a bottom lock, the velocity needs to be estimated by the state estimator.

IMU output frequency is configured to 100 Hz and will be buffered in between update cycles. In normal operation only the mean orientation will be further processed, however, if there is no DVL measurement available for more than three seconds, the buffered acceleration and turn rate will be used in conjunction with the previous state prediction to interpolate a velocity.

An USBL does not have per se a regular output frequency and the raw measurements can not be taken for the state estimation directly as it measures the relative position to a transmitting device. The preprocessing of the USBL measurements is the DNL algorithm described in the previous chapter. DNL yields the global vehicle position and the heading as output. Because of the irregular DNL output, which depends on the applied communication scheme, the state estimation needs to cope with long durations in which a position fix is not available.

On every cycle of the state estimation, the measurements of all available sensor readings are collected and preprocessed by the observation model. Due to the varying update rates of the sensors, the dimension of the output measurement state varies as well. During the correction step, only the observed state parameters are considered and the other dimensions will be neglected. If no sensor updates where received in a estimation cycle, the correction step is skipped an the estimation relies solely on the predicted state.

6. Evaluation

This chapter will be used to asses the models and algorithms developed in this work. A paramount portion of this chapter is therefore devoted to the explanation of the conducted experiments as well as the interpretation of their results in the first section. In the second section, those results will then be discussed and contemplated in a broader sense.

6.1. Experiments

The experiments in this section will be partly based upon each other, where first a module is evaluated, which is later used in a more complicated experimental set-up. Because data from real experiments is very hard to obtain in this field, several of the successive experiments will be based on data of only a few actual sea trials. Therefore, the sea trials will be explained in the beginning of this section. In the follow up section the USBL model will be evaluated and compared with measurements of the real sensor. Based on that, the accuracy of the DNL algorithm gets approved with data from the USBL model as well as measurements from sea trials. Finally, the cooperative localization capabilities of DNL will be investigated in multi-vehicle experiments.

Boxplots are a compact way of depicting the important parameters of a distribution, and are therefore used throughout this chapter. Figure 6.1 shows a boxplot and how it is connected with a normal distribution. On each box, the central mark indicates the median, and the bottom and top edges of the box indicate the interquartile range (IQR) of the 25th and 75th percentiles, respectively. The whiskers extend to 1.5*IQR. Every data point further away from the median is considered an outlier and is plotted individually using a '·' symbol. Boxplots give a good expression about the distribution of data samples and will be used to aid the interpretation of the experimental results.
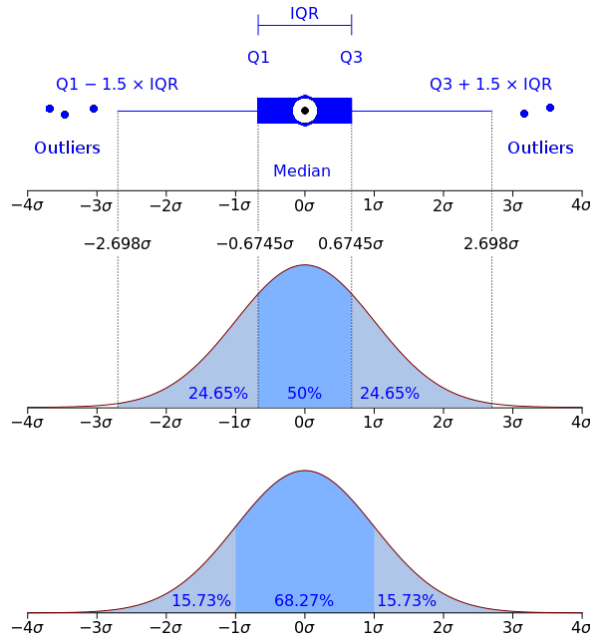
Figure 6.1.: Relationship between a box plot and a Gaussian distribution.

6.1.1. Sea Trials

During the SMIS project (see 1.2), several sea trials were conducted to test the platform in different stages of the development. A central aspect of many trials has been the analysis of the communication and acoustic localization performance, especially for long ranges. While every sea trial has propelled the development of the SMIS system, only a few experiments can be used to evaluate the algorithms contributed by this work. This is due to the very same problem which is approached by this thesis: underwater localization. A reliable ground truth of the position of a mobile submersible is very hard to obtain without proper equipment. One way to produce high accuracy ground truth data is to use a LBL system at the test side as reference. Another option is to capture acoustic or optical images with the target vehicle and register the images with a reference map of the test side. Both methods require elaborated preparation and costly hardware which was neither available during the SMIS project nor within this thesis. As a result, other methods needed to be applied in order to generate a synthetic ground truth with the given resources. This section will explain the set-up of selected experiments which have been used to evaluate the algorithms developed in this work.

6.1.1.1. POS485

The sea trial catalogued as POS485 [59] took place in the middle Atlantic ocean onboard the research vessel Poseidon from 13/05/2015 to 30/05/2015. During this trial

several depth related tests have been conducted for the SMIS project. The most relevant experiment for this work are the long range test for the acoustic communication and localization which took place on 25/05/2015. For this experiment a so called access point (AP) with an attached USBL modem was deployed to the sea bed at around $5000m$ below sea level. The AP itself consists of a frame with buoyancy bodies and a weight. With the weight the AP has a negative buoyancy causing it to descend to the ground. The weight can be released by an acoustic signal, resulting in a positive buoyancy and the surfacing of the AP.

The USBL modem on the AP was programmed to ping a ship mounted USBL modem periodically. On the other side the USBL modem on the ship pinged the submersed USBL periodically encoding its current position and position uncertainty in each ping. Both USBLs logged all incoming messages as well as the signal strength for the duration of the experiment. While the AP descended, the ships USBL received pings with abating intensity until the AP reached a depth of around $1600m$. At this point no more signals were received at the ship's USBL, presumably because of the acoustic noise made by the research vessels engine and propeller. The USBL on the AP however still received the pings sent by the ship. During the submergence of the AP, the research vessel kept its position and was able to detect the APs position via its echo sounder. Upon landing, the approximate position of the AP was confirmed with the echo sounder and the research vessel held its position for around 136 minutes to produce localization data at the AP's USBL. Afterwards, the research vessel started to depart from the AP's position until a distance of 0.5 nautical miles or around $0.9km$. The ship then made a full circle keeping the same distance to the AP. After completing the trajectory, the horizontal distance to the AP was increased to one nautical mile. Again the research vessel kept the distance while circling around the position of the AP. Upon completion of a quarter circle, the horizontal distance was again increased to three and four nautical miles, where the same procedure was executed before the weight of the access point was released and the AP surfaced.

During the whole experiment, the USBL on the AP received pings from the ship's USBL and measured the angle of arrival of those signals. By post-processing the collected data it was possible to determine the APs position and orientation. Together with the known position of the research vessel this set-up led to a reliable data set for the evaluation of the USBL localization capabilities.

6.1.1.2. EMB113

The sea trial EMB113 tock place in the Baltic sea on-board the research vessel Elisabeth Mann Borgese in the time from 24/09/2015 to 30/09/2015. This expedition was mainly focused on tuning of the AUV motion controllers. It was planned to conduct the tuning tests in the relatively deep gotland basin, however bad weather conditions in the test area lead to a replanning. Finally, the experiments were conducted in the wind protected area of the southern Arkona basin close to the Island Rügen. Here the weather conditions were acceptable. However the shallow water of only around $15m$

Figure 6.2.: Research vessel Poseidon in the middle Atlantic sea (left) and submersible access point with attached USBL modem (right).

at some places was suboptimal for the experiments. Not only was it difficult to execute the manoeuvres required for the depth controller but also the acoustic channel properties in the shallow water were cumbering. Despite the shortcomings of the test side, the experiments where executed successfully during September 28th and 29th. A falsely calibrated DVL led to difficulties in the localization of the AUV during the 28th. The error was fixed and on September 29th valuable data could be collected regarding the acoustic localization performance, hence the set-up will be explained here in more detail.

Subject of the tests on the 29th September was the fine tuning of the depth and heading controller of the AUV as well as the performance analysis of the acoustic localization. The AUV sensory navigation equipment included DVL, INS, pressure sensor as well as an USBL. The USBL was programmed to periodically sent state information of the AUV to another USBL which was mounted on the ship. Likewise, the ships USBL sent periodic states of the research vessel as well as steering commands to the AUV. Both USBL had the ACK flag enabled, meaning that they requested an acknowledge of the receiver for every sent message. Every received acknowledgement will trigger an USBLLONG measurement as described in section 5.2. While the research vessel was anchored for the duration of the experiment, the AUV was remotely controlled by an operator on the ship via acoustic link. In order to test heading and depth controller, the AUV undertook a series of manoeuvres including meandering, spiralling up and down, slowly descending in a straight line and many more as can be seen in figure 6.3. For the evaluation of the acoustic localization performance, the AUV position needs to be known precisely. Unlike in the previously described experiment, no real ground truth could be obtained for the AUV state. Instead the logged sensor information was used to estimate the AUV position and pose in post-processing. For this purpose an extended Kalman filter (EKF) was applied that fused the sensor read-

ings from IMU, DVL, pressure sensor as well as the USBLLONG measurements made by the research vessel to track the AUV. A detailed explanation on the implementation of the EKF can be found in [17]. Note that the USBL readings of the AUV have not been used in the EKF as they will be subject of the following performance analysis and their usage would introduce correlations between the state estimation and the USBL performance. With an average depth of around $30m$ the conditions for acoustic localization are rather bad. It is important to note that the USBL measurements of this day showed big noise in the elevation angle caused by multipath propagation and reflections from the sea bed and the water surface. Although all apparent outliers were removed before applying the EKF, it is still possible that noisy USBL measurements distort the state estimation of the AUV.

6.1.2. Evaluation of the USBL Modem Model

In this subsection, the USBL modem model from section 5.2 will be compared to measurements that were taken with the real sensors. With the immense costs of field experiments in the area of maritime technology, simulation is the only viable option to conduct the experiments needed for this thesis. In this regard, a big effort was made to match the model as closely as possible to the performance of the real sensor, to minimize the simulation gap and produce results that resemble the actual system. A particular importance was given to the USBL sensor since it is the most important sensor for the investigation on the cooperative localization.

6.1.2.1. Determining the Hydrophone Positions

Probably the most important tuning parameter for the USBL model is the location of the hydrophones inside the sensor's reference frame. Slight deviations in the hydrophone position will result in huge angle differences. The exact location of the hydrophones is not stated by the manufacturer, however it is possible to obtain them by reverse engineering. Given sufficient samples of ΔT and their pairing direction measurements we can convert formula 5.13 to yield the position differences between hydrophone pairs from equation 5.11 via the least square method. In order to do so, we need to construct a helper matrix A from the direction measurement $\vec{d}$ that holds information derived by the knowledge of the hydrophone array set-up, so that

$$S = \Delta T A^+ \tag{6.1}$$

where $A+ = (A^\mathsf{T} A)^{-1} A^\mathsf{T}$ is the pseudo-inverse of A. Each row in A determines how the x, y and z components of $\vec{d}$ influence the ΔT measurements. Columns in A stand for position components of the hydrophones. The following assumptions can been made based on the known array layout

$$h_{x_1} = h_{x_3}, h_{y_1} = -h_{y_3}, h_{z_1} = h_{z_3} \tag{6.2}$$
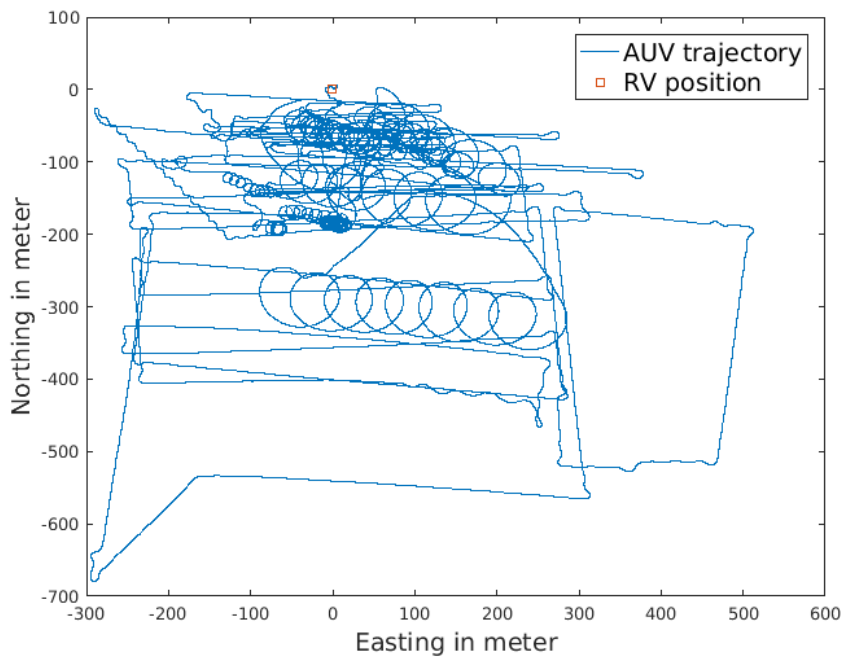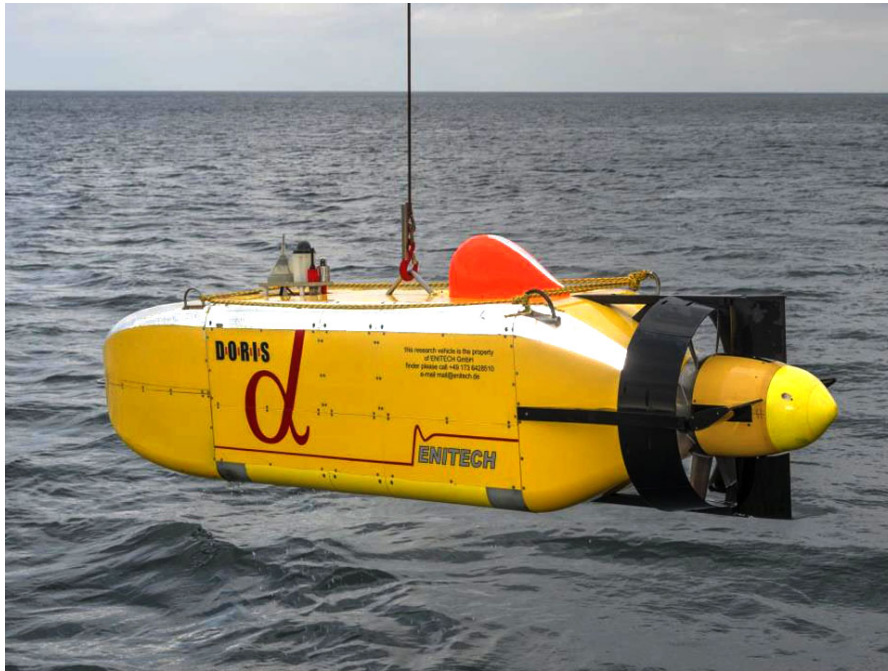
Figure 6.3.: Recovery of AUV 'Doris' from the Baltic sea (top). Trajectory of the AUV during the trial of the 29th Sep. 2015 estimated by an EKF (bottom).

$$h_{x_2} = -h_{x_4}, h_{y_2} = h_{y_4}, h_{z_2} = h_{z_4} \tag{6.3}$$

$$h_{x_5} = 0, h_{y_5} = 0 \tag{6.4}$$

where h_{x_i}, h_{y_i} and h_{z_i} denote the position of hydrophone i in the sensors reference frame. Based on those assumptions the helper matrix A can be constructed. Since there are multiple possible ways in which A can be constructed, the aim here is to solve for as many of the remaining unknown variables as possible. One possible form of A is

$$A = \begin{bmatrix} \vec{d_x} & \vec{d_y} & \vec{d_z} & 0 & 0 & 0 & -\vec{d_z} \\ 0 & 0 & \vec{d_z} & -\vec{d_x} & \vec{d_y} & \vec{d_z} & -\vec{d_z} \\ \vec{d_x} & -\vec{d_y} & \vec{d_z} & 0 & 0 & 0 & -\vec{d_z} \\ 0 & 0 & \vec{d_z} & \vec{d_x} & \vec{d_y} & \vec{d_z} & -\vec{d_z} \\ \vec{d_x} & \vec{d_y} & \vec{d_z} & \vec{d_x} & -\vec{d_y} & -\vec{d_z} & 0 \\ -\vec{d_x} & -\vec{d_y} & -\vec{d_z} & \vec{d_x} & \vec{d_y} & \vec{d_z} & 0 \\ \vec{d_x} & -\vec{d_y} & \vec{d_z} & \vec{d_x} & -\vec{d_y} & -\vec{d_z} & 0 \\ \vec{d_x} & -\vec{d_y} & \vec{d_z} & -\vec{d_x} & -\vec{d_y} & -\vec{d_z} & 0 \end{bmatrix} \in \mathbb{R}^{8 \times 7}. \tag{6.5}$$

In this form, matrix A has the maximal rank of five, meaning the equation system 6.1 can solve up to five variables in S. By solving the equation for many ΔT and $\vec{d}$ pairs in a least square fashion. Figure 6.4 shows the results of this procedure for the dataset of sea trial 6.1.1.2. As can be seen in the graphs, two of the seven variables ($x_{1,3}$ and $y_{2,4}$) show a big dispersion. They can not be solved with the chosen matrix A. However the other variables indicate good results with only minor deviation. For the final result we substitute

$$h_{x_1} = h_{x_3} = 0, h_{y_2} = h_{y_4} = 0 \tag{6.6}$$

Note that all ΔT and $\vec{d}$ measurements have been made by the same USBL. Other USBL models will have different array configuration and even other devices of the same model might show slightly different hydrophone positions due to variations in the production.

6.1.2.2. Evaluating the Direction Computation

With the hydrophone positions determined in the previous section it is now possible to evaluate how good the USBL model from section 5.2 can mimic the real device given the same time difference of arrival measurements. For the evaluation the ΔT measurement made by the real USBL device during sea trial 6.1.1.2 were fed into the USBL model to calculate the direction of arrival. The results in figure 6.5 show the difference between the direction of the real USBL and the direction computed by the model, for all samples of that experiment. With a difference of only two times the angle resolution stated by the manufacturer, the model can be said to almost imitate the real USBL device given the same ΔT values. This is an important achievement since many of the upcoming experiments will be based on that USBL model.
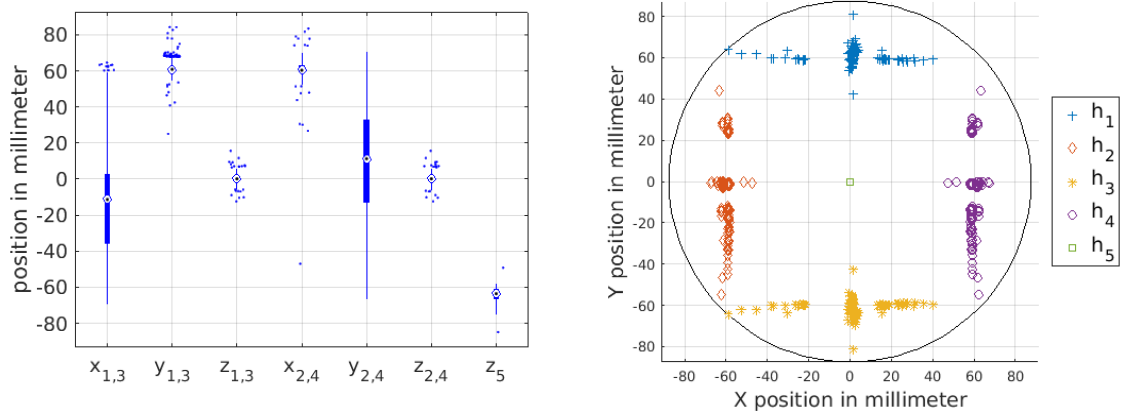
Figure 6.4.: Results of the position estimation for the hydrophones based on real data from sea trial 6.1.1.2. The box plot on the left side shows estimation uncertainty for each axis and hydrophone. On the right side the estimated hydrophone positions in the x-y plane of the USBL frame are shown for hydrophones $1 - 5$. Here the big circle illustrates the outer bounds of the transducer head.
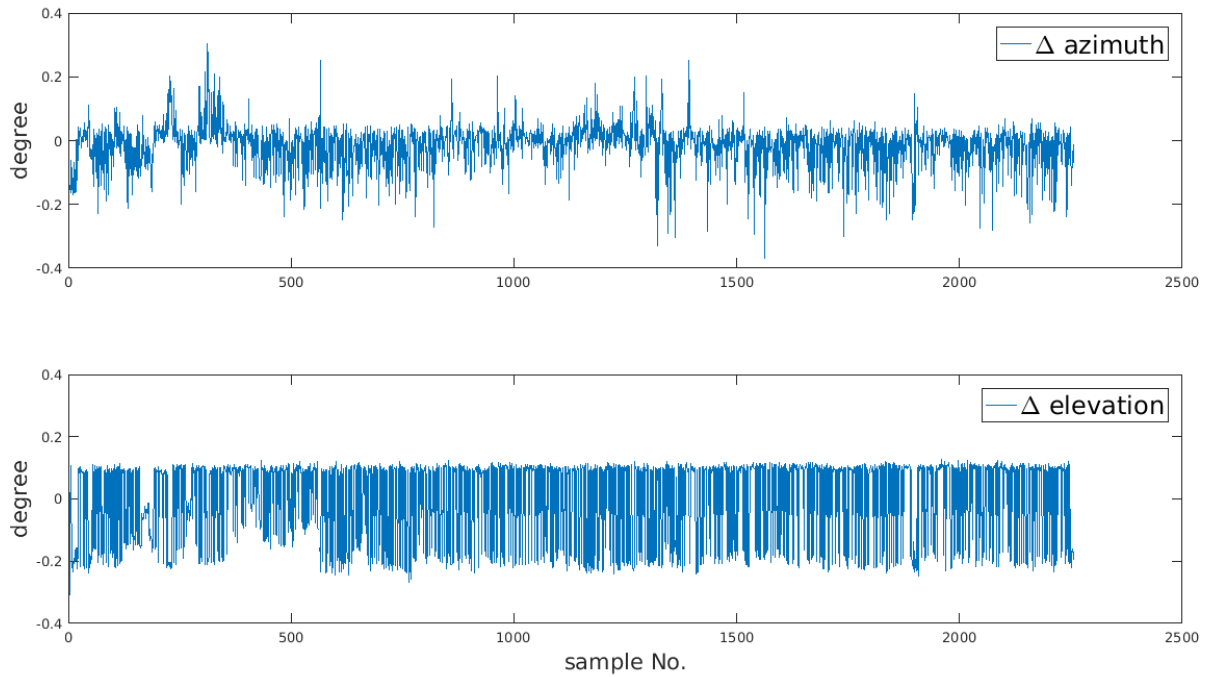
Figure 6.5.: Difference in the angle of arrival calculation between the USBLANGLE measurements from sensor and model, based on the measured time difference of arrival of sea trial 6.1.1.2.

6.1.2.3. Identifying the Noise Distribution

After the USBL model was successfully evaluated for given ΔT measurements, this section tries to identify the influence of noise in the time difference of arrival. As already described in section 5.2, the signal detection on the lowest level depends on correlation processes. To model the correlation process would be out of the scope of this thesis, as it would require knowledge of the internal signal processing algorithms used by the USBL. Instead, we can try to identify the noise influence empirically based on some collected measurement data. Here the data from sea trial 6.1.1.1 is the only reliable source since a real ground truth is required. Therefore, the deviation between ground truth and noisy measurement needs to be determined on the signal detection level. Unfortunately, ΔT measurement output was not featured on the USBL firmware at the time of the experiment. With the USBL model however, it is possible to derive the ΔT from $\vec{d}$ measurements and vice versa. By doing so for the direction measurements of the access point and the $\vec{d}$ derived from both the known positions of the access point and the research vessel, we can get the two sets ΔT_{USBL} and ΔT_{GT}. Now we calculate the divergence of the USBL time difference of arrival measurements from the expected ground truth for each measurement in the data set by

$$\epsilon_t = \Delta T_{USBL} - \Delta T_{GT} \in \mathbb{R}^8. \tag{6.7}$$

By drawing the sample standard deviation of ϵ_t over all samples, the σ_t values in table 6.1 could be obtained for each of the eight hydrophone pairs. To identify the distribution of the noise a Kolmogorow-Smirnow-Test as well as a Lilliefors-Test have been carried out with the null hypothesis that ϵ_t is normally distributed with zero mean and σ_t as in table 6.1. It was confirmed that all ϵ_t are indeed normally distributed for a 5% significance level. The p-value of the Kolmogorow-Smirnow-Test is listed in the table as well. On the right side of Figure 6.6 the empirical cumulative distribution function of $\epsilon_{t,7}$ is compared to a CDF of a normal distribution. In order to give an impression of how the noise in the ΔT measurement affects $\vec{d}$, the left side of the figure shows the elevation component of the measured angle next to the ground truth data. From the standard deviations in the table it is visible that pairs that include the vertically offset hydrophone 5 do show a smaller deviation. Due to the vertical signal direction of close to $90°$ elevation the Δt of pairs $5-8$ are close to zero, because the signal arrives as nearly the same time at both hydrophones. It can be argued that the higher fluctuation for these pairs is not solely based on sensor noise but also includes quantisation errors that stem from the limits of the recording device. Therefore hydrophone pairs $1-4$ seem to offer a more reliable value. Concluding the investigations on the time detection, the noise value for the USBL model was set to $\sigma_t = 0.1050\mu s$ for the remainder of the experiments.

In this subsection important parameters for the fine-tuning of the USBL sensor model were identified. Summarizing the outcome, it can be concluded that the model closely resembles the performance of the real sensor within only plus-minus two times the

Table 6.1.: Standard deviation of the ΔT noise and p-value of the Kolmogorov-Smirnow-Test for each hydrophone pair.

Pair No.	ΔT pair	p-value	σ_t
1	$\Delta t_{1,5}$	0.3964	$0.1036\mu s$
2	$\Delta t_{2,5}$	0.8313	$0.1063\mu s$
3	$\Delta t_{3,5}$	0.3016	$0.1040\mu s$
4	$\Delta t_{4,5}$	0.7477	$0.1054\mu s$
5	$\Delta t_{1,2}$	0.9904	$0.1486\mu s$
6	$\Delta t_{4,1}$	0.2505	$0.1479\mu s$
7	$\Delta t_{3,2}$	0.2505	$0.1479\mu s$
8	$\Delta t_{3,4}$	0.9904	$0.1486\mu s$
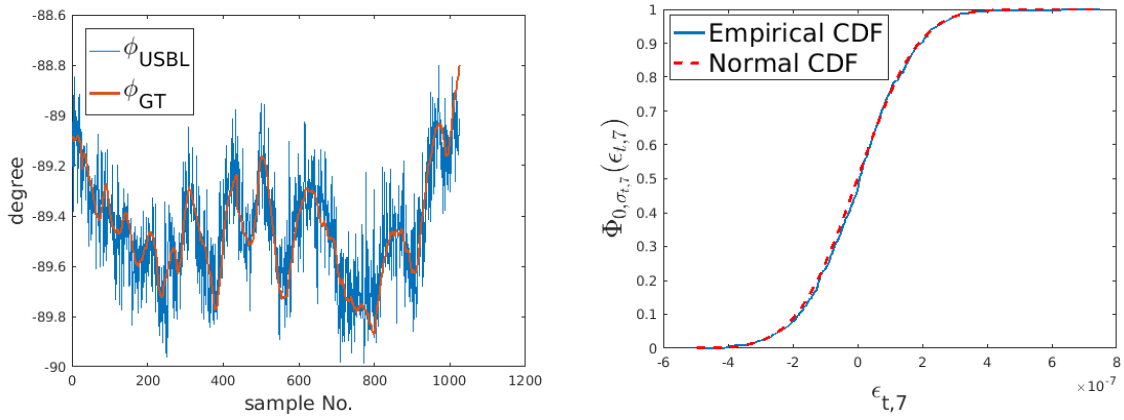
Figure 6.6.: Noise in the time measurements affect the direction measurement. The left side shows the elevation component of the measurement in blue and ground truth in red. On the right side the empirical cumulative distribution function for the Δt noise of hydrophone pair 7 is compared against a normal distribution with $\sigma_{t,7}$.

sensor resolution. The good results show that the model can be used in order to produce near reality measurement, thereby minimizing the simulation gap and providing a powerful tool for the analysis of USBL sensors in general. The USBL sensor model is an important contribution of this thesis, as the author could not find an in depth analysis on the localization capabilities of this specific USBL in the literature and the manufacturer provided only limited information on the topic.

6.1.3. Systematic Analysis of DNL

In this section the deepsea network localization as described in section 4.2 will be evaluated. The algorithm consists of two independent estimators, one for the vehicle heading and one for the position. For both estimators a statistical performance analyses was conducted in simulation before they were evaluated on the data collected during the sea trials mentioned in section 6.1.1.

6.1.3.1. Statistical Analysis of Heading Estimation

Two independent sources contribute to the performance of the DNL heading estimation. The USBL measurement and the position estimates of sender and observer. First we will assess the possible accuracy of each source separately before the overall performance is analysed.

For the DNL heading estimation, the USBL AOA measurement is used to calculate the bearing angle to the sender in the north-east plane. Since the AOA is measured in the sensor frame of the USBL it needs to be transformed onto the north-east plane. Here the noisy roll and pitch of the state estimation has to be used, which introduces uncertainty into the estimation. Furthermore, the AOA measurement itself is subject to noise, which needs to be considered. The algorithm takes these error influences into account and estimates the heading $\hat{\psi}_b$ of the incoming acoustic signal in vehicle frame, as well as the assumed variance of this estimation $\hat{P}_{\psi_b}$. In order to verify the quality of these estimation, a statistical analysis has been conducted in simulation. The analysis takes discrete samples of AOA and applies $N = 500$ runs of the algorithm for each sample point. The AOA is measured with the USBL model which will introduce some measurement noise. For each run, the USBL was assigned with a random orientation. Additive white Gaussian noise (AWGN) was applied to that orientation according to Σ_{ypr}, representing the orientation uncertainty of a state estimate. The orientation uncertainty needs to be known by the algorithm, however in real applications it can only be approximated and may differ from the true distribution. In the experiments this is modelled by applying a scaling factor to the covariance matrix, so that $\hat{\Sigma}_{ypr} = s\Sigma_{ypr}$ is the distorted covariance passed to the algorithms. When $s > 1$ the assumed orientation uncertainty $\hat{\Sigma}_{ypr}$ is bigger than the reality and the resulting estimate of $\hat{\sigma}_{\psi_b}$ will have a positive offset and for $s < 1$ the

offset is negative. The heading estimated by DNL was compared to the real heading and the estimated uncertainty was equally compared against the true circular sample standard deviation given by

$$\sigma_{\psi_b} = \sqrt{-2\ln\left(\frac{1}{N-1}\sum_{i=0}^{N-1} z^{(\hat{\psi}_b^{(i)} - \psi_b)}\right)} \tag{6.8}$$

with $z^\psi = e^{i\psi}$. To evaluate the uncertainty estimation we compute the average circular standard deviation estimate for each AOA as

$$\bar{\hat{\sigma}}_{\psi_b} = \sqrt{-2\ln\left(\frac{1}{N}\sum_{i=0}^{N-1} 1 - \hat{P}_{\psi_b}^{(i)}\right)} \tag{6.9}$$

The results indicate that the azimuth part in the AOA is indifferent for the algorithm performance. Different elevation angles however will lead to a change in estimation quality as shown in figure 6.7. The diagrams show the spread of the estimation error for two different Σ_{ypr} and scaling factor $s = 1$. Each box in the figure represents the statistical properties of the estimation error at a given elevation. The sample standard deviation as well as the estimated standard deviation are displayed as lines. Estimation error and estimated variance increase drastically with elevation angles close to $\pm 90°$ because here the direction of arrival is parallel to the down axis, in which case the AOA yields no information about the heading. For the majority of AOA however the average estimation error is well beneath one degree. The estimated standard deviation is often slightly higher than the sampled one, which reflects the conservative assumptions made for the tuning parameters of the algorithm.

 Besides the USBL measurement noise, also the position uncertainties of sender and observer contribute to the heading estimation quality. The angle of the arriving signal in the navigation frame $\{\psi_n, \phi_n\}$ can be determined by the position estimates. For the heading estimation we are only interested in the azimuth estimation and the respective uncertainty of this estimation $\hat{P}_{\psi_n}$. The estimation uncertainty originates from the uncertainty of the position beliefs of each vehicle. In order to investigate the influence of the position uncertainties to the heading estimation, an experiment has been set up, similar to the one described above. The heading is estimated from the positions of two vehicle, where the position estimate of each vehicle is given by $\hat{p} \sim \mathcal{N}(\mu_{pos}, \Sigma_n)$. The estimation method takes as input the position estimates and the estimated position uncertainties $\hat{\Sigma}_n = s\Sigma_n$ of each vehicle, where s is an factor that represents the error in the uncertainty belief. In the experiment the horizontal distance between the μ_{pos} was increased successively and for every horizontal distance $N = 500$ heading estimates have been performed. The results can be seen in figure 6.8 for different Σ_n and $s = 1$. Like in the previous experiment, the boxes illustrate the statistics of the estimation error and the sample standard deviation and averaged estimated standard deviation are visualized as lines. The figure shows that the estimation error drops with bigger distances, as can be expected. Estimated standard
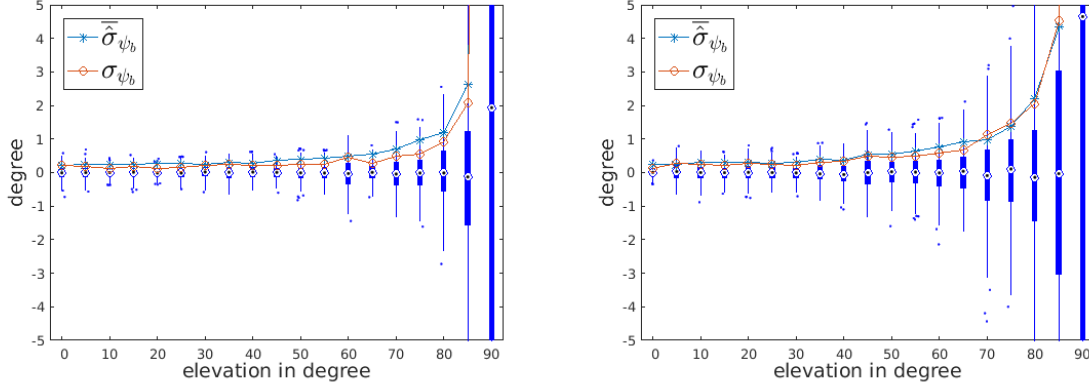
$$\Sigma_{ypr} = \mathrm{diag}(0.1°, 0.03°, 0.03°)^2 \qquad \Sigma_{ypr} = \mathrm{diag}(1°, 0.3°, 0.3°)^2$$

Figure 6.7.: Statistical analysis of estimation error for ψ_b in vehicle frame. The estimated standard deviation averaged over all runs is marked as $'*'$ and the true sample standard deviation with $'\circ'$. For every position on the x-axis 500 estimation samples have been analysed.
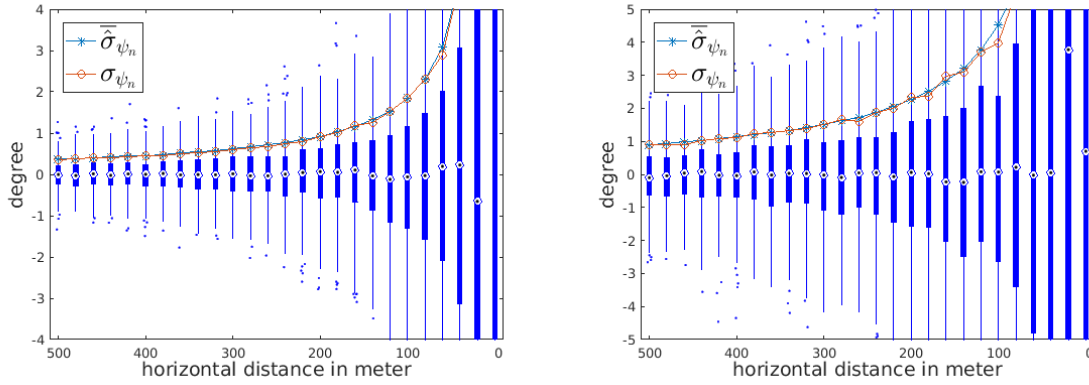
$$\Sigma_n = \mathrm{diag}(5, 5, 0.1)^2 \qquad \Sigma_n = \mathrm{diag}(30, 30, 0.1)^2$$

Figure 6.8.: Statistical analysis of DNL ψ_n estimation error. The estimated standard deviation averaged over all runs is marked as $'*'$ and the true sample standard deviation with $'\circ'$. For every position on the x-axis 500 estimation samples have been analysed.

deviation and sample standard deviation match each other with minor differences. Even for positions with a high uncertainty the estimation can produce reliable azimuth values given a big enough horizontal distance. Similar to experiment above the scaling factor s produces an positive offset of $\hat{\sigma}_{\psi_n}$ when greater than one and a negative offset when smaller than one.

91

6.1.3.2. Evaluation of Heading Estimation

The previous experiments show the theoretical estimation performance for $\hat{\psi}_n$ and $\hat{\psi}_b$. To get the actual estimation quality for the heading, both estimates need to be combined. Since the estimates are not correlated the estimated variances can be added to get the resulting heading variance. The overall performance of the heading estimate depends on the spacial relation between sender and observer. Bigger horizontal distance and small elevation angles increase performance, hence the heading estimation works best for horizontal communication between distant participants. This is given for example in a network of AUVs that monitor a large area of seabed.

The experiments described above take into account erroneous measurements and estimations for all the input variables that are used for the heading estimation. However errors in the belief of the covariance matrices have been simulated only by a scaling factor. It is possible that the estimation performance for the variance drops when the form of $\hat{\Sigma}_n$ and $\hat{\Sigma}_{ypr}$ differ essentially from the real distribution. Further more, systematic measurement errors like refraction effects, where not considered in this simulation.

A third experiment, based on the data of sea trial 6.1.1.2, was conducted in order to investigate the estimation performance in a real scenario. In this trail an AUV state has been reconstructed by an EKF from INS/DVL and pressure measurements of the submersible as well as USBLLONG measurements of the AUV, made from the nearby research vessel [17]. The vehicle state was estimated with a frequency of $10Hz$ and includes position, velocity, orientation as well as the respective covariance matrix given by the filter. The filter solution will be taken as the ground truth for this experiment. During the experiment the research vessel sends its position and position uncertainty to the AUV via acoustic link. These informations, together with AOA measurements made by the USBL mounted on the AUV, will be used for a DNL heading estimation. In this experiment we investigate how close the estimated heading matches the synthetic ground truth given by the EKF. Since the DNL estimation does not have a fixed output frequency, only those EKF states have been considered which are timely aligned with an USBL measurement. An excerpt of the results can be seen in figure 6.9. The upper diagram shows the heading of the EKF $\hat{\psi}_{EKF}$ and the DNL heading estimate $\hat{\psi}_{DNL}$ next to each other. In the lower diagram the difference between both headings is displayed as well as the estimated standard deviation $\hat{\sigma}_\psi$ by DNL. During the time frame shown in the diagrams, the vehicle conducted a lawn mower motion where it keeps the heading for some time, then turns by 90 degrees two times and repeats. The ripples in the heading signal originate from the prototypic heading controller[1] of the AUV, adjusting to a new heading set-point. Those ripples can be used to observe how the DNL heading estimations matches with the EKF solution. By observing the two signal structures it appears that both estimations captured the same ripple features, however the DNL heading seems to have an systematic offset that alternates over time around $\pm 4°$. This systematic error is not represented by

---

[1]Tuning the heading controller was part of the sea trial objectives.

the estimated standard deviation either. After deeper observation of the underlying sensor data, a correlation between the heading difference and the vehicles roll and pitch rotation rate was found. This could indicate that the DNL heading estimation may degrade with fast roll and pitch angle velocities. On the other hand, the USBL data used by the EKF is known to have a high noise in the elevation measurement, originating from the shallow water and hence poor channel properties at the mission site. Further investigations have shown that the noisy elevation measurement impair the position estimation of the EKF. Although the vehicle depth can be reliably determined by the pressure sensor, a faulty elevation angle would decrease the belief of the horizontal distance between research vessel and AUV. Such an error is likely to produce the systematic angle difference shown in figure 6.9. Because a real ground truth is not available, it is not possible to reliably tell which estimation is more trustworthy from the data. The general correspondence of both estimates however seem to verify that the DNL heading can be used under real circumstances.
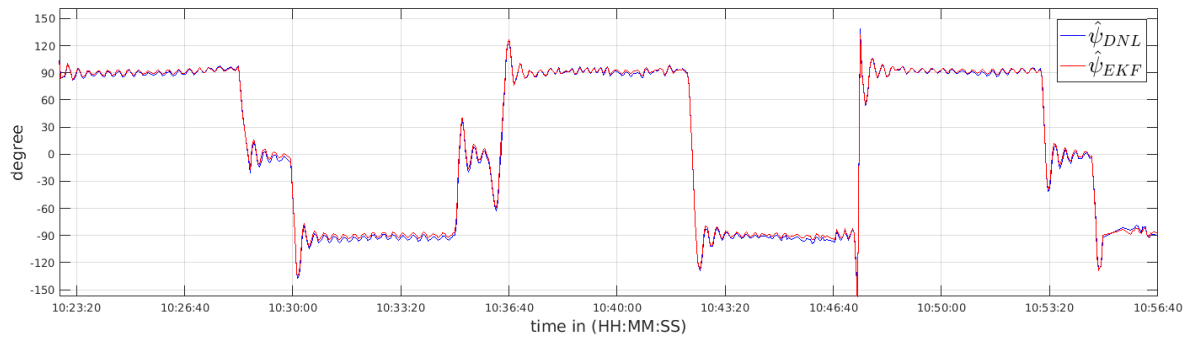
Estimated heading of EKF and DNL
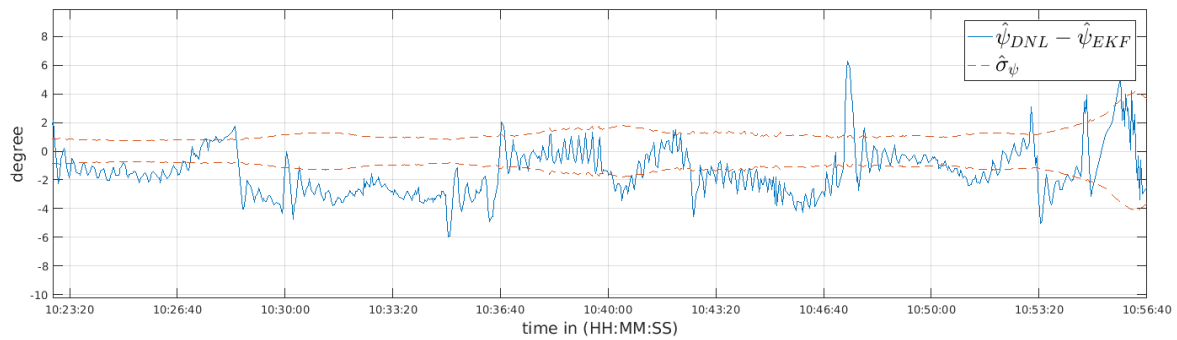
Heading difference and estimated standard deviation of DNL

Figure 6.9.: Comparison between an EKF and DNL heading estimations based on data of sea trial 6.1.1.2. In the top graph the heading estimates of the EKF and DNL are shown, while the bottom graph shows the angle difference between those two and the standard deviation estimated by the DNL algorithm. During the excerpt, a typical lawnmower trajectory was conducted by the AUV.

6.1.3.3. Statistical Analysis of Position Estimation

In 4.2 two different position estimation methods are described, depending on the available measurement data. The first method uses the position of sender and receiver as well as a USBLLONG measurement. Another method is used when only USBLANGLE data is available. In order to investigate the performance of both methods a statistical analysis was conducted in the simulation, similar to the experiments for the heading estimation above. Two nodes, one sending and one receiving, are placed in the scene at positions μ_{p_1} and μ_{p_2} respectively. The relative position between both is change by increasing the elevation angle in steps but keeping the slant range constant. For each elevation angle the algorithm has been run $N = 500$ times to give statistically significant data. For each run an USBL measurement was triggered with the USBL model and the measurement was used in combination with the position estimates of the vehicles. Each vehicle estimates its position separately for every run according to $\hat{p} \sim \mathcal{N}(\mu_p, \Sigma_n)$ and its position covariance by $\hat{\Sigma}_n = s_p \Sigma_n$. Furthermore, the orientation of the receiving vehicle is randomized for every run in order to account for the varying USBL sensibility. The receiver estimates its real orientation μ_q according to $\hat{q} \sim \mathcal{N}(\mu_q, \Sigma_{ypr})$ and the orientation covariance as $\hat{\Sigma}_{ypr} = s_q \Sigma_{ypr}$. In order to reduce complexity and get unbiased position estimations, the channel has been simulated with a constant sound velocity throughout the water profile. The same set-up has been used to evaluate both methods.

When an USBLLONG measurement is available, the receiver can estimate its position according to the DNL approach in chapter 4.2. Figure 6.10 illustrates the estimation error for a slant range of $2000m$ as box plot over different elevation angles. The averaged estimated covariance $\bar{\hat{\sigma}}$ and the sample covariance σ are superimposed as lines. Note that only the horizontal position components are interesting, since the vertical component can be measured precisely with a pressure sensor. In this setup the uncertainties for position and orientation have been choose to be rather big with $\Sigma_n = \mathrm{diag}(5m, 5m, 0.1m)^2$ in order to investigate the performance in a bad case scenario. Nevertheless the horizontal position could be estimated with a standard deviation of only around $6m$ in the horizontal directions for all different elevation angles. The estimated standard deviation also matches the sample standard deviation up to a minor difference. Like expected, the position error is slightly increased in comparison to the error of the USBL measurement alone. This is due to the impact of the noisy orientation measurements. When there is only a USBLANGLE measurement available, the position can still be estimated with another estimation method. The only difference between USBLLONG and USBLANGL measurements is that the slant range was measured in the first case. Instead of measuring the slant range it is possible to estimate it using the position estimations of sender and receiver. Using the same experimental set-up as above we can evaluate the slant range estimation.

Figure 6.11 shows the results of the experiment as box plot with slant range errors. Again the estimated and sample standard deviation are superimposed as lines. We see that the estimation error decreases as the elevation angle approaches $90°$. In this
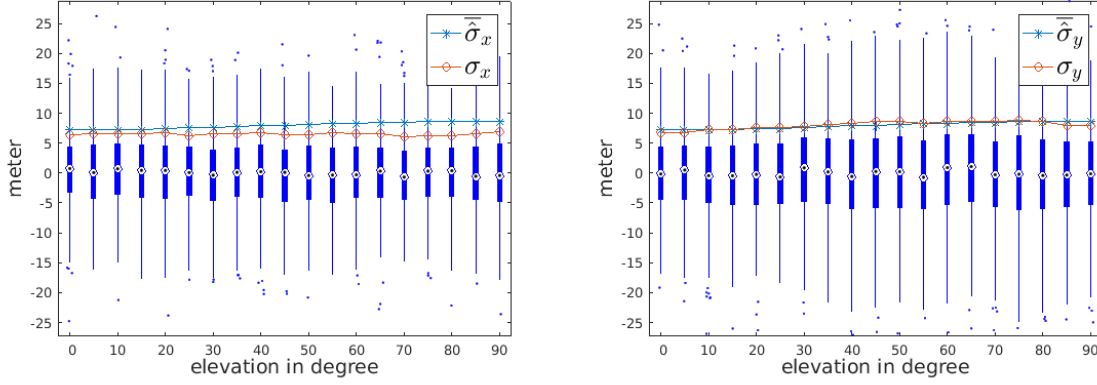
Error in X direction   Error in Y direction

Figure 6.10.: Position estimation performance using the position of sender and receiver as well as USBLLONG measurement for a slant range of $2000m$. The sender has a position covariance of $\Sigma_n = \text{diag}(5m, 5m, 0.1m)^2$ and the receiver has a orientation covariance of $\Sigma_{ypr} = \text{diag}(1°, 0.3°, 0.3°)^2$. Each box represents the error deviation of $N = 500$ runs for the X and Y direction respectively.

case one vehicle is directly above the other, so that only the relatively precise depths add up in the estimation uncertainty. Also the estimated standard deviation matches the real sample deviation since there is no non-linear influence of the orientation uncertainty in this case. Note that the slant range estimation may even be more accurate than the USBLLONG slant range measurement under some circumstances, since it is not affected by the varying sound velocity of the channel.

Having a reliable estimate of the slant range enables the second step of the estimation method. Using the slant range from above, we can now extend the USBLANGLE measurement in order to get the relative position between sender and receiver. From here on we can use the same procedure as with a USBLLONG, except that the resulting covariance matrix will be a combination of slant range uncertainty and USBL measurement uncertainty. Figure 6.12 illustrates the so achieved estimation error for the given scenario. When compared to the results from figure 6.10, we get a similar localization performance with a standard deviation around $6m$ for most elevation angles. At the $90°$ elevation mark the figure shows an increased error despite that the slant range estimation for this elevation is most precise. Also the estimated standard deviation for this method is slightly higher, since the slant range uncertainty is bigger than for a USBLLONG measurement.
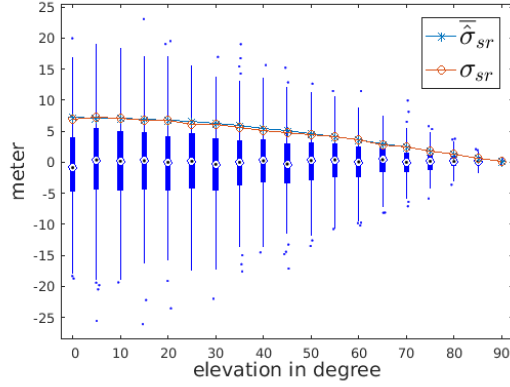
Figure 6.11.: Slant range estimation error using positions of sender and receiver for a slant range of $2000m$. Both vehicles have a position covariance of $\Sigma_n = \text{diag}(5m, 5m, 0.1m)^2$
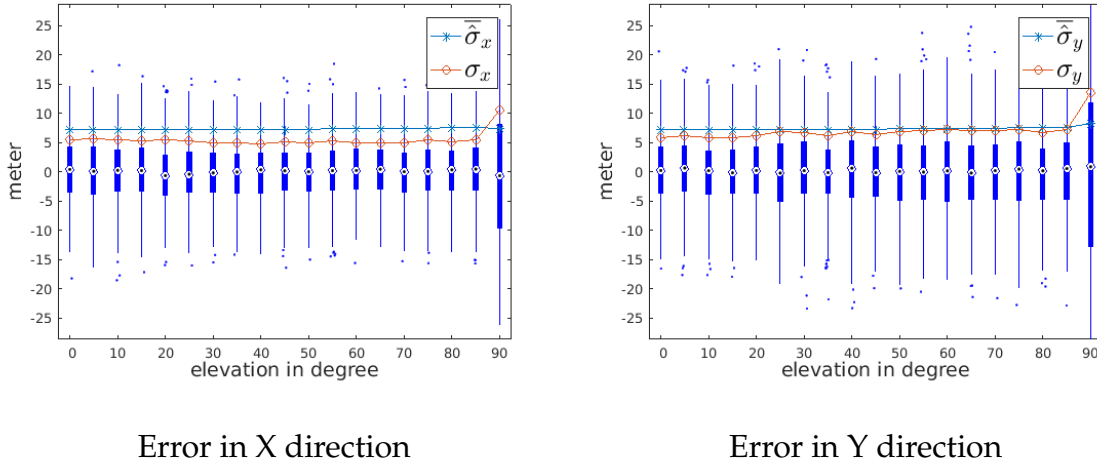
Error in X direction

Error in Y direction

Figure 6.12.: Position estimation error using slant range estimation and USBLANGLE measurements for a slant range of $2000m$. Sender and receiver have a position covariance of $\Sigma_n = \text{diag}(5m, 5m, 0.1m)^2$ and the receiver has a orientation covariance of $\Sigma_{ypr} = \text{diag}(1°, 0.3°, 0.3°)^2$. Each box represents the error deviation of $N = 500$ runs for the X and Y direction respectively.

6.1.3.4. Evaluation of Position Estimation

The results confirm the theoretical capability of the DNL localization in simulation. For the evaluation under real conditions, data of the sea trial 6.1.1.1 will be used. During this trial a so called access point with an USBL modem was submerged to a depth of $5002m$. After touchdown the access point remained stationary, while it was pinged periodically by a USBL modem from the research vessel. Each ping contained a data package with the research vessels position and uncertainty. Upon reception of a ping, an USBLANGL measurement is triggered at the USBL modem on the access point. The access point position was determined in post processing, using all available data from USBL and the sonar of the research vessel. Since the access point location might still be unreliable, a big position uncertainty of $\Sigma_n = \text{diag}(100m, 100m, 100m)^2$ was assumed. The set-up is illustrated in 6.13.

With the position of sender and receiver as well as the USBLANGLE measurements
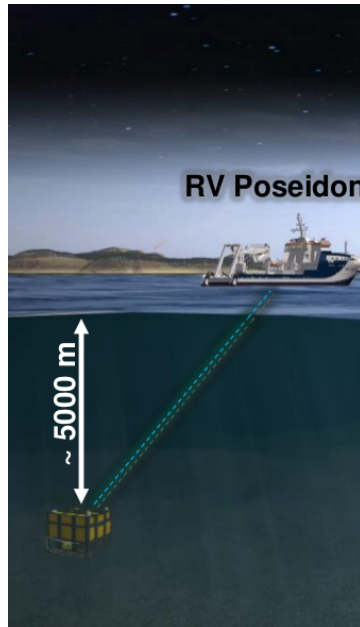
Figure 6.13.: Illustration of experimental set-up used in sea trial POS485. The submerged access point at a depth of around 5000 meter recorded periodic DNL message, which where broadcasted from the research vessel via the acoustic link.

it was now possible to conduct DNL position estimations. Figure 6.14 shows the estimation error and the estimated standard deviation for the given sample set of 1024 USBL measurements. The ratio of errors that are smaller than the estimated standard deviation is 67.97% for X and 71.0% for Y direction, which gets close to the 68.27% of a perfect estimation given a normal distribution. This suggests that the error distribution can in deed be estimated as Gaussian and that the estimator got close to

the true error distribution for this data set. The main contribution to the position error comes from the noise of the USBL measurements. For the given constellation of nearly $90°$ elevation and $5002m$ slant range, the USBL model predicts an standard deviation of arounet and for $s < 1$ the offset is negative. The heading estimated by DNL was compared to the real heading and the estimated uncertainty was equally compared against the true circular sample standard deviation given bd $25m$ in X and Y direction respectively. Further error influences are the slant range estimation and the uncertainty in orientation which was assumed to be $\Sigma_{ypr} = \text{diag}(0.1°, 0.03°, 0.03°)^2$.

It has to be mention that refraction effects have not been accounted for in these estimations, as the relative position between sender and receiver is mostly vertical with only minor horizontal difference. In this case the refraction due to sound speed variations can be omitted. For bigger horizontal distances however refraction effects may impair the USBL measurements systematically.

Summarizing the results of this section, it can be said that the Deep-Sea Network
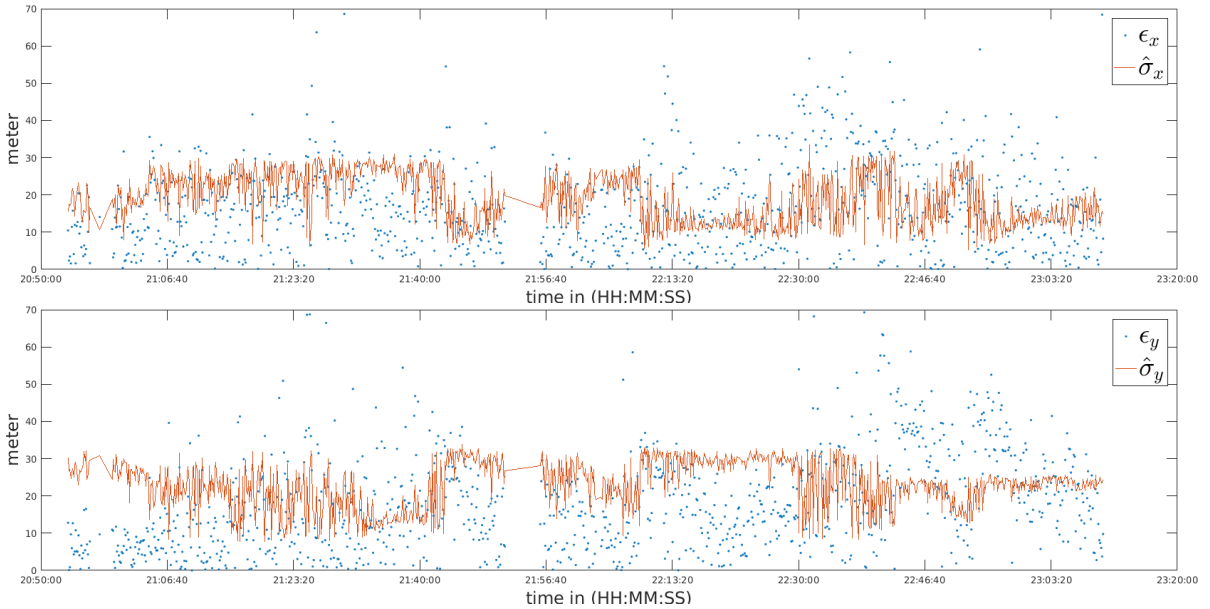
Figure 6.14.: Evaluation of the DNL localization on data of the sea trial 6.1.1.1. The blue dots represent the position estimation error in X (top) and Y (bottom) direction and the line indicates the estimated localization uncertainty for each dimension.

Localization is capable of enhancing the performance of traditional navigation filter by adding heading and position estimations with reliable uncertainty bounds. This is done by combining communication and localization schemes that utilize the available informations in the channel without the need to actively communicate. It was shown that the two way communication needed for the USBL slant range measurement can be substituted with an slant range estimation with only minor loss of precision in the examined scenarios.

6.1.4. Multi-Vehicle Experiments

In this section the DNL algorithm will be analysed in a simulated set-up with multiple vehicles in order to identify its performance in a cooperative localization scheme. For this, the simulation framework as described in the previous chapter 5 will be utilized.

6.1.4.1. DNL aided localization

To evaluate the performance of DNL in a multi-vehicle arrangement, two simulated experiment with 10 AUVs were conducted. In the first experiment the AUVs will only have access to proprioceptive sensors, performing dead reckoning for their localization. The second experiments introduces a USV at the surface providing geo-reference for the submersibles via DNL. A concept of this experimental set-up is shown in 6.15

The USV is stationary and equipped with a downward pointing USBL modem. It
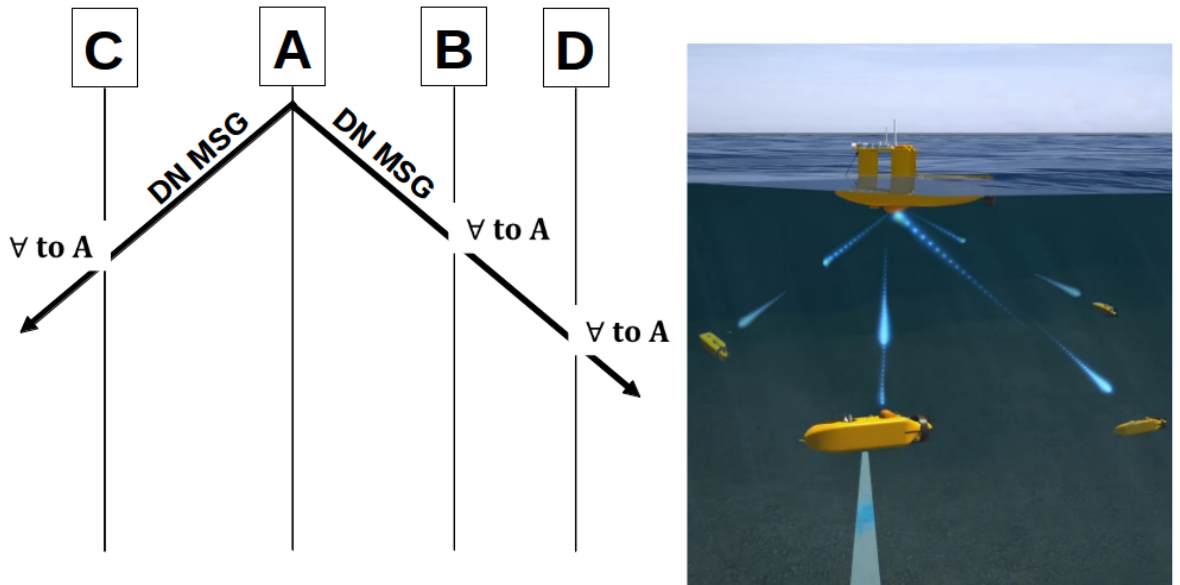
Figure 6.15.: Concept of experiment set-up with one surface vehicle as broadcaster and multiple submersibles as silent receiver.

can determine its position with a variance of $\Sigma_n = \mathrm{diag}(3m, 3m, 1m)^2$ and periodically broadcasts a DNL message every 20 seconds over the acoustic link.
The AUVs start with random orientation at horizontal location within a distance of $500m$ to the USV and a depth of $2000m$. Each AUV begins with perfect knowledge about its state and performs a random walk, changing its heading every 60 seconds, while maintaining a depth of $2000m$. The sensor equipment of the AUVs corresponds to that of a SMIS AUV with MEMS-based IMU, DVL, barometer and USBL-Modem.

In order to ensure bottom lock for the DVLs, the sea ground is simulated as a plane at $2050m$ depth. Sensor fusion on the AUVs will be executed by the particle filter explained in 5.3. The results from both experiments will be compared below.

For the sake of an easier visualization and comparison of position deviations, errors in the X and Y dimension will be summarized into a one dimensional error metric according to

$$\epsilon_h = \sqrt{\epsilon_x^2 + \epsilon_y^2} \qquad (6.10)$$

for the horizontal error and

$$\sigma_h = \sqrt{\lambda_1 + \lambda_2} \qquad (6.11)$$

for the horizontal standard deviation, where λ_1 and λ_2 are the non-zero eigenvalues of the horizontal part of Σ_n. In figure 6.16 the median growth rate of the horizontal position variance over time for both DR and the DNL aided localization is shown as it was predicted by the particle filter. For the DR case the variance grows linearly as can be expected considering the given sensor set-up with IMU and DVL. The DVL provides velocity fixes with a relatively stable noise. Over time, errors in the velocity and orientation measurements add up when they are integrated to get the position, resulting in an growing position variance. In the second case, exteroceptive measurements are supplemented by the position and heading output of the DNL approach which results in a much slower expansion of variance. For as static configuration the covariance is expected to converge towards a plateau which is dependent on the accuracy of the position fixes. When this happens, the localization is said to be in a steady state. In graph 6.16 we can see a slight increase in covariance even in the later stage, which conflicts with the expectations. One possibility is, that the simulation time was simply to short for the system to converge. Another explanation to this behaviour could be that the majority of the vehicles are moving away from the USV, thus increasing the uncertainty of the mean DNL position fix. To test this assumption, the simulation time was increased and the locomotion pattern of the AUVs was changed to a more deterministic and spatially confined meandering motion in the next experiments.

Figure 6.17 shows the individual error evolution for the first three AUVs in both scenarios, with and without DNL. From the trajectories of horizontal error and standard deviation it is visible that error growth is restricted in the DNL aided localization. Another interesting aspect of the progression in the position estimation error is the spiking behaviour. Every spike corresponds to the PF creating or dismissing a particle cluster, thereby changing the mean of all particle enough to cause a sudden jump in position estimation. In this experiment, the effect is most apparent in the vehicle that use only DR, however the same applies to the DNL aided localization as well.

We can further investigate the output of the DNL algorithm before it was fused with the other sensor readings. In figure 6.18 we see a statistical analysis of the DNL estimation error of all 10 AUVs. The bars show the estimation error while the red lines show the median of the estimated standard deviations $\hat{\sigma}$ for that bin. As can be seen
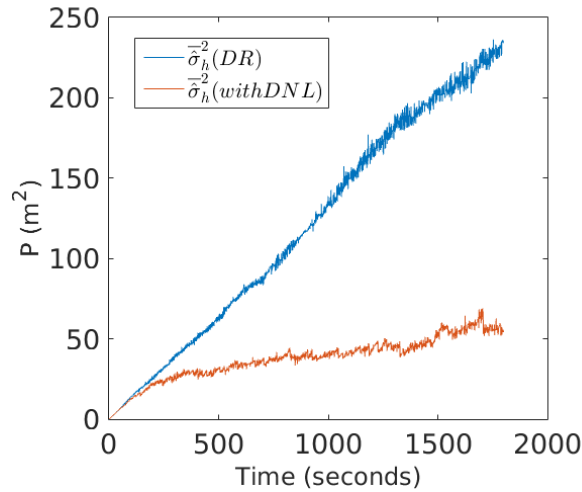
Figure 6.16.: Median evolution of horizontal position covariance over 10 AUVs for dead reckoning and DNL aided localization.
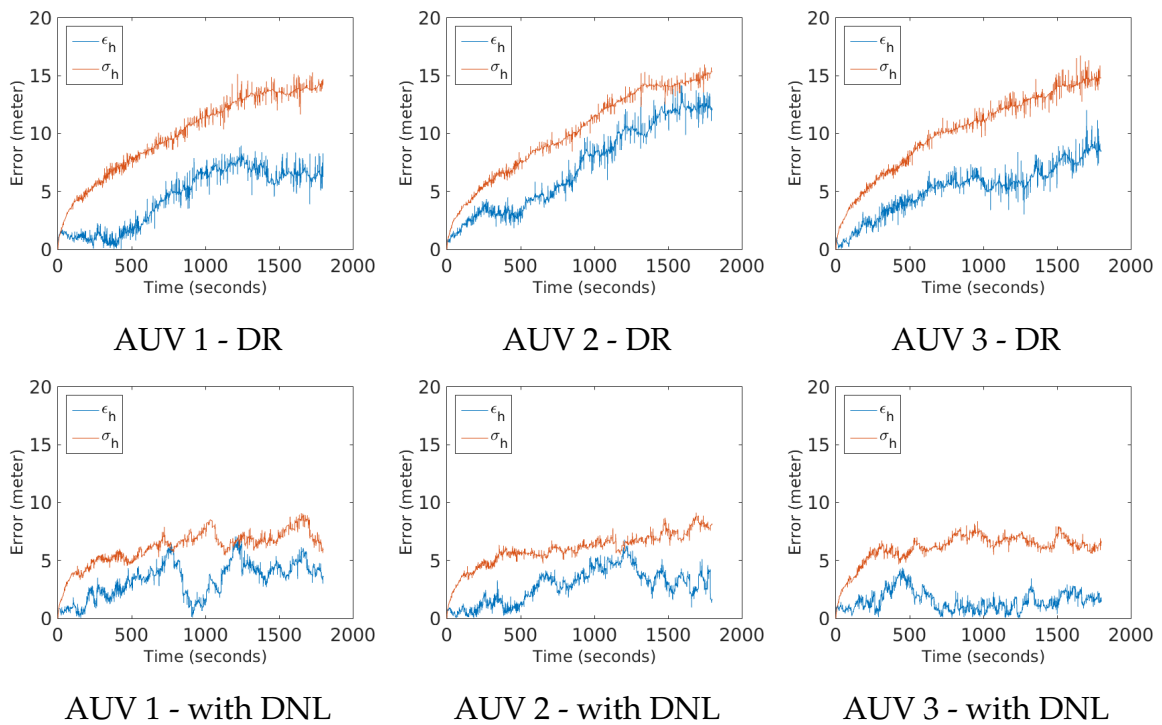
Figure 6.17.: Evolution of horizontal position error and standard deviation over time for the first three AUVs. The upper Row shows results with dead reckoning and the lower row shows results with cooperative localization.

101

in the histogram, bins on the corners are under-represented in this experiment and have only limited expressiveness. Nevertheless, the deviation margins that were predicted by DNL are met. For the limited amount of samples in this experiment, the estimated heading variance is even more conservative than the real error that was made.

DNL range estimation error   DNL position estimation error

DNL heading estimation error   DNL sample histogram
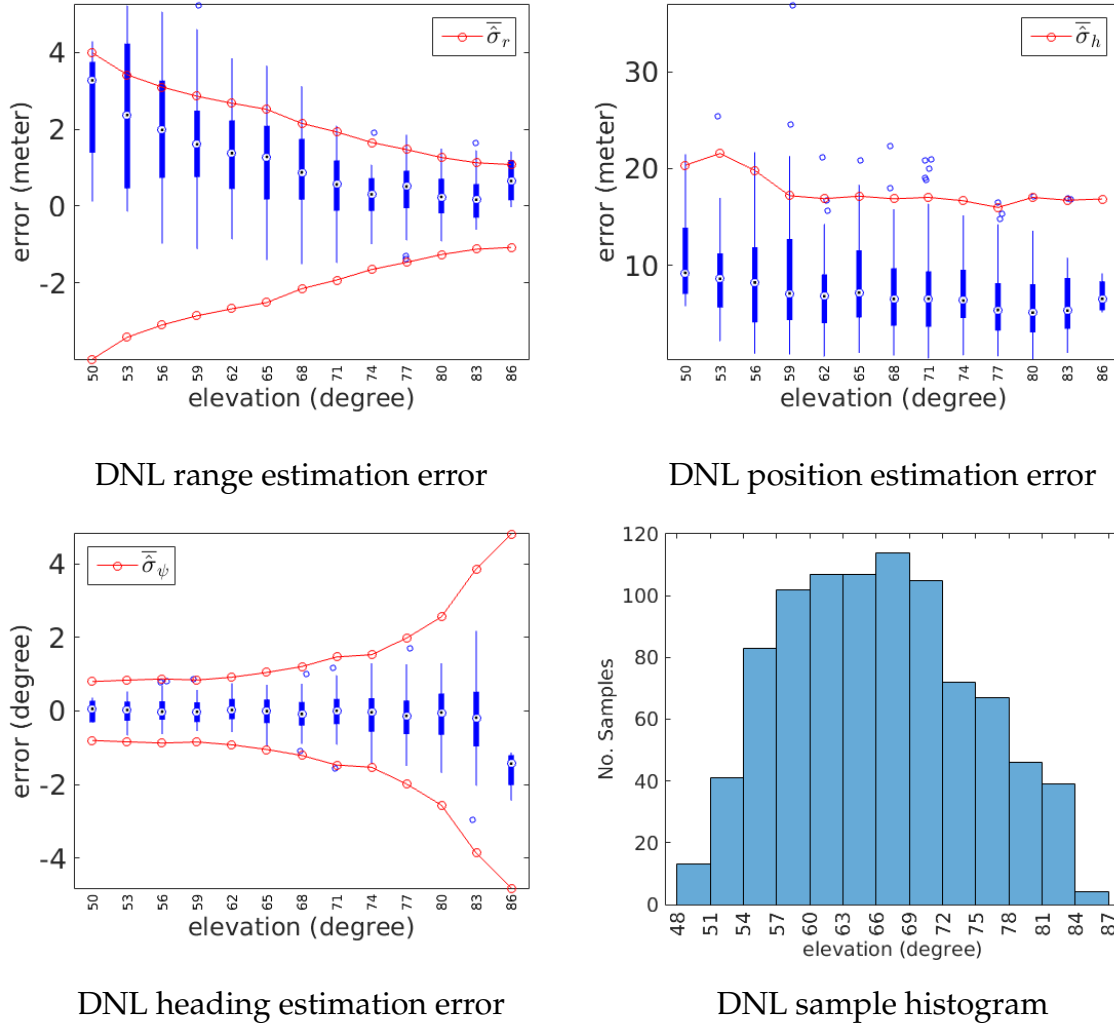
Figure 6.18.: DNL estimation error and median standard deviation estimation of all 10 AUVs binned over elevation angle.

This experiment shows a typical navigation scenario where a surface vehicle provides geo-reference for the underwater fleet. The experimental set-up was chosen to investigate the capability of DNL to utilize the transmission of one sender for the localization of multiple receiver.

6.1.4.2. **Multi-Hop with Directed Communication**

When a receiver node in the network can not be reached directly by the sender node, the information can nevertheless arrive at the receiver by routing it over one or more other nodes. The same principle can be applied in CL where the geo-referenced location of one node can support the localization of other nodes that are not directly connected. In the next experiment, the focus was set on analysing the influence of mulithops communication to the localization performance of DNL.

To test the multi-hop influence, the experimental set-up will consist of one USV at the surface that is connected to only one AUV close to the bottom. This AUV will function as relay for another four AUVs that can receive messages from the relay AUV but are out of range of the USV. Like in the previous experiment, the USV will perimodically broadcast DNL messages. However, in this case, only the AUV relay will receive them to support its own localization. The AUV relay will itself broadcast DNL messages periodically, which are received by the four AUVs that form the leafs of the directed communication graph. All AUVs will be placed in the same horizontal plane as in the previous experiment. The simulated time was increased to 100 minutes, in order to better analyse the convergence behaviour of the localization uncertainty. For the same reason, all AUVs will perform a meander motion instead of random walk. This will ensure that their relative position to the relay AUV does not change unpredictably over the time of the experiment. The set-up is displayed in figure 6.19.

Communication Scheme		
Vehicle	$t_{start}(sec.)$	$\Delta t_{period}(sec.)$
AUV5	10	60
USV	0	60
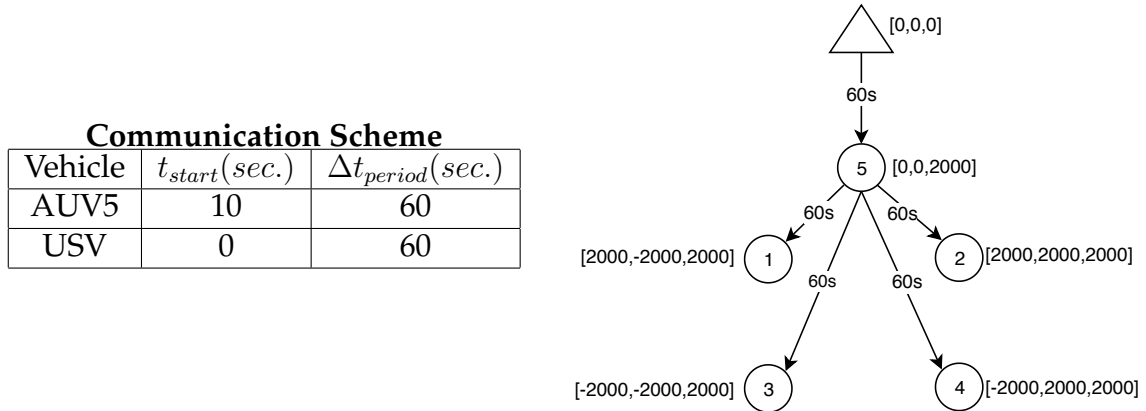
Figure 6.19.: Concept of experimental set-up with communication scheme left and communication graph right. The USV emits a DNL message every 60 seconds which is received by AUV5. Subsequently AUV5 broadcast a DNL message to AUVs 1-4.

The diagram depicts a directed communication graph with the following properties: each shape represents a vehicle (circles for AUVs, triangle for USV), the number in the shapes denotes the vehicle ID. Shapes are connected with arrows, showing the direction of communication. Brackets next to the shape denote the start position in meter

and north-east-down coordinates. In the adjacent table the communication scheme is described for each vehicle. In this experiment the USV and the AUV relay with ID five both sent at a period of 60 seconds, however the AUV has an additional offset of 10 seconds before it starts its first transmission. This 10 seconds delay will ensure that the AUV relay has enough time to receives the DNL message from the USV and incorporates this information into its own localization, before it broadcast its own position belief to the other AUVs.

The results of this experiment can be observed in figure 6.20. In the diagrams, the horizontal position error of the particle filter is shown as well as the estimated standard deviation. Grey lines indicate the times at which a DNL message was received and integrated into the position belief. When we compare the evolution of the error with the previous experiment, we can see that the covariance of the AUVs grows much faster, but reaches a steady state after some time. In this scenario the average position standard deviation plateaus after around 1500 seconds. Due to muli-hop, the uncertainties of USV and the AUV relay add up to the DNL covariance of the AUVs that are the leafs of the connection graph. This also results in an higher error in the steady state.

Figure 6.21 shows the performance of DNL before it was incorporated into the particle filter. With only four AUVs to analyse, the box plots visualization from the previous experiment is not very expressive. Instead the diagrams show the mean DNL estimation errors of the four leaf AUVs over time. AUV relay as sender and the leaf AUVs as receiver are all located in the same horizontal plane. For the slant range estimation this is the worst case scenario since the horizontal position covariance of sender and receiver directly translates into the slant range uncertainty estimate. The heading estimation on the other hand works best when sender and receiver are in the same plane, since in this case the accuracy of the heading only depends on the proportion between cumulative position covariance and distance between sender and receiver. Due to the high slant range uncertainty, the DNL position covariance is increased likewise. Since in this experimental set-up, the distance between the sender and the receiver AUVs is roughly the same and also doesn't change considerably over time, the position covariance also remains rather stagnant for the whole experiment duration. By comparing the mean localization performance of the PF in figure 6.20 and DNL in figure 6.21 it can be observed that the DNL performance seems to be the limiting factor in the steady state of the PF, since the PF localization performance converges to the same error/covariance margin as the DNL alone. This can only be expected since the position error will grow until it gets capped by a position fix and DNL is the only source of position fix to the four leaf nodes.

6.1.4.3. Multi-Hop with Meshed Network

The previous two experiments utilized a communication scheme with a unidirectional communication flow. In this experiment we want to investigate the influence of a communication scheme where all AUVs share their position estimation with DNL
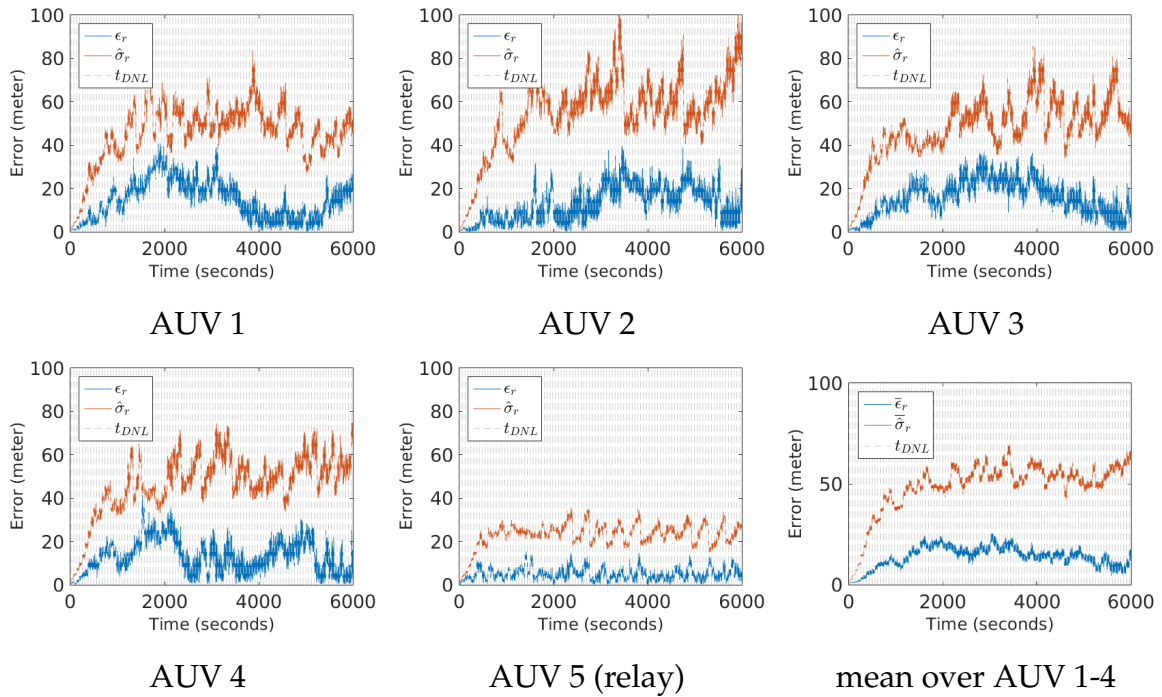
Figure 6.20.: Evolution of horizontal position error and estimated standard deviation by the particle filter. AUV 5 receives DNL messages from USV and in turn propagates DNL messages to AUV 1-4. Each vertical line represents the timing of a received DNL message.
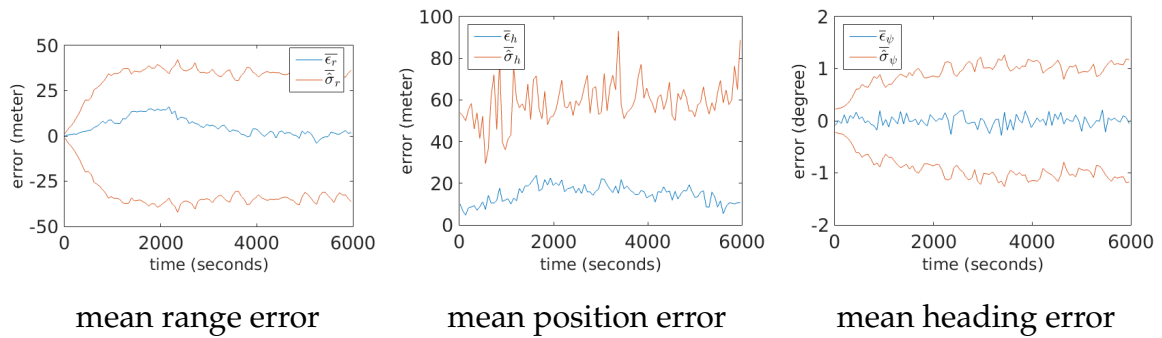
Figure 6.21.: Mean DNL estimation error and estimated standard deviation for the multi-hop case with directed communication. The mean was taken over AUV1-AUV4 on estimates that originated from the same DNL message.

messages. For this, the previous experiment is slightly modified. All vehicle position remain the same, but the communication scheme is changed so that each of the five AUVs broadcasts a DNL message every 10 minutes. To spread the DNL messages more evenly over time, each vehicle will start at a different time offset with its transmission in a round robin fashion. AUV1 starts at t=0, AUV2 starts at t=2min, AUV3 starts at t=4min AUV4 starts at t=6min, AUV5 starts at t=8min. In addition the USV will transmit a DNL message every 10 minutes with AUV5 as the only recipient. The set-up is summarized in figure 6.22.

Communication Scheme

Vehicle	$t_{start}(sec.)$	$\Delta t_{period}(sec.)$
AUV1	0	600
AUV2	120	600
AUV3	240	600
AUV4	360	600
AUV5	480	600
USV	470	600
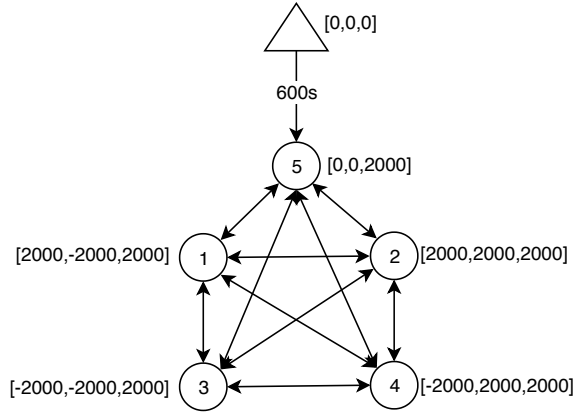
Figure 6.22.: Concept of experimental set-up with communication scheme left and communication graph right. AUV1-AUV5 perform a round robin communication scheme where each 120 second another vehicle transmits a DNL message. The USV inserts a DNL message every 600 seconds which is received only by AUV5.

Figure 6.23 shows the position error of the PF. Here the evolution of covariance and the localization error grow faster than in the previous experiments. This can be expected since the frequency of geo-referenced updates from the USV has been reduces by a factor of 10. However, even the performance of dead reckoning alone seems to be by far superior to the results of this experiment. From the sudden jumps in the uncertainty when ever a DNL message arrived, we can see the influence of DNL to the localization performance. In the results, a DNL message will in most cases increases the covariance of a vehicle, which is seen most prominently for AUV5. Here the covariance increases when the vehicle receives a DNL message from another AUV and it decreases every 600 seconds, when the geo-referenced USV is the originator of the message.

The same can be observed when looking at the mean DNL estimation errors in figure 6.24. In this experiment a steady state has not been reached within the simulated time window. The AUVs in this set-up seem to accumulate uncertainty quicker than the occasional injection of a geo-reference by the USV can reduce it. From the dotted vertical lines we can see that some of the AUVs have a irregular reception pattern,
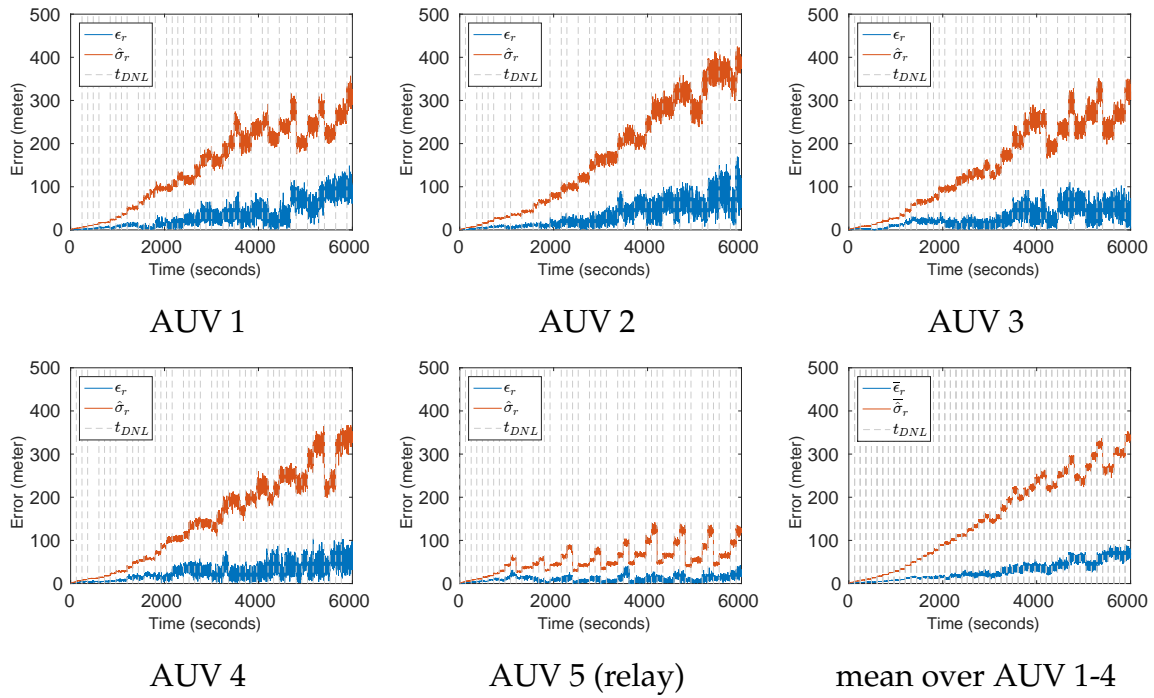
Figure 6.23.: Evolution of horizontal position error and estimated standard deviation by the particle filter. Every AUVs transmit cyclic DNL message every 10 minutes. In addition AUV 5 receives DNL messages from USV every 10 minutes. Each vertical line represents the timing of a received DNL message.
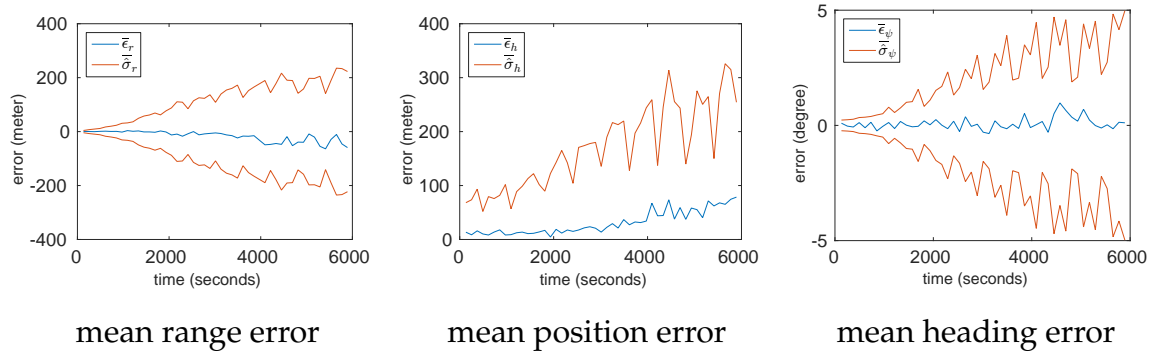
Figure 6.24.: Mean DNL estimation error and estimated standard deviation for the multi-hop case with a meshed network. The mean was taken over AUV1 - AUV4 on estimates that originated from the same DNL message.

meaning that some of the DNL messages have not reached this vehicle. In how far overhearing a message affects the vehicle localization is hard to judge in this scenario. Another reason for the decline of localization performance is that the chosen network topology creates a self reinforcing feedback loop. When the slant range is estimated conservatively, it results in a higher position covariance which in turn will lead to a higher uncertainty in the slant range in the next iteration. The same applies if the uncertainty estimate is to optimistic. For the DNL approach it is crucial that the underlying covariances of USBL measurement, sender and receiver position closely approximate realistic values. This is an important insight and helps to better understand the results.

6.1.4.4. Multi-Hop with Meshed Network and One Way Travel Time

The previous experiment showed that DNL provided bad results in a network configuration with sparse updates from a geo-referenced node. One of the main reason for this is that in the described form, DNL relies on the position estimates of sender and receiver to estimate the slant range and its uncertainty. It is however possible to measure the slant range directly if all vehicles have a sufficiently exact and synchronized clock. USBL with synchronized clocks can measure the one-way travel-time (OWTT) of a signal and infer from that the slant range. In this subsection we will repeat the previous experiment but with USBL modems that can measure the slant range via OWTT.

The localization error of the particle filter for each vehicle is shown in figure 6.25. Unlike in the previous experiment, the position covariance of every vehicle assumes a steady state after around 1000 seconds. By replacing the slant range estimation with an actual measurement, the self-reinforcing process has been halted. Also the DNL estimation results from before the fusion compare to the multi-hop result as can be seen in figure 6.26. In this experiment the number of geo-reference injections from the USV is even less by a factor of ten, while the localization performance stays roughly the same.

Figure 6.27 compares the error evolution of a directed communication pattern with the error evolution using a meshed communication pattern, with and without OWTT respectively. When using a directed communication pattern, a steady state was reached and the localization uncertainty stopped growing. After introducing the meshed communication pattern, the mean localization error as well as the uncertainty grow rapidly, even with frequent geo-reference injections from the USV. It appears that the additional uncertainty growth was introduces by the meshed communication strategy. This growth can mostly be attributed to the feedback loop created by the slant range estimation. When using slant range measurements via OWTT instead, this feedback loop is resolved and the localization becomes stable again, even for the
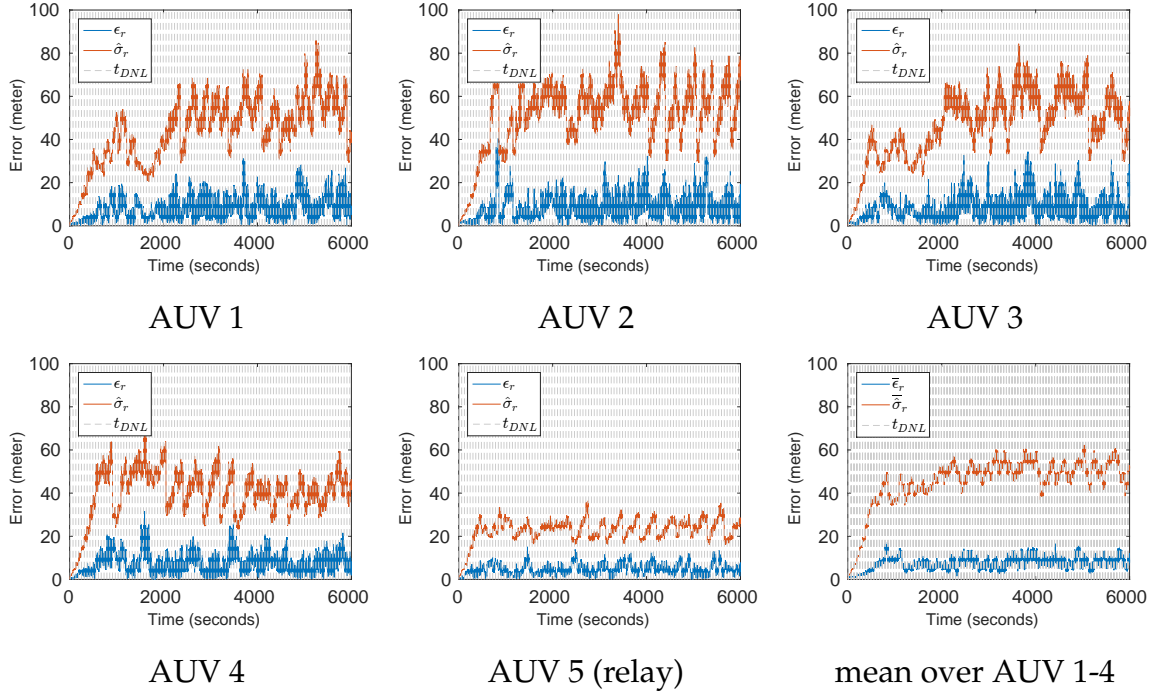
Figure 6.25.: Evolution of horizontal position error and estimated standard deviation by the particle filter. Every AUVs transmit cyclic DNL message every 10 minutes. In addition AUV 5 receives DNL messages from USV every 10 minutes. Vehicles can measure the slant range via OWTT. Each vertical line represents the timing of a received DNL message.
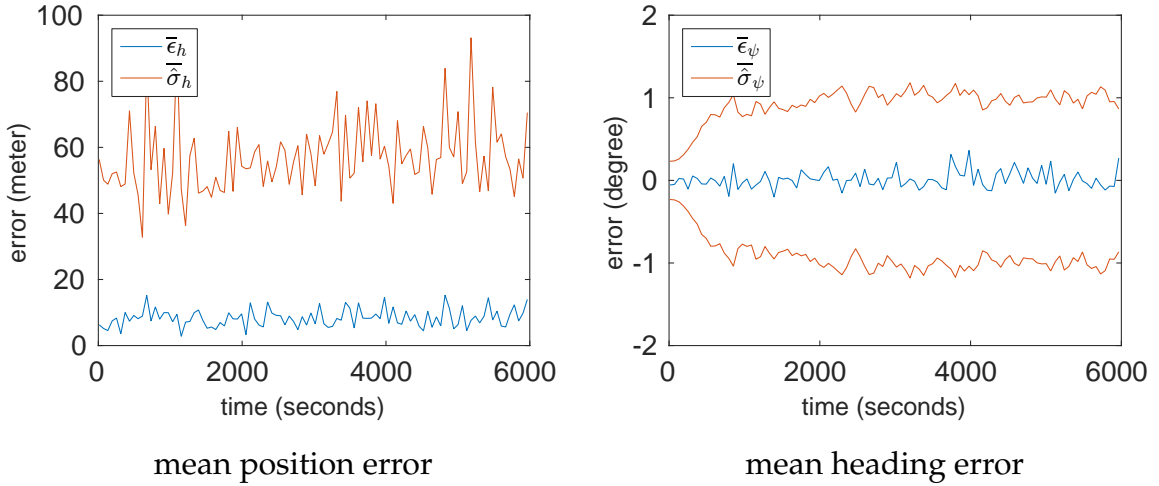
Figure 6.26.: Mean DNL estimation error and estimated covariance for the multi-hop case with a meshed network and OWTT enabled. The mean was taken over AUV1-AUV4 on estimates that originated from the same DNL message.

meshed communication pattern.
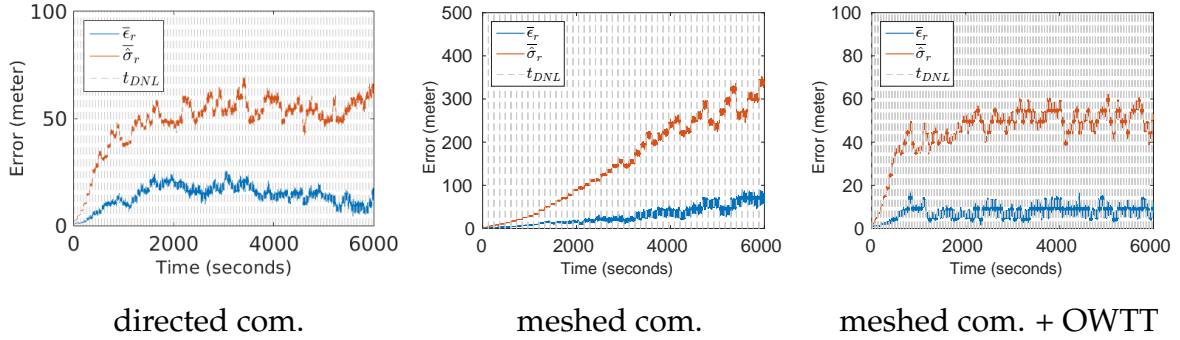
Figure 6.27.: Comparison of mean position error and estimated position covariance over AUV1-4 for different multi-hop experiments. On the left with a directed communication graph, in the middle with a meshed communication graph and on the right with a meshed communication graph and OWTT measurements.

6.2. Discussion

This section will be used to reflect on the most important insights from the experiments and discuss their implications.

In the first part of the experiments, the USBL model has been evaluated. The results suggest that the developed sensor model produces outputs that are comparable to those of the real sensor. It would be desirable to evaluate the model on a larger dataset however. The lack of reliable references data for the USBL measurements has been a difficult hindrance throughout this work. Since this is general problem of the underwater localization field, an open database where ground-truth data is mapped against USBL measurements would be a huge benefit for the whole research community.

In the second part, the experiments continued with feasibility and performance tests of the DNL approach. The systematic rasterization of the spherical space gave insights in which cases a good performance can be expected and where the approach has its limitations. During the evaluation with real sensor data, the DNL approach has shown to work as expected with reliable estimates of the covariance. An important insight from the analysis is that the quality of yaw and range estimators have a inversely proportional tendency for most application relevant set-ups. While the yaw estimator works best when sender and receiver are in the same horizontal plane, the range estimation performs best in a vertically aligned set-up. Here as well the amount of available reference data for the evaluation has been limited and doesn't represent a diverse enough data set.

After the base framework of DNL has been evaluated, the cooperative localization experiments could take place in the last part of the experiments section. In the previous experiments it was possible to investigate the DNL separately from the localization of a vehicle. This changed in the multi vehicle experiments where DNL was embedded in the vehicle localization and will affect its state estimation. This makes it harder to analyse, especially since DNL builds upon the vehicles state estimation and now there is a mutual influence between state and DNL estimation. Also for the first time in this work the agents use a particle filter for the sensor fusion. Particle filters are known to cope better with non-linear problems like the cooperative localization, which is why a particle filter was chosen for this work, however there is also a series of drawbacks.

The utilized PF in this work tends to produce many sudden state changes, e.g. when a cluster of particles gets replaced in a re-sampling step. This discontinuity causes an increase of the state variance and thus a degradation of the DNL estimation. Furthermore, a PF is a stochastic process and not deterministic, which makes it harder to untangle the influence of DNL to the end result. Finally, another property of the PF required special consideration when designing the experiments. When using PF, the timing of DNL messages is important, because the PF needs time to recover to a reasonable uncertainty bound after a DNL update. When receiving a DNL message, the filter updates its internal state, discarding outlying particles and thus reducing the variance. While this is generally a desired behaviour, when there are many DNL message in quick succession the variance is reduced without gaining accuracy. On the other hand, if the DNL update is too conservative, the covariance of the PF will increase disproportionately. For the given PF, the DNL injections should not exceed a maximal frequency of one message per minute. These insights show that DNL is susceptible to wrong uncertainty information, or in other words relies on correct covariance data from the sensor fusion. While there is certainly a way of fixing the behaviour of the PF for most of the problems mentioned here, it was not the goal of this work to develop a robust particle filter. In hindsight a deterministic filter like an EKF or UKF might have been better suited for the investigation of the DNL approach. Nevertheless, the multi-vehicle experiments showed some interesting results. When restrained to a strictly directional communication graph, the DNL approach has shown to limit the localization error of the AUVs, even if only one AUV has access to the geo-referenced signals from the USV. Furthermore the system can cope with communication loss and sparse geo-reference updates. By introducing OWTT measurements, it is even possible to retain the steady state over a period of several minutes and possibly longer without updates from the surface vessel. This is an important feature for the application of mobile underwater sensor networks as it demonstrates that a team of AUVs can temporally maintain its localization capability even without supporting infrastructure like a surface vehicle.

7. Conclusion & Outlook

This chapter will conclude this work by briefly summarizing the results and highlighting the contributions made. An outlook into possible future research directions will finalize this work.

7.1. Conclusion

7.1.1. USBL Model

The USBL model which has been developed in this work can be used for a variety of useful applications. In this work, the model has been utilized mainly for the error estimation of USBL measurements. However, it can also be used for calibrating the hydrophone positions of a real USBL as shown in section 6.1.2.1. Another possible application is to improve sensor measurements by correcting for vehicle motion and sound speed errors, either by post-processing after the deployment or online if the necessary information is available.

7.1.2. DNL Characteristics

In this section, it will be discussed whether the DNL algorithm proposed in this thesis fulfils the requirements that were collected in chapter 3. This is done separately for each requirement.

Localization is supported for fully mobile networks
This requirement is met as long as every node is able to estimate its approximate position and is equipped with a compatible USBL modem. Since vehicles need to keep track of their position in order to navigate, this condition is generally met for mobile nodes. Furthermore, static nodes e.g. anchored nodes can be integrated into the network seamlessly as long as they are equipped with an acoustic modem and have knowledge of their location. In this regard the DNL approach does not differentiate between the locomotion capability of any node.

Procedure does not rely on a particular network topology or communication protocol

Apart from the header, which needs to be included into the data packets, DNL does not rely on a special communication protocol and will work with arbitrary media access schemes. An important property of the proposed algorithm is the equal treatment of each node. This ensures that DNL will work with arbitrary network topologies.

It is important to note that the localization quality is not unaffected by the topology. In general the connectivity of a node, and hence the network topology, will influence the amount of data packets that this node receives. In this sense, the topology affects the number of DNL estimates for a specific node. Also the relative position of sender and receiver, in particular the depth difference, will affect the quality of the DNL estimate. In multi-hop topologies where no range measurement is available, e.g. via OWTT, the application of DNL is not advisable since it may even deteriorate localization performance.

Every agent can use CL to self-localize

The preconditions for an agent to use DNL are: The agent must be equipped with an USBL receiver to eavesdrop on network traffic and it must be aware of its approximate position. Other than that, there are no limitation on the type of agents that can utilize DNL for self-localization.

Computation complexity remains the same, independent from network size

The algorithm retains a constant complexity independent from the number of participants in the network. Many of the current CL approaches utilize past states e.g. in the form of pose graphs, which demand a higher computation time for each consecutive pose estimation. Since the DNL approach does not utilize past states, the amount of necessary computations remains the same for each DNL estimation. Further, the required memory also remains constant since the broadcasted position of the transmitter is only used for the current estimation and can be discarded afterwards. The decisive factor that determines the number of DNL estimates per time slot is the amount of data packets that have been received in one period. If the network traffic is high, many DNL estimates will be triggered. In this situation, an agent with limited computation power has the option to not use every received data packet for localization.

Localization performance improves with network size

Intuitively it can be presumed that, the more DNL packets one node receives from other nodes, the more information it has at its disposal in order to estimate the own position. However, in the conducted experiments this has not been the case. On the contrary, it was observed that the localization performance dropped with increasing frequency of received DNL packages. As discussed in the previous chapter, this can be attributed to the utilized particle filter and is not an intrinsic property of DNL.

Unfortunately, the experiments do not give enough indication to determine whether this property would be satisfied with another filter technique.

When CL is performed by an agent, the localization quality is better than its dead reckoning capability
The experiments showed that, if at least one node has access to absolute positioning information, the covariance of each node in the same network is bounded unlike in the dead reckoning case. If there is no direct connection between a leaf node and a node with absolute positioning information, the covariance of intermediate nodes accumulate and the leaf node will have a higher covariance at steady state. The DNL localization quality in the short term depends on the network topology and communication scheme of the network. In single hop networks with a geo-referenced node as transmitter the performance of DNL has been superior to a MEMS-based DR. If there are multi-hop nodes or no geo-reference is available, localization covariance with DNL can quickly exceed the covariance of DR localization.

Acoustic interference with payload sensors should be avoided
When looking at a sensor node, the strongest disturbances with acoustic payload sensors occur when sending messages over the acoustic link. This is because the intensity of outgoing signals is orders of magnitude greater than the attenuated signals that arrive at this node from remote sources. With DNL a node does not need to send an acoustic signal in order to get a localization fix, which helps to avoid unnecessary acoustic interference between payload sensors and the acoustic modem.

7.1.3. Cooperative Localization with DNL

The results of the experiments showed that DNL can improve the localization and heading estimate of deep diving submersibles, under certain preconditions. The core idea of DNL is to integrate the location of a sender together with a measurement of the relative position between sender and receiver into a position estimate of the receiving node. Here the slant range is estimated by also taking the own position estimate into account. Through this step each DNL estimate becomes dependent on its own previous position belief. When DNL is feed into the navigation solution, this creates a self-reinforcing feedback loop which may corrupt the localization.
Because of the interdependence in the slant range estimate, both sender and receiver need to maintain a proper estimate of their position uncertainty in order to yield a good DNL position estimate. This premise limits the scenarios in which DNL can improve the localization performance to those cases where a sender has access to geo-reference. While this is a strong limitation for a cooperative localization method, many of the currently applied underwater localization techniques share the same restriction. This drawback can be compensated however by replacing the slant range estimation with a measurement via OWTT, which is demonstrated in the final experiment.

As a cooperative localization approach, the purpose of DNL is to improve the navigation capability of participating agents. However, the focus in the design was not to maximize the localization accuracy of an agent. It was rather meant as a mechanism to restrict the indefinite uncertainty growth during deep dives for a large group of agents. Scalability is an important characteristic of DNL, which distinguishes it from most of the other cooperative localization approaches in the underwater domain. Also the silent nature and the low complexity are deliberate design choices that followed practical considerations, with the goal to enable navigation for large fleets of unmanned underwater vehicle.

Both, DNL and USBL model have been deployed on the computer of a USBL device without disturbing the original driver software, which shows how resource-efficient the approach is. Since no additional hardware is required to use DNL, its integration becomes effectively free of charge.

7.2. Contribution

The combination of communication and localization is still tenuously studied in the underwater domain. In the last decade, new technologies matured that merge underwater communication and localization in a single compact device, which lead to the emergence of new possibilities in underwater localization. This work adds to the research process in this field by proposing a cooperative localization mechanism that is based on message exchange between agents in conjunction with relative bearing measurements of a sending agent.

Compact devices for underwater communication and positioning have been an important enabling technology for the development of autonomous underwater vehicle. Manufacturers pursued different measurement approaches to tackle the problem. This work contributed an extensive USBL localization model for the Evologics USBL modem that was not found in the literature in such detail. The model is able to compensate measurement errors from vehicle motion and incorrect sound velocity assumptions. It can estimate an error margin for a given measurement and it can be used to simulate measurements.

Most of the acoustic localization methods found in the literature concentrate their efforts to determine the position only. In the DNL approach, also the vehicle heading is included, since it is a crucial information for the navigation and the interpretation of other sensor readings.

Localization remains one of the biggest challenges for deep diving AUVs. Current deep diving AUVs require an expensive suite of sensors to reliably determine their position over an extended period of time. Therefore, the deployment of a AUV fleets is often economically prohibitive. The gyroscope makes up a good part of the overall cost for sensors. The price for a navigation rated ring laser or fibre optic gyroscope lies in the middle six digit range. Inertial navigation sensors with MEMS-based gyroscopes come at a price that is two orders of magnitude lower but with insufficient

precision. By integrating a cooperative localization scheme like DNL into the MEMS-based navigation it is feasible to increase the long term reliability. An interesting scenario would be to deploy two different classes of AUV, a cheaper version with limited navigation capabilities and another class that has good navigation capabilities and acts as relay and reference node for the other submersibles. This brings us a little step closer to the possibility of autonomous fleets of deep diving underwater vehicles that are required to explore and monitor the vast spaces under the surface of our oceans.

7.3. Outlook

Because every thesis is limited in time and effort, this work could not nearly cover all interesting aspects. This section will give a short summary of related topics that would be promising to investigate further.

The utilized particle filter has turned out to be a difficult base for the verification of the DNL approach. A deterministic filter like a EKF or UKF could help to reduce the problems related to sudden changes of position belief, thus making it easier to differentiate the influence of DNL to the navigation solution.

One of the major drawbacks of DNL is caused by the necessity of estimating the slant range. USBL modems with slant range measurement via OWTT have only emerged after the SMIS project. So for this work no real data could be gathered with this devices. The final experiment showed that slant range measurements could remove some of the limitations of the approach. It would be interesting to further analyse the DNL performance with OWTT, e.g. to test how long a group of AUVs could maintain a reasonable uncertainty threshold without geo-reference insertions.

So far, all AUV shared the same localization capabilities. It would be interesting to investigate the dynamics of a group with mixed capabilities. This could give answers to questions like, what is the minimal effort in sensor equipment that is necessary to maintain a given localization quality.

When dealing with groups of agents, interesting parameters for localization are the uncertainty increase or the approximated steady state threshold. Mourikis et. al. [28] have formalized a system to determine these values for their terrestrial robots performing CL. If their work could be adapted to the underwater case, it would be possible to predict the localization performance for a given group without running a tedious simulation.

Finally, it must be said that there are also many completely different interesting and promising approaches to improve navigation accuracy, like SLAM and Model-Aided navigation, which were not examined in detail in this work.

Appendix

A. Appendix 1

A.1. List of Abbreviations

AOA	Angle of Arrival
AP	Access Point
AUV	Autonomous Underwater Vehicle
CFD	Cumulative Distribution Function
CL	Cooperative Localization
CI	Covariance Intersection
DEIF	Distributed Extended Information Filter
DGPS	Differential Global Positioning System
DNL	Deep-Sea Network Localization
DOA	Direction Of Arrival
DR	Dead Reckoning
DVL	Doppler Velocity Log
EKF	Extended Kalman Filter
ENI	Energietechnik-Elektronik GmbH
GNSS	Global Navigation Satellite System
IMP	IMPaC Offshore Engineering GmbH
IMU	Inertial Measurement Unit
INS	Inertial Navigation System
IOW	Leibnitz-Institute for Baltic Sea Research Warnemuende
IQR	Interquartile Range
KF	Kalman Filter
KIT	Karlsruhe Institute of Technology
LBL	Long Base Line
MAC	Media Access Control
MAS	Multi Agent System
MEMS	Micro Electro Mechanical Systems
MUWAN	Mobile UnderWater Acoustic Networks
OWTT	One Way Travel Time
PF	Particle Filter
ROS	Roboter Operating System
ROV	Remotely Operated Vehicle
RPMG	Relative Position Measurement Graph
RTT	Round Trip Time

A. Appendix 1

SBL	Short Base Line
SBS	Sea-Bed Station
SLAM	Simultaneous Localization and Mapping
SMC	Sequential Monte-Carlo method
SMIS	Subsea Monitoring via Intelligent Swarms
TDOA	Time Difference of Arrival
TOA	Time of Arrival
TUB	Technical University of Berlin
UKF	Unscented Kalman Filter
UPF	Unscented Particle Filter
UPS	Underwater Positioning Scheme
URDF	Unified Robot Description Language
URO	University of Rostock
USBL	Ultra Short Base Line
USBLANGL	Ultra Short Base Line measurement without rang information
USBLLONG	Ultra Short Base Line measurement with rang information
USV	Unmanned Surface Vehicle
UT	Unscented Transformation
UWSN	UnderWater Sensor Networks
UWAN	UnderWater Acoustic Networks

List of Figures

List of Tables

List of Algorithms

Bibliography

[1] BGR. Marine mineralische Rohstoffe an der BGR. `https://www.bgr.bund.de/DE/Gemeinsames/Produkte/Downloads/Marine_Rohstoffe_Newsletter/Rohstoffwirtschaft/marine_mineralische_rohstoffe_2016.pdf`, 2016. Online; accessed 11 January 2020.

[2] Daniel OB Jones, Stefanie Kaiser, Andrew K Sweetman, Craig R Smith, Lenaick Menot, Annemiek Vink, Dwight Trueblood, Jens Greinert, David SM Billett, Pedro Martinez Arbizu, et al. Biological responses to disturbance from simulated deep-sea polymetallic nodule mining. *Plos One*, 12(2):e0171750, 2017.

[3] United States Geological Survey. Manganese nodules from the seafloor are often rich in metals like manganese, iron, nickel, copper, and cobalt. `https://upload.wikimedia.org/wikipedia/commons/7/76/Manganese_nodules.gif`, 2010. Online; accessed 11 January 2020.

[4] F. Boeck, M. Golz, S. Ritz, and G. Holbach. Smis - subsea monitoring via intelligent swarms, design challenges of an autonomous seabed station. In *ASME 2014 33rd International Conference on Ocean, Offshore and Arctic Engineering Volume 8B: Ocean Engineering*, San Francisco, California, USA, 2014.

[5] Florin Boeck, Matthias Golz, Sebastian Ritz, and Gerd Holbach. Smis-subsea monitoring via intelligent swarms, design challenges of an autonomous seabed station. In *ASME 2014 33rd International Conference on Ocean, Offshore and Arctic Engineering*, pages V08BT06A026–V08BT06A026. American Society of Mechanical Engineers, 2014.

[6] S. Ritz, G. Holbach, F. Boeck, and M. Golz. Challenges and specialties in design of an unmanned surface vehicle for hydrographic tasks. *Jahrbuch der Schiffbautechnischen Gesellschaft*, Volume 108:in Process, 2014.

[7] Erik Rentzow, Detlef Dewitz, Martin Kurowski, Bernhard P Lampe, Sebastian Ritz, Robert Kutz, Matthias Golz, and Florin Boeck. Design and automation of an ocean-going autonomously acting usv. In *OCEANS 2015-Genova*, pages 1–6. IEEE, 2015.

[8] Louis Whitcomb, Dana R Yoerger, Hanumant Singh, and Jonathan Howland. Advances in underwater robot vehicles for deep ocean exploration: Navigation, control, and survey operations. In *Robotics Research*, pages 439–448. Springer, 2000.

[9] Jim Partan, Jim Kurose, and Brian Neil Levine. A survey of practical issues in underwater networks. *ACM SIGMOBILE Mobile Computing and Communications Review*, 11(4):23–33, 2007.

[10] Xingxing Li, Xiaohong Zhang, Xiaodong Ren, Mathias Fritsche, Jens Wickert, and Harald Schuh. Precise positioning with current multi-constellation global navigation satellite systems: Gps, glonass, galileo and beidou. *Scientific reports*, 5, 2015.

[11] Inc Sea-Bird Electronics. *SBE 50 User Manual*, 2012.

[12] Luke Stutters, Honghai Liu, Carl Tiltman, and David J Brown. Navigation technologies for autonomous underwater vehicles. *IEEE Transactions on Systems, Man, and Cybernetics, Part C (Applications and Reviews)*, 38(4):581–589, 2008.

[13] Josep Aulinas. ≫ *Selective Submap Joining SLAM for autonomous vehicles* ≪. PhD thesis, Dissertation. Institute of Informatics, Applications, Computer Vision und Robotics Group, Universitat de Girona, 2011.

[14] Franco Hidalgo and Thomas Bräunl. Review of underwater slam techniques. In *Automation, Robotics and Applications (ICARA), 2015 6th International Conference on*, pages 306–311. IEEE, 2015.

[15] K. Vickery. Acoustic positioning systems. a practical overview of current systems. In *Proceedings of the 1998 Workshop on Autonomous Underwater Vehicles*, pages 5–17, Cambridge, MA, USA, 1998.

[16] Tao Bian, Ramachandran Venkatesan, and Cheng Li. Design and evaluation of a new localization scheme for underwater acoustic sensor networks. In *Global Telecommunications Conference, 2009. GLOBECOM 2009. IEEE*, pages 1–5. IEEE, 2009.

[17] David Oertel. *Deep Sea Navigation Improvement through online Calibration of Dynamic Models for Autonmous Underwater Vehicles*. PhD thesis, KIT, 2017.

[18] Ryan M Eustice, Hanumant Singh, and Louis L Whitcomb. Synchronous-clock, one-way-travel-time acoustic navigation for underwater vehicles. *journal of field robotics*, 28(1):121–136, 2011.

[19] Simon J Julier. The scaled unscented transformation. In *American Control Conference, 2002. Proceedings of the 2002*, volume 6, pages 4555–4559. IEEE, 2002.

[20] Wu Zhang, Min Liu, and Zong-gui Zhao. Accuracy analysis of unscented transformation of several sampling strategies. In *Software Engineering, Artificial Intelligences, Networking and Parallel/Distributed Computing, 2009. SNPD'09. 10th ACIS International Conference on*, pages 377–380. IEEE, 2009.

[21] Neil Gordon, B Ristic, and S Arulampalam. Beyond the kalman filter: Particle filters for tracking applications. *Artech House, London*, 830, 2004.

[22] Rudolph Van Der Merwe, Arnaud Doucet, Nando De Freitas, and Eric A Wan. The unscented particle filter. In *Advances in neural information processing systems*, pages 584–590, 2001.

[23] Hwee-Pink Tan, Roee Diamant, Winston KG Seah, and Marc Waldmeyer. A survey of techniques and challenges in underwater localization. *Ocean Engineering*, 38(14):1663–1676, 2011.

[24] Werner Weber, Jan Rabaey, and Emile HL Aarts. *Ambient intelligence*. Springer Science & Business Media, 2005.

[25] Stergios I Roumeliotis and Ioannis M Rekleitis. Analysis of multirobot localization uncertainty propagation. In *Intelligent Robots and Systems, 2003.(IROS 2003). Proceedings. 2003 IEEE/RSJ International Conference on*, volume 2, pages 1763–1770. IEEE, 2003.

[26] Stergios I Roumeliotis and Ioannis M Rekleitis. Propagation of uncertainty in cooperative multirobot localization: Analysis and experimental results. *Autonomous Robots*, 17(1):41–54, 2004.

[27] Anastasios I Mourikis and Stergios I Roumeliotis. Performance bounds for cooperative simultaneous localization and mapping (c-slam). In *Robotics: Science and Systems*, pages 73–80. Boston, MA, 2005.

[28] Anastasios I Mourikis and Stergios I Roumeliotis. Performance analysis of multirobot cooperative localization. *IEEE Transactions on robotics*, 22(4):666–681, 2006.

[29] Guangjie Han, Jinfang Jiang, Lei Shu, Yongjun Xu, and Feng Wang. Localization algorithms of underwater wireless sensor networks: A survey. *Sensors*, 12(2):2026–2061, 2012.

[30] Vijay Chandrasekhar, Winston KG Seah, Yoo Sang Choo, and How Voon Ee. Localization in underwater sensor networks: survey and challenges. In *Proceedings of the 1st ACM international workshop on Underwater networks*, pages 33–40. ACM, 2006.

[31] Xiuzhen Cheng, Haining Shu, Qilian Liang, and David Hung-Chang Du. Silent positioning in underwater acoustic sensor networks. *Vehicular Technology, IEEE Transactions on*, 57(3):1756–1766, 2008.

[32] Cláudia Soares, João Gomes, Beatriz Ferreira, and João Paulo Costeira. Locdyn: Robust distributed localization for mobile underwater networks. *arXiv preprint arXiv:1701.08027*, 2017.

[33] Beatriz Quintino Ferreira, João Gomes, Cláudia Soares, and João P Costeira. Collaborative localization of vehicle formations based on ranges and bearings. In *Underwater Communications and Networking Conference (UComms), 2016 IEEE Third*, pages 1–5. IEEE, 2016.

[34] Narcs Palomeras, Natalia Hurts, and Marc Carreras. Auv/asc cooperative survey. In *SEVENTH INTERNATIONAL WORKSHOP ON MARINE TECHNOLOGY Martech 2016*, volume 7, pages 71–73, 2016.

[35] Michael Kaess, Ananth Ranganathan, and Frank Dellaert. isam: Incremental smoothing and mapping. *IEEE Transactions on Robotics*, 24(6):1365–1378, 2008.

[36] Been Kim, Michael Kaess, Luke Fletcher, John Leonard, Abraham Bachrach, Nicholas Roy, and Seth Teller. Multiple relative pose graphs for robust cooperative mapping. In *Robotics and Automation (ICRA), 2010 IEEE International Conference on*, pages 3185–3192. IEEE, 2010.

[37] Alexander Cunningham, Manohar Paluri, and Frank Dellaert. Ddf-sam: Fully distributed slam using constrained factor graphs. In *Intelligent Robots and Systems (IROS), 2010 IEEE/RSJ International Conference on*, pages 3025–3030. IEEE, 2010.

[38] Alexander Bahr, John J Leonard, and Maurice F Fallon. Cooperative localization for autonomous underwater vehicles. *The International Journal of Robotics Research*, 28(6):714–728, 2009.

[39] Liam Paull, Mae Seto, and John J Leonard. Decentralized cooperative trajectory estimation for autonomous underwater vehicles. In *Intelligent Robots and Systems (IROS 2014), 2014 IEEE/RSJ International Conference on*, pages 184–191. IEEE, 2014.

[40] Sarah E Webster, Jeffrey M Walls, Louis L Whitcomb, and Ryan M Eustice. Decentralized extended information filter for single-beacon cooperative acoustic navigation: Theory and experiments. *IEEE Transactions on Robotics*, 29(4):957–974, 2013.

[41] Jeffrey M Walls and Ryan M Eustice. An exact decentralized cooperative navigation algorithm for acoustically networked underwater vehicles with robustness to faulty communication: Theory and experiment. In *Robotics: Science and Systems*, 2013.

[42] Jeffrey M Walls, Alexander G Cunningham, and Ryan M Eustice. Cooperative localization by factor composition over a faulty low-bandwidth communication channel. In *Robotics and Automation (ICRA), 2015 IEEE International Conference on*, pages 401–408. IEEE, 2015.

[43] Alejandro Ribeiro, Georgios B Giannakis, and Stergios I Roumeliotis. Soi-kf: Distributed kalman filtering with low-cost communications using the sign of innovations. *IEEE Transactions on signal processing*, 54(12):4782–4795, 2006.

[44] Tim Bailey, Mitch Bryson, Hua Mu, John Vial, Lachlan McCalman, and Hugh Durrant-Whyte. Decentralised cooperative localisation for heterogeneous teams of mobile robots. In *Robotics and Automation (ICRA), 2011 IEEE International Conference on*, pages 2859–2865. IEEE, 2011.

[45] John R Spletzer. *Sensor fusion techniques for cooperative localization in robot teams*. PhD thesis, Citeseer, 2003.

[46] K.G. Kebkal, Oleksiy Kebkal, Ievgenii Glushko, Veronika Kebkal, Luis Sebastiao, Antonio Pascoal, Joao Gomes, Jorge Ribeiro, Silva H., and Miguel Ribeiro. Underwater acoustic modems with integrated atomic clocks for one-way travel-time underwater vehicle positioning. UACE2017 4th Underwater Acoustics Conference and Exhibition, 09 2017.

[47] Stojanovic, Militsa. Exploration and Exploitation in Actuated Communication Networks. `http://millitsa.coe.neu.edu/?q=node/13`, 2017. Online; accessed 17 February 2017.

[48] Sergej Neumann, David Oertel, Heinz Wörn, Martin Kurowski, Detlef Dewitz, Joanna J Waniek, David Kaiser, and Robert Mars. Towards deep-sea monitoring with smis-experimental trials of deep-sea acoustic localization. In *Proceedings of the 18th International Conference on Climbing and Walking Robots*. World Scientific, 2015.

[49] Neumann Sergej, Oertel David, and Wörn Heinz. Deep net localization - eavesdropping in mobile acoustic underwater sensor networks. In *Techno-Oceans 2016*. IEEE, 2016.

[50] Joanna Waniek. Cruise report rv poseidon cruise no. 470 [pos470], from 25.05.2014 to 15.06.2014, malaga (spain) - funchal (portugal). Cruise Report doi:10.3289/CR_POS470, Leibniz Institut für Ostseeforschung Warnemünde, Rostock, Germany, July 2014.

[51] EvoLogics GmbH. *S2C Reference Manual*, standard edition, 2016.

[52] EvoLogics GmbH. *Products / Underwater USBL Positioning Systems / S2CR 7/17 USBL — EvoLogics GmbH*, 2017.

[53] Michael B Porter and Homer P Bucker. Gaussian beam tracing for computing ocean acoustic fields. *The Journal of the Acoustical Society of America*, 82(4):1349–1359, 1987.

[54] Michael B Porter, Heat, Light, and Sound Research Inc. Acoustics toolbox, 2009.

[55] David Oertel, Sergej Neumann, H. Worn, M. Golz, and Joanna Waniek. Reducing elevation angle errors of long-range deep-sea acoustic localization by ray tracing and depth measurements. pages 178–183, 07 2016.

[56] Xavier Lurton and Darrell R Jackson. An introduction to underwater acoustics. *The Journal of the Acoustical Society of America*, 115(2):443–443, 2004.

[57] Konstantin G Kebkal, Oleksiy G Kebkal, Rudolf Bannasch, and Sergey G Yakovlev. Performance of a combined usbl positioning and communication system using s2c technology. In *2012 Oceans-Yeosu*, pages 1–7. IEEE, 2012.

[58] Joel Reis, Marco Morgado, Pedro Batista, Paulo Oliveira, and Carlos Silvestre. Design and experimental validation of a usbl underwater acoustic positioning system. *Sensors*, 16(9):1491, 2016.

[59] Joanna Waniek. R.v. poseidon cruise report pos485. Fahrtbericht doi:10.3289/CR_POS485, Leibniz Institute for Baltik Sea Research, Warnemnde, Warnemünde, Germany, Oktober 2015.

[60] Neumann Sergej, Oertel David, and Wörn Heinz. Self-localization by eavesdropping in acoustic underwater sensor networks. In *Proceedings of the International Conference on Multisensor Fusion and Integration for Intelligent Systems*. IEEE, 2016.

[61] Nihal Yatawara, Bovas Abraham, and John F MacGregor. A kalman filter in the presence of outliers. *Communications in Statistics-Theory and Methods*, 20(5-6):1803–1820, 1991.

[62] W Flenniken, J Wall, and D Bevly. Characterization of various imu error sources and the effect on navigation performance. In *ION GNSS*, pages 967–978, 2005.

[63] Keyu Chen, Maode Ma, En Cheng, Fei Yuan, and Wei Su. A survey on mac protocols for underwater wireless sensor networks. *Communications Surveys & Tutorials, IEEE*, 16(3):1433–1447, 2014.

[64] Ian F Akyildiz, Dario Pompili, and Tommaso Melodia. Underwater acoustic sensor networks: research challenges. *Ad hoc networks*, 3(3):257–279, 2005.

[65] John Heidemann, Milica Stojanovic, and Michele Zorzi. Underwater sensor networks: applications, advances and challenges. *Philosophical Transactions of the Royal Society of London A: Mathematical, Physical and Engineering Sciences*, 370(1958):158–175, 2012.

[66] John Heidemann, Wei Ye, Jack Wills, Affan Syed, and Yuan Li. Research challenges and applications for underwater sensor networking. In *Wireless Communications and Networking Conference, 2006. WCNC 2006. IEEE*, volume 1, pages 228–235. IEEE, 2006.

[67] Giuseppe Casalino, Alessio Turetta, Enrico Simetti, and Andrea Caiti. Rt 2: A real-time ray-tracing method for acoustic distance evaluations among cooperating auvs. In *OCEANS 2010 IEEE-Sydney*, pages 1–8. IEEE, 2010.

Bibliography

[68] Finn Bruun Jensen. *Computational ocean acoustics*. Springer Science & Business Media, 1994.

[69] Liam Paull, Sajad Saeedi, Mae Seto, and Howard Li. Auv navigation and localization: A review. *Oceanic Engineering, IEEE Journal of*, 39(1):131–149, 2014.

[70] A Alcocer, P Oliveira, and A Pascoal. Underwater acoustic positioning systems based on buoys with gps. In *Proceedings of the Eighth European Conference on Underwater Acoustics*, volume 8, pages 1–8, 2006.

[71] Magne Mandt, Kenneth Gade, and Bjørn Jalving. Integrating dgps-usbl position measurements with inertial navigation in the hugin 3000 auv. In *Proceedings of the 8th Saint Petersburg International Conference on Integrated Navigation Systems, Saint Petersburg, Russia*, 2001.

[72] Maurice Fallon, Georgios Papadopoulos, John Leonard, and Nicholas Patrikalakis. Cooperative auv navigation using a single maneuvering surface craft. *I. J. Robotic Res.*, 29:1461–1474, 10 2010.

[73] Paul Rigby, Oscar Pizarro, and Stefan B Williams. Towards geo-referenced auv navigation through fusion of usbl and dvl measurements. In *OCEANS 2006*, pages 1–6. IEEE, 2006.

[74] Hsin-Hung Chen. In-situ alignment calibration of attitude and ultra short baseline sensors for precision underwater positioning. *Ocean Engineering*, 35(14):1448–1462, 2008.

[75] Jan Opderbecke. At-sea calibration of a usbl underwater vehicle positioning system. In *OCEANS'97. MTS/IEEE Conference Proceedings*, volume 1, pages 721–726. IEEE, 1997.

[76] Mrinal K Sen, LN Frazer, S Mallick, and NR Chapman. Analysis of multipath sound propagation in the ocean near 49 n, 128 w. *The Journal of the Acoustical Society of America*, 83(2):588–597, 1988.

[77] Konstantin G Kebkal and Rudolf Bannasch. Sweep-spread carrier for underwater communication over acoustic channels with strong multipath propagation. *The Journal of the Acoustical Society of America*, 112(5):2043–2052, 2002.

[78] KG Kebkal and R Bannasch. Separation of time-varying multipath arrivals by converting their time delays into their frequency reallocations. 3 rd ica/eaa int. In *Symp. on Hydroacoustics, Annual J*, volume 4, pages 119–126, 2001.

[79] Richard M Murray. Recent research in cooperative control of multivehicle systems. *Journal of Dynamic Systems, Measurement, and Control*, 129(5):571–583, 2007.

[80] Seokhoon Yoon and Chunming Qiao. Cooperative search and survey using autonomous underwater vehicles (auvs). *IEEE Transactions on Parallel and Distributed Systems*, 22(3):364–379, 2011.

[81] Steffen, Jan. Tiefseetiere gesucht, Manganknollen gefunden. `http://www.geomar.de/uploads/media/pm_2015_02_SO237-Manganknollen.pdf`, 2015. Online; accessed 11 January 2020.

[82] Schwarz-Schampera, Ulrich. Untersuchungen zu Rohstoffpotenzialen und Umwelteinfluessen. *Pressemitteilung BGR*, 2017. Online; accessed 13 February 2018.

[83] Tim Cowles, John Delaney, John Orcutt, and Robert Weller. The ocean observatories initiative: Sustained ocean observing across a range of spatial scales. *Marine Technology Society Journal*, 44:54–64, 2010.

[84] A Plueddemann, R Weiler, J Barth, and U Send. The coastal and global scale nodes of the ocean observatories initiative. In *OCEANS 2009, MTS/IEEE Biloxi-Marine Technology for Our Future: Global and Local Challenges*, pages 1–7. IEEE, 2009.

[85] MBARI. Imaging autonomous underwater vehicle. `http://www.mbari.org/at-sea/vehicles/autonomous-underwater-vehicles/`, 2016. Online; accesse 20 February 2017.